Poster Session

-Poster Session-

The poster number with "S" is eligible for the Best Student Poster Award nomination.

P01S Angle-resolved photoemission spectroscopy of Dirac nodal-line superconductor ZrSi1-xPxSe

K. Ideura[a], Y. Nishioka[a], K. Kuroda[a,b,c], A. Ino[d,e], Y. Miyai[a], S. Ideta[a,d], K. Shimada[a,c,d], H. Kito[f], I. Hase[f], S. Ishida[f], H. Fujihisa[f], Y. Gotoh[f], Y. Yoshida[f], A. Iyo[f], H. Ogino[f], H. Eisaki[f],K. Kawashima[f,g], A. Kimura[a,b,c]

a Graduate School of Advanced Science and Engineering, Hiroshima University, Japan
b International Institute for Sustainability with Knotted Chiral Meta Matter (WPI-SKCM2), Japan
c Research Institute for Semiconductor Engineering, Japan
d Research Institute for Synchrotron Radiation Science, Hiroshima University, Japan
e Kurume Institute of Technology, Japan
f National Institute of Advanced Industrial Science and Technology (AIST), Japan
g IMRA JAPAN Co., Ltd., Japan

P02S Electronic states in superconducting type-II Dirac semimetal: 1T-PdSeTe

Yogendra Kumar[a], Shiv Kumar [b], Yenugonda Venkateswara [c,d], Ryohei Oishi[a], Jayata Nayak [d], R.P. Singh[f], Takahiro Onimaru[a], Yasuyuki Shimura[a], Chaoyu Chen [e], Shinichiro Ideta [b], Kenya Shimada [b,g,h]

a Graduate School of Advanced Science and Engineering, Hiroshima University, Japan
b Research Institute for Synchrotron Radiation Science (HiSOR), Hiroshima University, Japan
c Department of Physics, SUNY Buffalo State University, USA
d Department of Physics, Indian Institute of Technology, India
e Songshan Lake Materials Laboratory, China
f Department of Physics, Indian Institute of Science Education and Research, India
g The International Institute for Sustainability with Knotted Chiral Meta Matter (WPI SKCM2), Hiroshima University,Japan
h Research Institute for Semiconductor Engineering (RISE), Hiroshima University,Japan

P03 Developments of ARPES Studies at HiSOR BL-1: Towards HiSOR-II Projects II

Shin-ichiro Ideta[a,b], Masashi Arita[a], Yudai Miyai[b], Yogendra Kumar[b], and Kenya Shimada[a,b,c,d]

a Research Institute for Synchrotron Radiation Science (HiSOR), Hiroshima Univ., Japan
b Graduate School of Advanced Science and Engineering, Hiroshima Univ., Japan
c Research Institute for Semiconductor Engineering, (RISE), Hiroshima Univ., Japan
d International Institute for Sustainability with Knotted Chiral Meta Matter (WPI-SKCM 2), Japan

P04S ARPES study of FexTiS2 ($x = 0 \leq x \leq 0.33$)

K. Kimura[a], Y. Nakashima[b], Y. Tanimoto[b], H. Sato[c], M. Arita[c], Y. Miyai[b], S. Ideta[c], K. Shimada[c], T. Bizen[d], M. Miyata[e], M. Koyano[d]

a Faculty of Science, Hiroshima University, Japan
b Graduate School of Advanced Science and Engineering, Hiroshima University, Japan
c Hiroshima Research Institute for Synchrotron Radiation Science, Hiroshima University, Japan
d School of Materials Science, Japan Advanced Institute of Science and Technology, Japan
e Global Zero Emission Research Center, National Institute of Advanced Industrial Science and Technology, Japan

-Poster Session-

The poster number with "S" is eligible for the Best Student Poster Award nomination.

P05 Temperature dependence of the coupling parameter in the strange metal state of heavily overdoped cuprate superconductor

Y. Miyai[a], S. Ideta[b], M. Arita[b], K. Tanaka[c] ,M. Oda[d], T. Kurosawa[e] and K. Shimada[b,f,g]

a Graduate School of Advanced Science and Engineering, Hiroshima University, Japan
b Hiroshima Synchrotron Radiation Center, Hiroshima University, Japan
c UVSOR-III Synchrotron, Institute for Molecular Science, Japan
d Department of Physics, Hokkaido University, Japan
e Faculty of Science and Engineering, Muroran Institute of Technology, Japan
f Research Institute for Semiconductor Engineering (RISE), Hiroshima University, Japan
g The International Institute for Sustainability with Knotted Chiral Meta Matter (WPI-SKCM2), Hiroshima University, Japan

P06S Unraveling the Electronic Structure of Altermagnetic MnTe via Photoemission Spectroscopy

Kazi Golam Martuza[a], Yogendra Kumar[a], Shiv Kumar[b,c], Shin-ichiro Ideta[b] and Kenya Shimada[b,d,e]

a Graduate School of Advanced Science and Engineering, Hiroshima University, Japan
b Research Institute for Synchrotron Radiation Science (HiSOR), Hiroshima University,Japan
*c Institute of Microelectronics, Agency for Science, Technology and Research (A*STAR), Singapore*
d International Institute for Sustainability with Knotted Chiral Meta Matter (WPI-SKCM2), Hiroshima University, Japan
e Research Institute for Semiconductor Engineering (RISE), Hiroshima University, Japan

P07S Comprehensive Study of Electronic States Induced by Quantum Charge Fluctuations in Electron-doped High-Tc Cuprate Superconductors

H. Yamaguchi[a], Y. Onishi[a], Y. Miyai[a], M. Atira[b], H. Sato[a,b], D. Song[f], K. Tanaka[e], K. Shimada[a,b,c,d], S. Ideta[a,b]

a Graduate School of Advanced Science and Engineering, Hiroshima Univ.,Japan
b Hiroshima Synchrotron Radiation Center (HiSOR), Hiroshima Univ., Japan
c Research Institute for Semiconductor Engineering, (RISE), Hiroshima Univ.,Japan
d International Institute for Sustainability with Knotted Chiral Meta Matter (WPI-SKCM2), Japan
e UVSOR-Ⅲ Synchrotron, Institute for Molecular Science.,,Japan
f Blusson Quantum Matter Institute,University of British Columbia, Canada

P08 Metallization of boron-doped amorphous carbon films

Yuji Muraoka[a], Sho Enomoto[b], Subaru Nakashima[c], Takanori Wakita[d], Takayoshi Yokoya[a] and Kohei Yamagami[e]

a RIIS. Okayama Univ., Japan
b ELST. Okayama Univ., Japan
c Fac. of Sci. Okayama Univ., Japan
d JASRI. 6-6-11-901 Aramaki Aoba, Aoba-ku, Sendai, Miyagi 980-8579, Japan
e JASRI. 1-1-1, Kouto, Sayo-cho, Sayo-gun, Hyogo 679-5198, Japan

P09 Current Activities of Research and Education on BL-5 (FY2024)

T. Yokoya[a,b], T. Wakita[a] and Y. Muraoka[a,b]

a Research Institute for Interdisciplinary Science, Okayama University
b Research Laboratory for Surface Science, Okayama University, Japan

-Poster Session-

The poster number with "S" is eligible for the Best Student Poster Award nomination.

P10 Photoelectron spectroscopy and local structure of the Se chain confined in single carbon nanotube

R. Nishikawa[a], K. Mimura[b], Y. Tanimoto[c], H. Sato[d], S. Islam[a], T. Miyanaga[e], and H. Ikemoto[a]

a Department of Physics, University of Toyama, Japan
b Department of Physics and Electronics, Osaka Metropolitan University, Japan
c Graduate School of Advanced Science and Engineering, Hiroshima University, Japan
d Hiroshima Research Institute for Synchrotron Radiation Science, Hiroshima University, Japan
e Department of Mathematics and Physics, Hirosaki University, Japan

P11S Observation of electronic structure of chiral magnet GdNi3Ga9 by ARPES

Y. Tanimoto[a], Y. Nakashima[a] H. Sato[b], M. Arita[b], Y. Miyai[a], K. Shimada[c], K. Tanaka[c], S. Nakamura[d], S. Ohara[d]

a Graduate School of Advanced Science and Engineering, Hiroshima University, Japan
b Hiroshima Research Institute for Synchrotron Radiation Science, Japan
c UVSOR synchrotron Facility, Institute for Molecular Science, Japan
d Graduate School of Engineering, Nagoya Institute of Technology, Japan

P12S Effects for the Electronic Structure by Oxygen Deficiency on the double-layer Cuprate High-Tc Superconductor, Bi2212

K. Kawamoto[a], H. Yamaguchi[b], Y. Miyai[b], Y. Onishi[b], M. Arita[c], K. Shimada[b,c,d,e], and S. Ideta[b,c]

a Faculty of Science, Hiroshima Univ., Japan
b Graduate School of Advanced Science and Engineering, Hiroshima Univ., Japan
c Research Institute for Synchrotron Radiation Science (HiSOR), Hiroshima Univ., Japan
d Research Institute for Semiconductor Engineering, (RISE), Hiroshima Univ., Japan
e International Institute for Sustainability with Knotted Chiral Meta Matter (WPI-SKCM2), Japan

P13S ARPES and IPES Studies for the Electronic Structure Derived by Quantum Charge Fluctuations on the Single-layer Cuprate Superconductor

Y. Onishi[a], Y. Miyai[a], Y. Tsubota[a], K. Tanaka[c], S. Ishida[d], H. Eisaki[d], H. Sato[b], M. Arita[b], K. Shimada[a,b], and S. Ideta[a,b]

a Graduate School of Advanced Science and Engineering, Hiroshima Univ., Japan
b Hiroshima Synchrotron Radiation Center (HiSOR), Hiroshima Univ., Japan
c UVSOR-Ⅲ Synchrotron, Institute for Molecular Science, Japan
d National Institute of Advanced Industrial Science and Technology (AIST), Japan

P14S Oxygen-termination effect of the spin-dependent electronic states in FeCo/Rh(001) thin film

Kaori Kunitomo[a], Kazuki Sumida[b], Koji Miyamoto[b], and Taichi Okuda[b,c,d]

a Graduate School of Advanced Science and Engineering, Hiroshima University, Japan
b Research Institute for Synchrotron Radiation Science (HiSOR), Hiroshima University, Japan
c International Institute for Sustainability with Knotted Chiral Meta Matter (WPI SKCM2) Hiroshima University, Japan
d Research Institute for Semiconductor Engineering (RISE) Hiroshima University, Japan

-Poster Session-

The poster number with "S" is eligible for the Best Student Poster Award nomination.

P15S Anisotropic Topological Surface States Induced by One-Dimensional Structure and Their Thickness Dependence

R. Yamamoto[a], Y. Fujisawa[b], K. Sumida[b], H. Sato[b], K. Miyamoto[b], and T. Okuda[b,c,d].

a Graduate School of Advanced Science and Engineering Hiroshima University, Japan
b Research Institute for Synchrotron Radiation Science (HiSOR), Hiroshima University, Japan
c International Institute for Sustainability with Knotted Chiral Meta Matter (WPI-SCKM2), Hiroshima University, Japan
d Research Institute for Semiconductor Engineering (RISE), Hiroshima University, Japan

P16S The observation of electronic structures on Pt/Fe/MgO and the design of operand sample holder

T. Asano[a], K. Sumida[b], T. Okuda[b,c,d], and K. Miyamoto[b]

a Graduate School of Advanced Science and Engineering, Hiroshima University, Japan.
b Research Institute for Synchrotron Radiation Science (HiSOR), Hiroshima University, Japan.
c International Institute for Sustainability with Knotted Chiral Meta Matter (SKCM2), Hiroshima University, Japan.
d Research Institute for Semiconductor Engineering (RISE), Hiroshima University, Japan

P17S Improving the accuracy of spin detection using lock-in techniques

Yuma Ikeo[a], Koji Miyamoto[b] , and Taichi Okuda[b,c,d]

a Faculty of Science, Hiroshima University, Japan
b Research Institute for Synchrotron Radiation Science (HiSOR), Japan
c International Institute for Sustainability with Knotted Chiral Meta Matter (WPI-SCKM2), Hiroshima University, Japan
d Research Institute for Semiconductor Engineering (RISE), Hiroshima University, Japan

P18S Structural Dynamics of α1-Acid Glycoprotein in the Membrane Interaction Revealed by Time-Resolved Vacuum-Ultraviolet Circular Dichroism

Satoshi Hashimoto[a] and Koichi Matsuo[a,b,c]

a Graduate School of Advanced Science and Engineering, Hiroshima University, Japan
b Research Institute for Synchrotron Radiation Science, Hiroshima University, Japan
c International Institute for Sustainability with Knotted Chiral Meta Matter (WPI-SKCM2), Hiroshima University, Japan

P19S Structural Dynamics of β-Lactoglobulin in the Interaction Processes with Sodium Dodecyl Sulfate Micelles Observed by Time-Resolved Vacuum-Ultraviolet Circular Dichroism

Satoshi Hashimoto[a] and Koichi Matsuo[a,b,c]

a Graduate School of Advanced Science and Engineering, Hiroshima University, Japan
b Research Institute for Synchrotron Radiation Science, Hiroshima University, Japan
c International Institute for Sustainability with Knotted Chiral Meta Matter (WPI-SKCM2), Hiroshima University, Japan

P20S Development of a Vertical Circular Dichroism Apparatus for Measuring Aggregated Biomolecules

Aoyama Kuya[a], Imaura Ryota[a], Hashimoto Satoshi[a], Haga Tastuki[a], Mohamed Ibrahim[b], Matsuo Koichi[a,b]

a Graduate School of Advanced Science and Engineering, Hiroshima University, Japan
b Research Institute for Synchrotron Radiation Science, Hiroshima University, Japan

-Poster Session-

The poster number with "S" is eligible for the Best Student Poster Award nomination.

P21 Monitoring the Self-Assembly of Alginate Induced by Calcium Ions Using Circular Dichroism

Tatsuki Haga[a], Masaya Yoshid[a], Takeharu Haino[a], Koichi Matsuo[b] and Mohamed I.A. Ibrahim[b]

a Graduate School of Advanced Science and Engineering, Hiroshima University.
b Research Institute for Synchrotron Radiation Science (HiSOR), Hiroshima University, Japan.

P22S Optical Activity Emergence of Amino-acid Films under Circularly Polarized Lyman-α Light Irradiation

Gen Fujimori[a,b], Masahiro Kobayashi[c], Jun-ichi Takahashi[d], Hiroshi Ota[e,f], Koichi Matsuo[g], Yoshitaka Taira[e], Masahiro Katoh[e,g], Kensei Kobayashi[a,b], Yoko Kebukawa[b], Hiroaki Nakamura[c]

a Yokohama National University, Japan
b Institute of Science Tokyo, Japan
c National Institute for Fusion Science, Japan
d Kobe University, Japan
e UVSOR Synchrotron Facility, Japan
f Japan Synchrotron Radiation Research Institute, Japan
g Research Institute for Synchrotron Radiation Science, Japan

P23S Determination of organic molecular film thickness on gold substrates using soft X-ray photoelectron spectroscopy

Shogo Tendo[a], Kakuto Yoshioka[a], Akinobu Niozu[b], Shohei Asakura[a], Yuri Ohura[a], and Shin-ichi Wada[a,c]

a Graduate School of Advanced Science and Engineering, Hiroshima University, Japan
b Graduate School of Humanities and Social Sciences, Hiroshima University, Japan
c Research Institute for Synchrotron Radiation Science, Hiroshima University, Japan

P24S DFT calculations for NEXAFS analysis measured for organic molecules

Shohei Asakura[a], Hashimoto Genki[b], Ohura Yuri[a], Shogo Tendo[a], Kakuto Yoshioka[a], Akinobu Niozu[c], and Wada Shin-ichi[a,b,d]

a Faculty of Science, Hiroshima University, Japan
b Graduate School of Science and Engineering, Hiroshima University, Japan
c Graduate School of Humanities and Social Sciences, Hiroshima University, Japan
d Research Institute for Synchrotron Radiation Science, Hiroshima University, Japan

P25S Fluorine substitution dependence of ultrafast electron transport in biphenyl monolayers induced by resonant core-excitations

Hayate Inoue[a], Kakuto Yoshioka[b], Shohei Asakura[b], Yuri Ohura[b], Shogo Tendo[b], Akinobu Niozu[c], and Shin-ichi Wada[a,b,d]

a School of Science, Hiroshima University, Japan
b Graduate School of Advanced Science and Engineering, Hiroshima University, Japan
c Graduate School of Humanities and Social Sciences, Hiroshima University, Japan
d Research Institute for Synchrotron Radiation Science, Hiroshima University, Japan

P26 Structural analysis of Co/h-BN/Ni(111) using low-energy electron diffraction

Shen Zili[a] and Masahiro Sawada[b]

a Graduate School of Advanced Science and Engineering, Hiroshima University
b Research Institute for Synchrotron Radiation Science, Hiroshima University

P27 Magnetic and Transport Properties of Thin Films of MnTe Altermagnet Candidate

H.Sato[a] and Y.Fujisawa[b]

a Faculty of Science, hiroshima University
b HiSOR

-Poster Session-

The poster number with "S" is eligible for the Best Student Poster Award nomination.

P28S Activity and Characteristics of Ni-Based Hybrid Catalysts with Promoters for Ammonia Methanation

Reiji Sunamoto[a], Hiroki Miyaoka[a], Takayuki Ichikawa[a] and Hitoshi Saima[a]
a Hiroshima University, Japan

P29 Experimental Study on Single Electron Storage in 2024

Y. Asai[a], M. Shimada[b,c], H. Miyauchi[b,c] and M. Katoh[c,d]
a Graduate School of Advanced Science and Engineering Hiroshima University, Japan
b High Energy Accelerator Research Organization (KEK), Japan
c Research Institute for Synchrotron Radiation Science, Hiroshima University,
d UVSOR Synchrotron Facility, Japan

P30 Application of Machine Learning to Accelerator Beam Transport Systems

R. Sakurai[a],M. Shimada[a,b] , H. Miyauchi[a,b] , T. Obina[b] and M. Katoh[a,b,c,d]
a Faculty of Science, Hiroshima University, Japan
b High Energy Accelerator Research Organization (KEK), Japan
c Research Institute for Synchrotron Radiation Science, Hiroshima University
d UVSOR Synchrotron Facility, Japan

P31S Observing Electronic Dynamics within 100 fs in 2H-MoTe2 by Double-excitation Ultrafast Electron Diffraction

Yui Iwasaki[a], Gaël Privault[a], Haruki Taira[a], Ryota Nishimori[a], Takumi Fukuda[b], Muneaki Hase[a], Yusuke Arashida[a], and Masaki Hada[a]
a University of Tsukuba, Japan
b Okinawa Institute of Science and Technology, Japan

P32S Direct Measurement of Compressed Electron Pulse Duration through the Interaction with Terahertz Waves

Haruki Taira[a], Ryota Nishimori[a], Kaito En-ya[a], Godai Noyama[a], Gael Privault[a], Yusuke Arasida[a], Kou Takubo[b], Sin-ya Koshihara[b], Shoji Yoshida[a]
and Masaki Hada[a]
a University of Tsukuba, Japan
b Institute of Science Tokyo, Japan

P33S Hydration structure of inorganic salt solutions at various concentrations: A molecular dynamics approach

Ayana Sato[a], Nanami Shima[b], Osamu Takahashi[c]
a Department of Chemistry, Faculty of Science, Hiroshima Univ.
b Chemistry Program, Graduate School of Advanced Science and Engineering, Hiroshima Univ.
c Research Institute for Synchrotron Radiation Science, Hiroshima Univ.

P34S Concentration dependence of mixtures of water and 3-methylpyridine using MD simulations

Kouki Ozeki[a] and Osamu Takahashi[b]
a Department of Chemistry, Faculty of Science, Hiroshima Univ.
b Research Institute for Synchrotron Radiation Science, Hiroshima Univ

P35S Structure of maleic and succinic acid in aqueous solution by soft X-ray absorption spectroscopy

Risa Okada[a] and Ryosuke Yamamura[a] and Osamu Takahashi[b]
a Graduate School of Advanced Science and Engineering, Hiroshima University, Japan
b Research Institute for Synchrotron Radiation Science, Hiroshima University, Japan

-Poster Session-

The poster number with "S" is eligible for the Best Student Poster Award nomination.

P36S Theoretical calculations of resonant inelastic soft X-ray scattering based on semi-classical approximation -Application to methanol-

Hikari Sato[a] and Osamu Takahashi[b]
a Department of Chemistry, Faculty of Science, Hiroshima Univ.
b Research Institute for Synchrotron Radiation Science, Hiroshima Univ.

P37S Improvement of the calculation method for X-ray Emission Spectroscopy based on Slater's transition state theory

Yuika Watari[a] and Osamu Takahashi[b]
a Graduate School of Advanced Science and Engineering, Hiroshima Univ.
b Research Institute for Synchrotron Radiation Science, Hiroshima Univ.

24AG042 BL-1

Angle-resolved photoemission spectroscopy of Dirac nodal-line superconductor $ZrSi_{1-x}P_xSe$

K. Ideura[a], Y. Nishioka[a], K. Kuroda[a,b,c], A. Ino[d,e], Y. Miyai[a], S. Ideta[a,d], K. Shimada[a,c,d], H. Kito[f], I. Hase[f], S. Ishida[f], H. Fujihisa[f], Y. Gotoh[f], Y. Yoshida[f], A. Iyo[f], H. Ogino[f], H. Eisaki[f], K. Kawashima[f,g], A. Kimura[a,b,c]

[a]*Graduate School of Advanced Science and Engineering, Hiroshima University, Higashi-Hiroshima 739-8526, Japan*
[b]*International Institute for Sustainability with Knotted Chiral Meta Matter (WPI-SKCM²), Higashi-Hiroshima 739-8526, Japan*
[c]*Research Institute for Semiconductor Engineering, Higashi-Hiroshima 739-8527, Japan*
[d]*Research Institute for Synchrotron Radiation Science, Hiroshima University, Higashi-Hiroshima 739-0046, Japan*
[e]*Kurume Institute of Technology, Kurume 830-0052, Japan*
[f]*National Institute of Advanced Industrial Science and Technology (AIST), Tsukuba 305-8568, Japan*
[g]*IMRA JAPAN Co., Ltd., Kariya 448-8650, Japan*

Keywords: Superconductor, Dirac line node, Angle resolved photoemission spectroscopy

Recently, Dirac line node (DLN) has been observed in the superconductor ZrPSe, which belongs to the nonsymmorphic space group, with the P square lattice as the glide plane, forming at E-EF = -1.2 eV [1,2]. On the other hand, the Dirac semimetal ZrSiSe with the glide plane as Si does not exhibit superconductivity, and its DLN is located near the Fermi level [3]. This indicates that the substitution of P with Si causes the emergence of superconductivity and the change in the electronic structure. Therefore, by observing the evolution of the electronic structure with x in the mixed crystal $ZrSi_{1-x}P_xSe$, it is expected that the mechanism of superconductivity in ZrPSe will be elucidated. In this study, we performed angle-resolved photoemission spectroscopy (ARPES) on single crystal samples of $ZrSi_{1-x}P_xSe$ (x = 0.2, 0.45, 0.72, 1) to directly observe the electronic structure.

Figure 1 (a) shows the Fermi surface at x = 0.72. Electron pockets at the Γ point and point, as well as two large Fermi surfaces (α, β), were observed. As the energy moves away from the Fermi energy, the α and β approach each other and form a diamond shaped DLN at -1.15 eV. On the other hand, the Fermi surface at x = 0.2 shown in Figure 1 (b) has no electron pockets, and the α and β approached each other, and a DLN is formed at -0.2 eV. This observation indicates that the energy of the DLN changes continuously with the change in the substitution amount.

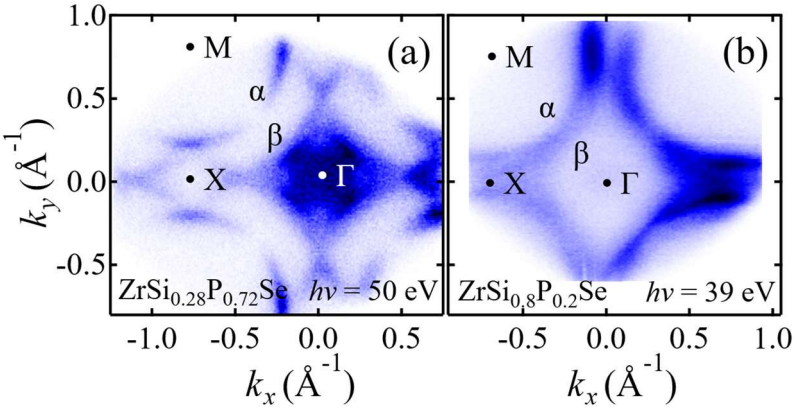

Figure 1: Fermi surface of $ZrSi_{1-x}P_xSe$, (a) x = 0.72 ($h\nu$ = 50 eV), (b) x = 0.2 ($h\nu$ = 39 eV)

In addition, the electron occupancy was determined from the area of the Fermi surface. For all Fermi surfaces (α, β, γ, ε), the electron occupancy increases as the amount of P increases. In particular, the increase is large for the α and β and small for the γ and ε. The total electron occupancy also increases with the amount of P . This means that the amount of change in the α and β accounts for most of the total change. This suggests that the P substitution introduces electrons into the DLN derived from the square lattice.

REFERENCES

1. H. Kito *et al*., J. Phys. Soc. Jpn. **83**, 074713 (2014).
2. S. Ishizaka *et al*., Phys. Rev. B **105**, L121103 (2022).
3. G. Gatti *et al*., Phys. Rev. Lett. **125**, 076401 (2020).

22AU002 BL-1 (HiSOR)

Electronic states in superconducting type-II Dirac semimetal: 1T-PdSeTe

Yogendra Kumar[1], Shiv Kumar[2], Yenugonda Venkateswara[3,4], Ryohei Oishi[1], Jayata Nayak[4], R.P. Singh [6], Takahiro Onimaru[1], Yasuyuki Shimura [1], Chaoyu Chen[5], Shinichiro Ideta[2], Kenya Shimada[2,7,8]

[1]Graduate School of Advanced Science and Engineering, Hiroshima University, Higashi-Hiroshima 739-8526, Japan
[2]Research Institute for Synchrotron Radiation Science (HiSOR), Hiroshima University, Higashi-Hiroshima 739-0046, Japan
[3]Department of Physics, SUNY Buffalo State University, Buffalo, New York 14222, USA
[4]Department of Physics, Indian Institute of Technology, Kanpur 208016, India
[5]Songshan Lake Materials Laboratory, Dongguan 523808, China
[6]Department of Physics, Indian Institute of Science Education and Research, Bhopal 462066, India
[7]The International Institute for Sustainability with Knotted Chiral Meta Matter (WPI-SKCM2), Hiroshima University, Higashi-Hiroshima 739-8526, Japan
[8]Research Institute for Semiconductor Engineering (RISE), Hiroshima University, Higashi-Hiroshima 739-8527, Japan

Keywords: Electronic structure, First-principles calculations, Spin-orbit, coupling, Dirac/Weyl semimetal, Superconductivity, Surface states, Topological materials, Topological superconductor.

Recently topological semimetals have attracted much interest for their non-trivial band structures [1-3] that can be categorized into Dirac semimetals (DSMs), Weyl semimetals (WSMs), and topological nodal-line semimetals based on their band crossing characteristics near the Fermi level [4]. Layered transition metal chalcogenides, found among DSMs and WSMs, are notable for their diverse physical properties like superconductivity and charge density wave (CDW), with promising applications [5].

We synthesized high-quality single crystals of the superconducting type-II Dirac semimetal 1T-PdSeTe using a two-step melting method and characterized their crystal quality via XRD, EPMA, and cross-sectional S-TEM with EDX. Scanning transmission electron microscopy confirmed a homogeneously mixed Se/Te distribution within the CdI_2-type lattice. Angle-resolved photoemission spectroscopy (ARPES) at HiSOR BL-1 and UVSOR BL5U beamlines, along with density functional theory (DFT) calculations using ordered/disordered supercell and slab models, revealed topological surface states, a surface Dirac cone, and a type-II bulk Dirac-like crossing along the Γ–A direction.

Compared to 1T-$PdTe_2$ (Tc = 1.6 K), PdSeTe exhibited an enhanced superconducting transition temperature (Tc = 3.2 K), likely due to chemical pressure effects rather than atomic disorder. The persistence of electronic band dispersion and local structures upon substitution suggests that the CdI_2-type lattice symmetry governs the band structure. These findings provide insights into the role of solid solutions in modifying surface and bulk electronic states and enhancing superconductivity in Dirac semimetals.

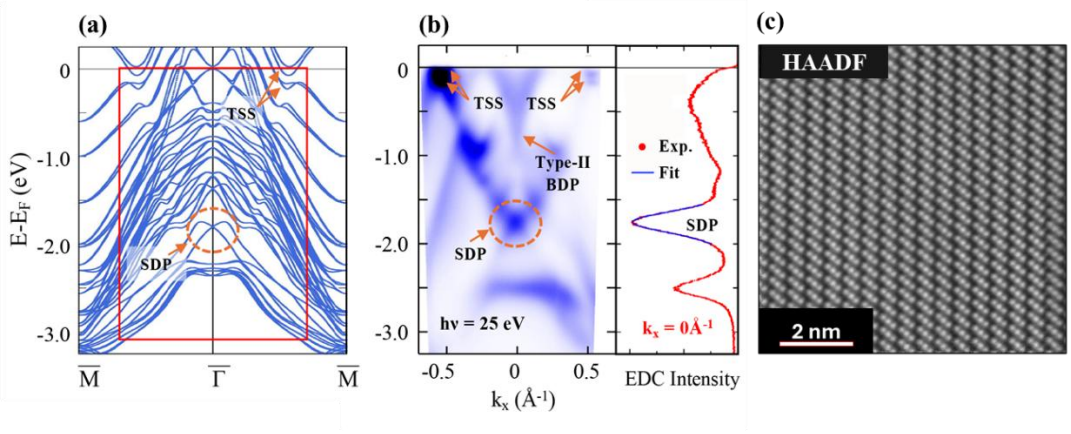

Fig. 1: (a) and (b) represent the simulated bands for slab (5 atomic layers) and measured ARPES spectrum along $\bar{M} - \bar{\Gamma} - \bar{M}$ direction with 25eV photon energy at 20K, respectively. (c) High-resolution STEM, High angle annular dark field (HAADF) image of the (100) plane of a 1T-PdSeTe crystal.

REFERENCES

1. M.Z. Hasan, C.L. Kane, Reviews of Modern Physics **82**, 3045-3067 (2010).
2. X.-L. Qi, S.-C. Zhang, Reviews of Modern Physics **83**, 1057-1110 (2011).
3. Y. Xia et al., Nature Physics **5**, 398-402 (2009).
4. B. Yan, C. Felser, Annual Review of Condensed Matter Physics **8**, 337-354 (2017).
5. K. Kim, *et al.*, PRB **97**, 165102 (2018).

Developments of ARPES Studies at HiSOR BL-1: Towards HiSOR-II Projects II

Shin-ichiro Ideta[a,b], Masashi Arita[a], Yudai Miyai[b], Yogendra Kumar[b], and Kenya Shimada[a,b,c,d]

[a] *Research Institute for Synchrotron Radiation Science (HiSOR), Hiroshima Univ., Higashi-Hiroshima 739-0046, Japan*

[b] *Graduate School of Advanced Science and Engineering, Hiroshima Univ., Higashi-Hiroshima 739-8526, Japan*

[c] *Research Institute for Semiconductor Engineering, (RISE), Hiroshima Univ., Higashi-Hiroshima 739-8527, Japan*

[d] *International Institute for Sustainability with Knotted Chiral Meta Matter (WPI-SKCM [2]), Higashi-Hiroshima 739-8526, Japan*

Keywords: Superconductivity, Cuprate, ARPES, Electronic structure.

The Hiroshima Institute for Synchrotron Radiation Science (HiSOR) is the synchrotron radiation facility established at Hiroshima University. A compact 700 MeV electron-storage ring produces synchrotron radiation in the ultraviolet (VUV) and soft x-ray range. Tunable photon energy in this range is indispensable and valuable for studying the fine electronic structures of novel materials such as superconductors, topological insulators, and Weyl semimetals, etc., employing high-resolution angle-resolved photoemission spectroscopy (APRES).

Recently, to perform surface mapping in synchrotron radiation, based on the research and developments, we have reduced the beam size of the synchrotron radiation by using a focusing mirror, and to perform detailed measurements by improving the accuracy of the manipulator system. In BL-1 (high-resolution ARPES beamline), the beam size of the synchrotron radiation is reduced by order of magnitude (beam size: ~70-100 μm). In addition, we have redesigned the sample holder for common use following the new installation of analyzers.

In this poster, we will show the details of recent developments in HiSOR beamline (BL-1) towards the HiSOR-II projects.

24BG005 BL-1, BL-7, BL-9A

ARPES study of Fe_xTiS_2 ($x = 0 \leq x \leq 0.33$)

K. Kimura[a], Y. Nakashima[b], Y. Tanimoto[b], H. Sato[c], M. Arita[c], Y. Miyai[b], S. Ideta[c], K. Shimada[c], T. Bizen[d], M. Miyata[e], M. Koyano[d]

[a]*Faculty of Science, Hiroshima University, Higashi-Hiroshima 739-8526, Japan*
[b]*Graduate School of Advanced Science and Engineering, Hiroshima University, Higashi-Hiroshima 739-8526, Japan*
[c]*Hiroshima Research Institute for Synchrotron Radiation Science, Hiroshima University, Higashi-Hiroshima 739-0046, Japan*
[d]*School of Materials Science, Japan Advanced Institute of Science and Technology, Nomi 923-1292, Japan*
[e]*Global Zero Emission Research Center, National Institute of Advanced Industrial Science and Technology, Tsukuba, Ibaraki 305-8569, Japan*

Keywords: intercalation, superlattice, angle resolved photoemission spectroscopy

1*T*-TiS_2 is non-magnetic layered material with 1*T*-CdI_2-type crystal structure. The hexagonal layer of Ti ions is sandwiched between the two hexagonal layers of S ions and the Ti ion is octahedrally coordinated with six S ions. The S-Ti-S triple layers are covalently bonded and these TiS_2 triple layers are weakly coupled with van der Waals (vdW) force. In the vdW gap located between the TiS_2 layers, the other 3*d* transition-metal *M* can be intercalated as M_xTiS_2. Among them, Fe_xTiS_2 exhibits a wide variety of magnetic properties [1]. With increasing the Fe concentration from $x = 0$, the cluster spin grass (CG) state with the Ising spins is found for $x < 0.20$. After exhibiting the antiferromagnetic (AFM) state from $x = 0.20$ to 0.28, the CG state is again realized for $0.28 < x < 0.38$ and the AFM state for $0.38 < x < 0.50$. Above $x = 0.50$, the ferrimagnetic behavior is observed. On the other hand, the Fe ion intercalated in the vdW gap between the TiS_2 layers occupy the octahedral site surrounded by six S ions. X-ray studies reveal the Fe random distribution for $x < 0.20$, while the formation of $2\sqrt{3}a \times 2a \times 2c$ superlattices due to the Fe ordering for $x = 0.25$ and $\sqrt{3}a \times \sqrt{3}a \times 2c$ superlattice for $x = 0.33$. The rich magnetic states of Fe_xTiS_2 are expected to link to the change in electronic band structure due to the Fe intercalation. In this study, we carried out angle-resolved photoemission spectroscopy (ARPES) to reveal the electronic band structure of Fe_xTiS_2 ($0 \leq x \leq 0.33$) at beamlines BL-1, BL-7 and BL-9A of Hiroshima Research Institute for Synchrotron Radiation Science (HiSOR).

Figures 1(a), (b) and (c) shows the ARPES intensity plots of TiS_2, $Fe_{0.25}TiS_2$ and $Fe_{0.33}TiS_2$, respectively, measured at $h\nu$=66 eV along the $\bar{\Gamma}$-$\bar{M}$ directions of the surface Brillouin zone, roughly corresponding to Γ-M direction of the bulk Brillouin zone, estimated from the $h\nu$-dependent measurements. The ARPES spectra were taken at 20 K and with *p*-polarized geometry. For TiS_2 in Fig. 1(a), we find an electron pocket derived from the Ti 3*d* states around the M point, which is resonantly enhanced in intensity around the Ti 3*p*-3*d* absorption region. Almost non-dispersive band is observed just below the electron pocket, which is assigned to the localized 3*d* states of the Ti ions self-intercalated in the vdW gap between TiS_2 layers. The electron pocket is hardly observed in the ARPES spectra with *s*-polarized geometry (not shown here), suggesting that it comes from the Ti $3d_{z^2}$ component. The parabolic band around the Γ point is due to the S 3*p* states.

The electron pocket around the M point is shifted to higher binding energy on going from TiS_2 (Fig. 1(a)) to $Fe_{0.25}TiS_2$ (Fig. 1(b)) and further to $Fe_{0.33}TiS_2$ (Fig. 1(c)) and as the results it becomes large. In addition, the parabolic S 3*p* band also becomes deeper with increasing the Fe concentration. These results indicate that electrons are transferred from the intercalated Fe ions to host TiS_2 layers. The dispersive Fe 3*d*-derived band is observed around $E_B = 0.4$ eV for $Fe_{0.25}TiS_2$ and $Fe_{0.33}TiS_2$ as shown by dashed lines in Figs. 1(b) and 1(c), reflecting the Fe ions align periodically in the vdW gap parallel to the TiS_2 layers (in plane). The periodicity of the Fe 3*d* band for $Fe_{0.25}TiS_2$ becomes half of that of $\bar{\Gamma}$-$\bar{M}$-$\bar{\Gamma}$ for TiS_2, reflecting the $2\sqrt{3}a \times 2a$ periodicity in plane for $x = 0.25$. The periodicity of the Fe 3*d* band becomes long for $Fe_{0.33}TiS_2$, which is qualitatively understood from the shorter $\sqrt{3}a \times \sqrt{3}a$ periodicity in plane for $x = 0.33$. In addition, the Fe 3*d* band is more dispersive for $Fe_{0.33}TiS_2$. On the other hand, the Fe 3*d* band is almost flat for $Fe_{0.10}TiS_2$ and

$Fe_{0.15}TiS_2$, indicating that the Fe 3*d* states almost localized due to the random distribution of the Fe ions.

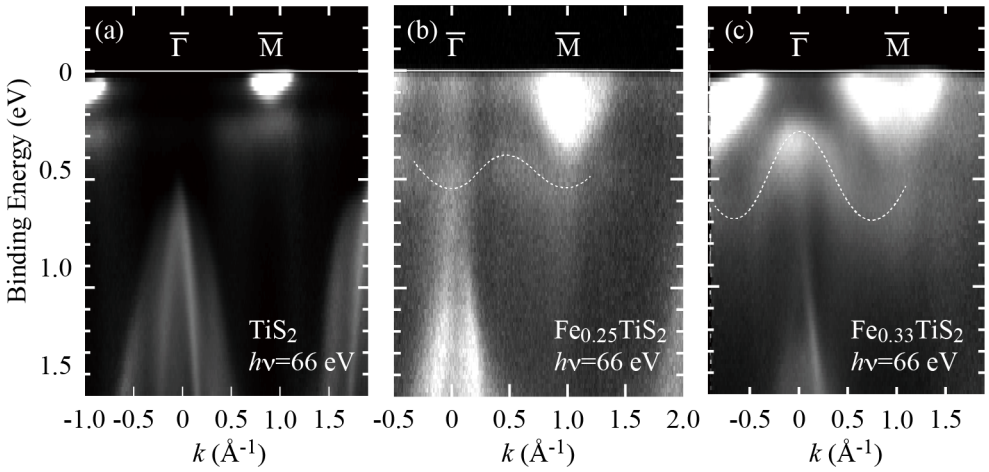

FIGURE 1. ARPES intensity plots of (a) TiS_2, (b) $Fe_{0.25}TiS_2$ and (c) $Fe_{0.33}TiS_2$ measured at $h\nu = 66$ eV along $\bar{\Gamma}$-$\bar{M}$ direction. Dashed lines in (b) and (c) are guide for the eye for the Fe 3*d* band.

We measured the ARPES spectra of TiS_2, $Fe_{0.25}TiS_2$ and $Fe_{0.33}TiS_2$ along the Γ-A direction with changing *hv* from 30 to 124 eV at 20 K with *p*-polarized geometry. We find that the Fe 3*d* bands for $Fe_{0.25}TiS_2$ and $Fe_{0.33}TiS_2$ exhibit the dispersion along the direction normal to the TiS_2 layers and has half period of the S 3*p* band, reflecting the 2*c* periodicity for $x = 0.25$ and 0.33.

REFERENCES

1. N. V. Selezneva, E. M. Sherokalova, A. Podlesnyak, M. Frontzek and N. V. Baranov, Phys. Rev. Mater. **7**, 014401 (2023).

20AU018, 22AG005, 22BG004 BL-1, BL-9A

Temperature dependence of the coupling parameter in the strange metal state of heavily overdoped cuprate superconductor

Y. Miyai[a], S. Ideta[b], M. Arita[b], K. Tanaka[c], M. Oda[d], T. Kurosawa[e] and K. Shimada[b,f,g]

[a] *Graduate School of Advanced Science and Engineering, Hiroshima University, Higashi-Hiroshima 739-8526, Japan*
[b] *Hiroshima Synchrotron Radiation Center, Hiroshima University, Higashi-Hiroshima 739-8526, Japan*
[c] *UVSOR-III Synchrotron, Institute for Molecular Science, Okazaki 444-8585, Japan*
[d] *Department of Physics, Hokkaido University, Sapporo 060-0809, Japan*
[e] *Faculty of Science and Engineering, Muroran Institute of Technology, Muroran 050-8585, Japan*
[e] *Research Institute for Semiconductor Engineering (RISE), Hiroshima University, Higashi-Hiroshima 739-8527, Japan*
[g] *The International Institute for Sustainability with Knotted Chiral Meta Matter (WPI-SKCM^2), Hiroshima University, Higashi-Hiroshima 739-8526, Japan*

Keywords: High-T_c superconductor, ARPES

Since the discovery of high-transition-temperature (T_c) superconductivity in cuprates, unusual physical properties due to strong correlations in the underdoped to the optimally-doped region including the metal-insulator transition [1], pseudogap state, spin and charge ordering [2,3], have attracted much interest and extensive studies have been done to elucidate their correlation to the mechanism of the high- T_c. In contrast, the electronic states in the overdoped region have been regarded as the Fermi liquid. However, non-Fermi liquid like behaviors such as the strange metal state [4], ferromagnetic fluctuation [5], and charge order [6], have been discovered in the overdoped region, renewing scientific interests of cuprate superconductors.

These physical properties originate from many-body interactions arising from the complex entanglement of the internal degrees of freedom of spin, charge, lattice, and orbital, and their contributions are reflected in the self-energy. In this study, we have investigated the distinct energy scales in the self-energy, namely low-energy kink (LEK) and high-energy anomaly (HEA), in heavily overdoped Bi-based high-T_c cuprates, $(Bi,Pb)_2Sr_2CuO_{6+\delta}$ (Pb-Bi2201) using high-resolution angle-resolved photoemission spectroscopy (ARPES).

We experimentally extracted the self-energy (Σ_{tot}) based on the Kramers-Kronigh relation. By introducing the model function, we successfully reproduced the self-energy responsible for the HEA (Σ_{HEA}) and extracted the self-energy responsible for the LEK (Σ_{LEK}) by subtracting Σ_{HEA} from Σ_{tot}. Figure 1(b) shows the temperature dependence of the coupling parameter, $\lambda(T)$, determined from the gradient of the real part of the self-energy at the Fermi level, as shown in Fig.1(a). One can see that $\lambda_{\mathrm{tot}} \sim 1$ at 300 K, indicating that the normal state is strongly correlated. Since Σ_{HEA} is dominant at 300 K, Σ_{HEA} should correspond to the self-energy in the strange metal state. On the other hand, we found that $\lambda_{\mathrm{LEK}}(T) = \lambda_{\mathrm{tot}}(T) - \lambda_{\mathrm{HEA}}$ deviates from the theoretical calculation based on the temperature-independent Eliashberg function of the electron-phonon interaction [7], revealing that the LEK is remarkably enhanced at low temperatures. It suggests an unexplored mechanism to enhance the coupling parameter emerging from entangled many-body interactions. Our results give insight into the unusual strange metal state as well as the

origin of the exotic superconductivity in cuprates.

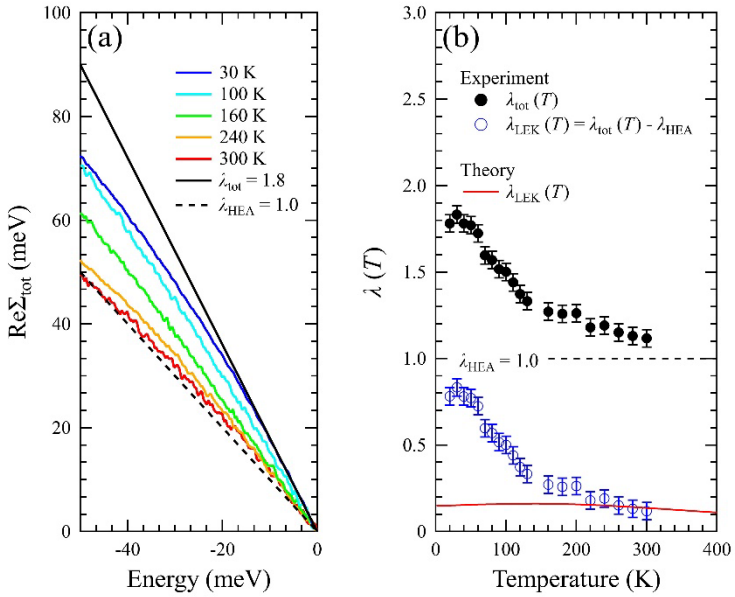

Figure 1 (a) The real part of the self-energy, $\mathrm{Re}\Sigma_{\mathrm{tot}}(\omega)$, for some representative temperatures. Black solid line indicates the magnitude of the coupling parameter calculated from $\mathrm{Re}\Sigma_{\mathrm{tot}}(\omega)$ at 300 K, while the black dashed line corresponds to the real part of the model self-energy for HEA, $\mathrm{Re}\Sigma_{\mathrm{HEA}}(\omega)$. (b) The temperature dependence of the coupling parameter. Black and blue dots indicate the total coupling parameter, $\lambda_{\mathrm{tot}}(T)$, and the coupling parameter for the LEK, $\lambda_{\mathrm{LEK}}(T) = \lambda_{\mathrm{tot}}(T) - \lambda_{\mathrm{HEA}}$, respectively, where λ_{HEA} denotes the coupling parameter for the HEA (black dashed line). The red curve shows the theoretical temperature dependence of the coupling parameter for LEK using the Eliashberg function in Ref.[7].

1. M. Imada *et al*., *Reviews of Modern Physics* **70**, 1039 (1998).
2. A. Damascelli *et al*., *Reviews of Modern Physics* **75**, 473 (2003).
3. J. A. Sobota *et al., Reviews of Modern Physics* **93**, 025006 (2021).
4. J. Ayres *et al*., *Nature* **595**, 661-666 (2021).
5. K. Kurashima *et al*., *Physical Review Letters* **121**, 057002 (2018).
6. Y. Y. Peng *et al*., *Nature Materials* **17**, 697 (2018).
7. W. Meeasana, *et al*., *Physical Review Letters* **96**, 157003 (2006).

23BG012 BL-1,9A

Unraveling the Electronic Structure of Altermagnetic MnTe via Photoemission Spectroscopy

Kazi Golam Martuza[a], Yogendra Kumar[a], Shiv Kumar[b,c], Shin-ichiro Ideta[b] and Kenya Shimada[b,d,e]

[a]*Graduate School of Advanced Science and Engineering, Hiroshima University, Japan 739-0046*

[b]*Research Institute for Synchrotron Radiation Science (HiSOR), Hiroshima University 739-0046, Japan*

[c]*Institute of Microelectronics, Agency for Science, Technology and Research (A*STAR), Singapore*

[d]*International Institute for Sustainability with Knotted Chiral Meta Matter (WPI-SKCM^2), Hiroshima University, Higashi-Hiroshima 739-0046, Japan*

[e]*Research Institute for Semiconductor Engineering (RISE), Hiroshima University, Higashi-Hiroshima 739-8527, Japan*

Keywords: MnTe, altermagnet, electronic structure, ARPES, RPES

Despite having zero net magnetization, the recently discovered alternmagnetism exhibits spin splitting in the momentum space and has attracted a lot of attention due to its unique magnetic characteristics and possible uses [1]. Antiferromagnetic semiconductor MnTe with the hexagonal NiAs-type structure has garnered a lot of interest lately as a typical altermagnet [2–5].

Using polarization-dependent angle-resolved photoemission spectroscopy (ARPES), we have examined the electronic band structure of bulk single-crystalline hexagonal MnTe (0001). MnTe single crystals were synthesized using a solid-state reaction technique and we cut out the (0001) plane of the single crystal. The samples went through multiple cycles of sputtering at 2 kV and 1.5 kV beam energy, followed by annealing at 400°C to provide a clean surface appropriate for ARPES measurements. Surface cleanliness was verified via Auger electron spectroscopy, and the crystalline surface order was confirmed by the presence of sharp hexagonal diffraction patterns in low-energy electron diffraction (LEED) measurements.

The polarization-dependent ARPES measurements were conducted at HiSOR BL-9A using an ASTRAIOS electron analyzer at the photon energy of 40 eV and the sample temperature of 200 K. The polarization direction of the incident light was set by adjusting the undulator magnet configuration. Figures 1(a) and 1(b) present the ARPES intensity maps near the chemical potential in the k_x-k_y plane, acquired using s- and p-polarization geometries, respectively. Although MnTe is a semiconductor, intrinsic hole doping shifts the chemical potential close to the top of the valence band. The enhanced photoemission intensity observed under s-polarization indicates that the electron wave functions exhibit odd symmetry with respect to the mirror plane, suggesting that the observed valence bands primarily arise from Mn $3d_{xy}$, Mn $3d_{yz}$, and Te $5p_y$ orbitals. The spectral intensity is strong around the $\bar{\Gamma}$ point and the ARPES intensity map along the $\overline{\Gamma K}$ direction in Fig. 1(c) reveals the presence of hole-like bands, consistent with theoretical predictions of the band structure [5,6]. The ARPES intensity mapping at the chemical potential in Fig. 1(a) is compatible with the hexagonal (0001) surface.

Figure 2 shows the resonance photoemission spectroscopy (RPES) of MnTe in the Mn 3p-3d excitation region taken at HiSOR BL-1 with changing photon energies from 43 eV up to 59 eV. The Mn 3d-derived spectral intensity is enhanced taken around 51 eV (on-resonance) and is suppressed taken around 47 eV (off-resonance), which is consistent with previous results on polycrystalline MnTe [7]. The leading peak at ~ -3 eV is derived from Mn 3d and the broad peak at ~8 eV is charge transfer satellite originated from strong electron correlation [7].

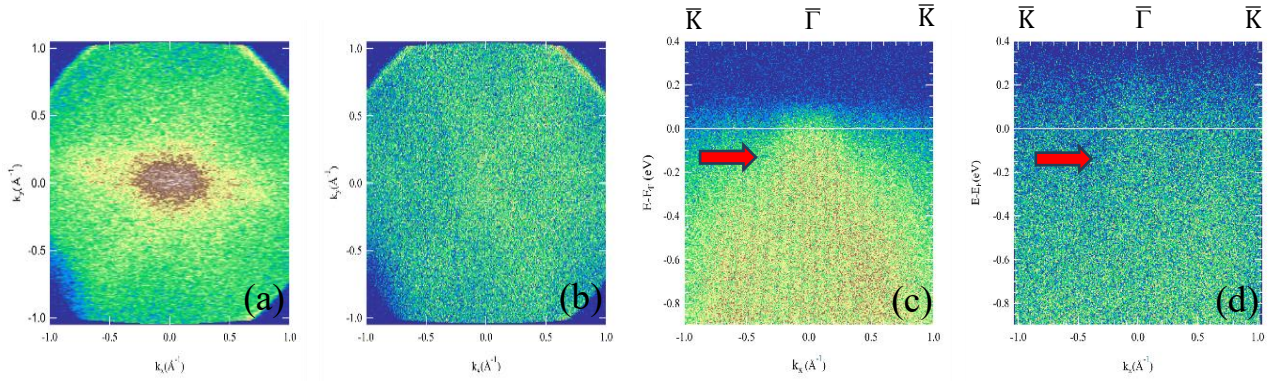

FIGURE 1. High-resolution ARPES results on MnTe (0001) single crystal taken at 200K and hν=40 eV. k_x-k_y mapping at the chemical potential with the s-polarization (a) and p-polarization (b) geometries. ARPES intensity map along the $\overline{\Gamma}\overline{K}$ high symmetry line with the s-polarization (c) and p-polarization (d) geometries.

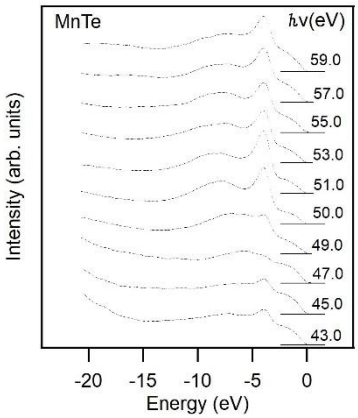

FIGURE 2: The RPES spectrum of MnTe in the Mn 3p-3d excitation region measured at 43-59 eV photon energy.

REFERENCES

[1] S. Lee et al., *Phys. Rev. Lett.,* 2024, 132, 036702.
[2] S. Mu et al., *Phys Rev Mater.,* 2019, 3, 025403.
[3] De Melo et al., *Journal of Crystal Growth*, 1991, 110, 445-451.
[4] H. Sato et al*., Journal of Magnetism and Magnetic Materials*, 1995, 140-144, 153-154.
[5] P. E. Faria Junior et al*., Phys. Rev. B*, 2023, 107, L100417.
[6] S. J. Youn et al., *Physica Status Solidi (B),* 2004, 241, 1411–1414.
[7] M. Taniguchi, et. al., *Journal of Electron Spectroscopy and Related Phenomena* 124(2-3), 2002, 107-125.

24AG037 BL-1, IPES

Comprehensive Study of Electronic States Induced by Quantum Charge Fluctuations in Electron-doped High-T_c Cuprate Superconductors

H. Yamaguchi[a], Y. Onishi[a], Y. Miyai[a], M. Atira[b], H. Sato[a,b], D. Song[f], K. Tanaka[e], K. Shimada[a,b,c,d], S. Ideta[a,b]

[a]*Graduate School of Advanced Science and Engineering, Hiroshima Univ., Higashi-Hiroshima 739-0046, Japan*
[b]*Hiroshima Synchrotron Radiation Center (HiSOR), Hiroshima Univ., Higashi-Hiroshima 739-0046, Japan*
[c]*Research Institute for Semiconductor Engineering, (RISE), Hiroshima Univ., Higashi-Hiroshima 739-8527, Japan*
[d]*International Institute for Sustainability with Knotted Chiral Meta Matter (WPI-SKCM^2), Higashi-Hiroshima 739-8526, Japan*
[e]*UVSOR-III Synchrotron, Institute for Molecular Science., Okazaki, Aichi 444-8585, Japan fStewart*
[f]*Blusson Quantum Matter Institute,University of British Columbia,Vancouver, BCV 6T1Z4,Canada*

Keywords: cuprate superconductors, charge fluctuation, electronic structure, ARPES, IPES

The mechanism for high-T_c cuprate superconductivity is realized by interaction between electrons and bosons. However, it has been a long-standing mystery to what extent which bosons play an important role to occur high-T_c superconductivity.

Recent resonant inelastic x-ray scattering (RIXS) experiments have been reported that charge excitations for high-T_c cuprate superconductors [1-3]. The contribution of the charge fluctuations to high-T_c cuprate superconductivity has started to pay attention for the physics of cuprate superconductivity. According to previous theoretical studies [4-7], using the layered *t-J* model, the electron self-energy is calculated and discussed about the effect of charge fluctuation for the electronic structure of cuprates.

In this study, we have performed an angle-resolved photoemission spectroscopy (ARPES) and inverse photoemission spectroscopy (IPES) to understand the electronic structure for the electron-doped cuprate $Nd_{1.85}Ce_{0.15}CuO_4$ in the occupied and unoccupied states, respectively. In addition to the experiments, we have performed *ab-initio* calculations to investigate the electronic structure as shown in Fig. 1. We have observed band dispersions and found some similar features corresponding to charge derived bands. In the poster presentation, we will show the experimental and theoretical results in details and discuss the effect from the charge fluctuation of cuprate superconductors.

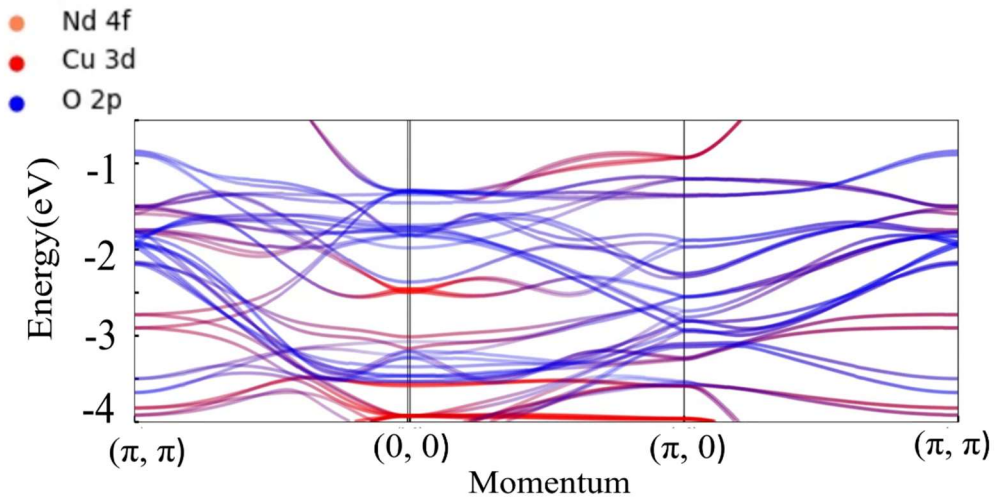

FIGURE 1. Bulk-band structure of Nd_2CuO_4 using DFT calculations. The color and intensity of the curves correspond to the weight of orbitals, Nd 4*f*, Cu 3*d*, and O 2*p*.

REFERENCES

1. J. Lin *et al*., Quantum Materials **5**, 4 (2020).
2. A. Singh *et al*., Phys. Rev. B **105**, 235105 (2022).
3. W. S. Lee *et al*., Nature Phys **10**, 883-889 (2014).
4. A. Greco *et al*., Commun Phys **2**, 3 (2019).
5. H. Yamase *et al*., Phys. Rev. B. **104**, 045141 (2021).
6. H. Yamase *et al*., Phys. Rev. B **109**, 1 (2024).
7. H. Yamase *et al*., Commun Phys **6**, 168 (2023).

BL-5

Metallization of boron-doped amorphous carbon films

Yuji Muraoka[a], Sho Enomoto[b], Subaru Nakashima[c], Takanori Wakita[d], Takayoshi Yokoya[a] and Kohei Yamagami[e]

[a]*RIIS. Okayama Univ. 3-1-1 Tsushima-naka, Tsushima, Kita-ku, Okayama 700-8530, Japan*
[b]*ELST. Okayama Univ. 3-1-1 Tsushima-naka, Tsushima, Kita-ku, Okayama 700-8530, Japan*
[c]*Fac. of Sci. Okayama Univ. 3-1-1 Tsushima-naka, Tsushima, Kita-ku, Okayama 700-8530, Japan*
[d]*JASRI. 6-6-11-901 Aramaki Aoba, Aoba-ku, Sendai, Miyagi 980-8579, Japan*
[e]*JASRI. 1-1-1, Kouto, Sayo-cho, Sayo-gun, Hyogo 679-5198, Japan*

Keywords: Metallization, Boron doped, Amorphous carbon, Film

Amorphous carbon (a-C) has excellent mechanical properties such as high hardness, high corrosion resistance, and low friction coefficient, and is therefore used as a coating material for automotive parts, molds, cutting tools, etc. On the other hand, the electrical properties of a-C are insulating, which makes it difficult to utilize this material for electrical devices. If a-C can be made conductive, a-C expands its application fields including electronics devices. Impurity doping is an effective approach to obtain the conductive a-C. However, metallic a-C has not yet been realized due to the presence of a high defect density that suppresses the carrier generation efficiency in a-C.

Q-carbon, a new allotrope of carbon, is discovered in 2015 [1]. This material is amorphous and consists of 80% sp^3 bonds and 20% sp^2 bonds. Interestingly, when Q-carbon is doped with boron, it becomes superconducting with the transition temperature of 36 K at boron-doping level of 17% [2]. This indicates that the boron-doped a-C can be metallic, and also that the carrier generation efficiency in the boron-doped Q-carbon is an order of magnitude higher than that of conventional a-C. Boron-doped Q-carbon provides a promising way for realizing the metallization of a-C.

Boron-doped Q-carbon is formed in a non-equilibrium process. This material is produced by the pulsed laser deposition of the amorphous film with boron and a-C mixture and subsequent pulsed laser annealing (PLA) of the B and C mixed films at room temperature and pressure in air, using a nanosecond pulsed UV excimer laser. During PLA, the films are melted to a highly undercooled state and subsequently rapid quenched to room temperature Since the duration of PLA is about only 200 ns, it is important to properly control the heat in quite short time to obtain this material. We have previously developed an adjusted pulsed laser annealing (adjusted PLA) method that allows thermal control through experimental parameters, and obtained the non-doped Q-carbon [3]. In this study, the boron-doped a-C films were prepared using the adjusted PLA method, and study on the electronic states were performed to investigate the metallic nature of the obtained films.

Starting material films of boron and a-C mixture (hereafter as-deposited films) were prepared on Al_2O_3(0001) substrates by using a pulsed laser deposition technique with a Nd:YAG laser (λ= 355 nm, τ = 5 ns). The film deposition was carried out at a substrate temperature of 300 K under a vacuum condition of 3×10^{-8} Torr. The film thickness is 150 nm, and the B/C ratio in the film is 35%. PLA was performed on the staring material films at ambient atmosphere and temperature using the Nd: YAG laser. The films with PLA (hereafter PLA-films) were obtained by irradiating one laser pulse through a converging lens to the surface of the starting material films. The energy density of PLA was set to 0.6 J/cm^2. The as-deposited and PLA-films were characterized by using synchrotron radiation photoelectron spectroscopy (PES) at HiSOR BL-5 and SPring-8 BL25SU. Monochromated X-ray of 700 and 1300 eV was used for measurements and the total energy resolution was set to about 80 and 170 meV for 700 and 1300 eV, respectively in the measurements at SPring-8 BL25SU. Before measurements, the samples were annealed at 120 ^{o}C under vacuum condition of 5×10^{-7} Pa for 30 min to obtain a clean surface. The Fermi level position was determined by measuring the Fermi edge of gold. All spectra were taken at 300 K.

Figure 1 shows the valence band spectra of the as-deposited and PLA-films. For the as-deposited film, the

valence band spectrum shows a broad structure. A fairly broad, intense peak located between 16 and 19 eV is mainly due to carbon 2*s* band, a broad shoulder located at about 11 to 14 eV is mainly due to the mixture of carbon 2*s* and 2*p* bands, and a very broad and decidedly weaker structures extending from 10 eV to the cutoff energy is mainly due to carbon 2*p* band. A broad peak at about 25 eV is due to the O 2*s* band which is a result of contamination in the film preparation process. The obtained result is in good agreement with that of amorphous carbon films reported previously [4]. For the PLA-film, the shape of valence band spectrum is similar to that of the as-deposited film. However, there is a difference between two spectra; the broad structure from 4 eV to the cutoff energy is more obvious in the PLA-film. This suggests that the valence band spectrum is changed by PLA. In order to see the top of valence band spectrum in more detail, the near Fermi level spectra of both as-deposited and PLA-films were collected. The result is shown in Figure 2. A finite intensity is observed at the Fermi level for the PLA-film, while it is not for the as-deposited film. This indicates that the PLA-films becomes metallic after PLA. The PES spectra of boron 1s core-level of the PLA-films is drastically changed compared to that of the as-deposited films (not shown), indicating that the boron atoms are incorporated in the PLA-films. The XPS measurements of valence band and B 1*s* core-level reveal that the film becomes metallic due to the boron doping by PLA. We will present the results of spectral analysis of C 1*s* and B 1*s* core-levels in both as-deposited and PLA-films.

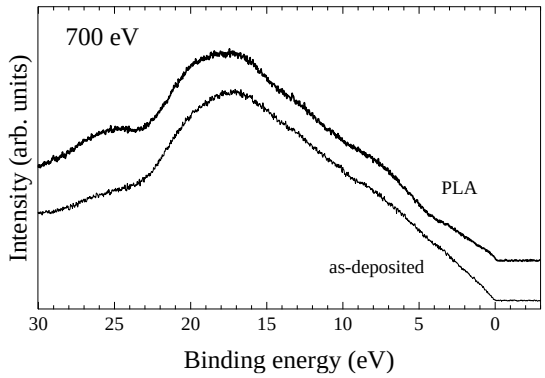

FIGURE 1. Valence band spectra for the as-deposited and PLA-films measured with a photon energy of 700 eV at 300 K.

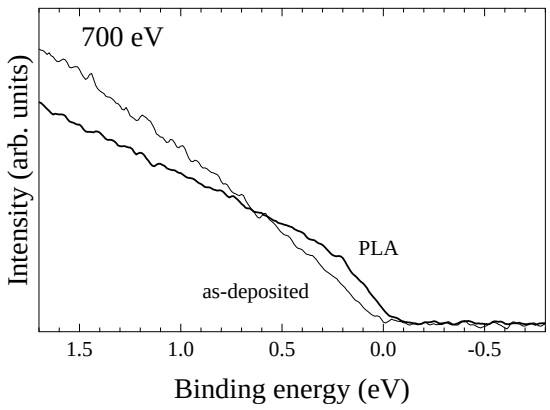

FIGURE 2. Near Fermi level spectra for the as-deposited and PLA-films.

REFERENCES

1. J. Narayan and A. Bhaumik, *J. Appl. Phys*. **118,** 215303 (2015).
2. A. Bhaumik, R. Sachan and J. Narayan, *ACS Nano* **11,** 5351-5357 (2017).
3. H. Yoshinaka, S. Inubushi, T. Wakita, T. Yokoya and Y. Muraoka, *Carbon* **167,** 504-511 (2020).
4. T. W. Scharf, R. D. Ott, D. Yang and J. A. Barnard, *J. Appl. Phys.* **85,** 3142-3154 (1999).

24AG019 BL-5

Current Activities of Research and Education on BL-5 (FY2024)

T. Yokoya[a,b], T. Wakita[a] and Y. Muraoka[a,b]

[a]*Research Institute for Interdisciplinary Science, Okayama University*
[b]*Research Laboratory for Surface Science, Okayama University, Okayama 700-8530, Japan*

Keywords: Photoemission spectroscopy, photoelectron emission microscopy

We present an overview of our resent research and educational activities on beamline 5 (BL5) in the fiscal year 2024. Our beamline has two experimental stations in a tandem way. The first station is equipped with an angle-resolved photoemission spectrometer (ARPES), a low energy electron diffraction (LEED) apparatus and an X-ray source. The hemispherical analyzer of ARPES spectrometer (HA54, VSW) has a mean radius of 50 mm and is mounted on a twin axis goniometer in ultra-high vacuum chamber. Using this goniometer, one can perform ARPES and photoelectron diffraction (PED) measurements. It is also possible to perform resonant photoemission spectroscopy (RPES) measurements by using photon energy tunability of synchrotron radiation with X-ray absorption spectroscopy (XAS) measurement. With the X-ray source (XR2E2, FISONS), we can perform an X-ray photoelectron spectroscopy (XPS) measurement for the chemical state analysis and the PED. At the second station, we have installed a photoelectron emission microscope (PEEM, 'PEEM III', Elmitec). PEEM provides a magnified image of lateral intensity distribution of photo-emitted electrons from a sample surface. The spatial resolutions are several ten nanometers with Hg lamp and a few micrometers with synchrotron radiation. The sample is transferred between the ARPES and the PEEM chamber in-situ, and one can perform measurements at both stations for the same sample.

In the recent researches on BL-5, we have studied the electronic structure of potassium doped aromatic molecule (K_x picene) [1], iron-based superconductor ($FeSe_xTe_{1-x}$) [2], transition metal dioxide films such as VO_2 thin films which exhibits a first-order metal-to-insulator transition at 340 K [3], CrO_2 thin films which are known as a half-metallic material [4], TaO_2 film which is stabilized with a new technique developed in our group [5], and phase-separated TiO_2-VO_2 films on mica substrates. We have also studied the electronic structures of a high-quality boron-doped diamond film which shows a signature of the highest superconducting transition temperature of 25 K [6] and a high quality single crystal of $YbFe_2O_4$ which is one of multiferroic materials [7], by utilizing RPES at B *K*- and Fe $M_{2,3}$- edges, respectively. In addition, we have studied the sp^3 content in diamond-like carbon films by using photoemission spectroscopy in order to optimize the conditions to produce Q-carbon (quenched carbon) which is a newly discovered amorphous phase of carbon with several exotic properties [8]. In the last few years, we have performed PEEM and TEY measurements at BL5 in HiSOR for a B-doped carbon nano wall film on a Si substrate and a micro-droplet of solidified L-boronophenylalanine on a Si substrate in order to investigate microscopic chemical states of trace B atoms in them from fine structures in local- and wide-area-XAS spectra near B *K*-edge and to visualize B distributions on their surfaces. For this kind of measurements with PEEM, we have developed a new auto-measurement system where we can obtain a serial PEEM images with excitation x-ray energies for a certain energy range with a fixed energy step.

Recently, we have prepared an auto-measurement system and an X-ray focusing capillary lens for photoemission holography (PEH) measurements. PEH is a method that has been greatly developed in Japan in recent years as a measurement method for elucidating the local structure of materials with an atomic resolution [9]. In particular, various results have been reported in the study of the three-dimensional atomic configurational structure around the dopants in crystals [10]. However, the opportunity to use state-of-the-art apparatuses (for example, DA30 analyzer and RFA of BL25SU at SPring-8) are limited. Although our photoelectron energy analyzer is an old model and it is difficult to separate and observe small shifts in core levels because of the energy resolution of 1-2 eV of the system, we expect that our apparatus will be used for preliminary experiments on undoped materials prior to experiments for doped samples using state-of-

the-art systems. It can also be used for educational purposes such as experiencing photoelectron holography experiments and learning the analysis methods.

We have used the BL-5 for education activity as well, for example, practical education for undergraduate students of Okayama University. The students have an opportunity to study the synchrotron radiation mechanism and to experience XPS measurement which is very useful for the surface science research. We accepted more than 100 students from 2006 to 2012. From 2014, we have started to join the practical lecture for experiments using the beamline end stations in HiSOR for both graduate school students of Hiroshima and Okayama Universities. In 2018, we have had a new project for education under a Japan-Asia youth exchange program in science supported by Japan Science and Technology Agency (JST), "Sakura Exchange Program in Science". We have accepted six students from Changchun University of Science and Technology in China.

REFERENCES

1. H. Okazaki *et al*., *Phys. Rev* **82**, pp. 195114 (5 pages) (2010).
2. Y. Yoshida *et al*., *J. Phys. Soc. Jpn* **78**, pp. 034708 (4 pages) (2009).
3. K. Saeki *et al*., *Phys. Rev* **80**, pp. 125406 (5 pages) (2009).
4. Y. Muraoka *et al*., *MRS Proceedings* **1406** (2012).
5. Y. Muraoka *et al*., *Thin Solid Films* **599**, pp. 125-132 (2016).
6. H. Okazaki *et al*., *Appl. Phys. Lett* **106**, pp. 052601 (5 pages) (2015).
7. K. Fujiwara *et al*., *Trans. Mater. Res. Soc. Jpn.* **41**, pp. 139-142 (2016).
8. H. Yoshinaka *et al*., *Carbon.***167**, pp. 504-511 (2020).
9. T. Matsushita *et al*. *Europhys. Lett*. **71**, 597 (2005). *Phys. Status Solidi B* **255**, 1800091 (6 pages) (2018).
10. K. Hayashi, T. Matsushita, *SPring-8 Research Frontiers* **2020**, pp. 12 -15 (2021).

23BG005 BL-7

Photoelectron spectroscopy and local structure of the Se chain confined in single carbon nanotube

R. Nishikawa[a], K. Mimura[b], Y. Tanimoto[c], H. Sato[d], S. Islam[a], T. Miyanaga[e], and H. Ikemoto[a]

[a]*Department of Physics, University of Toyama, Toyama 930-8555, Japan*
[b]*Department of Physics and Electronics, Osaka Metropolitan University, Sakai 599-8531, Japan*
[c]*Graduate School of Advanced Science and Engineering, Hiroshima University, Higashi-Hiroshima 739-8526, Japan*
[d]*Hiroshima Research Institute for Synchrotron Radiation Science, Hiroshima University, Higashi-Hiroshima 739-0046, Japan*
[e]*Department of Mathematics and Physics, Hirosaki University, Hirosaki 036-8561, Japan*

Keywords: Se chain, carbon nanotube, Photoelectron spectroscopy, EXAFS.

Trigonal selenium (t-Se) is the stable crystalline form in which Se atoms form three-turn helical chains with twofold covalent bonds, and these chains are stacked through interchain interactions. This hierarchical structure—where the helical chains constitute the primary structure and the stacked chains constitute the secondary one—is a characteristic feature of chalcogen elements, including Se. This unique characteristic arises from the four 4p valence electrons: two form covalent bonds, while the others form lone-pair (LP) bonds. The LP bonds are located at the top of the valence band, with a gap between the LP bands and the anti-bonding (σ*) bands, making t-Se a semiconductor. The physical properties are strongly correlated with its structure. Therefore, it is crucial to study both the electronic state and local structure. In this report, we present the electronic structure and the local structure of selenium chains confined within single-walled carbon nanotubes (Se@SWCNT), as determined by extended X-ray absorption fine structure (EXAFS) and photoelectron spectroscopy (PES) measurements.

Se@SWCNT was synthesized by heat treatment of a glass tube sealing Se and SWCNT. PES experiments were perfomed at BL-7 in HiSOR using 120 eV excitation photon energy at both room temperature (RT) and 20 K (LT). EXAFS measurements for the Se K-edge (12.7 keV) were conducted at BL12C in KEK-PF using transmission mode over a temperature range of 20–300 K.

Figure 1 shows the PES spectra of SWCNTs with and without Se, where the backgrounds were subtracted using the Shirley method [1]. Since the Se atoms are confined within the SWCNTs, their contribution is relatively small. The PES spectra of Se@SWCNT were obtained by subtracting the spectra of SWCNTs without Se from those with Se. A key observation is the spectral weight near the Fermi energy (E_F); nearly zero at RT while finite at LT. This suggests that Se@SWCNT could exhibit metallic behavior at LT, while at RT it behaves like a semiconductor similar to t-Se.

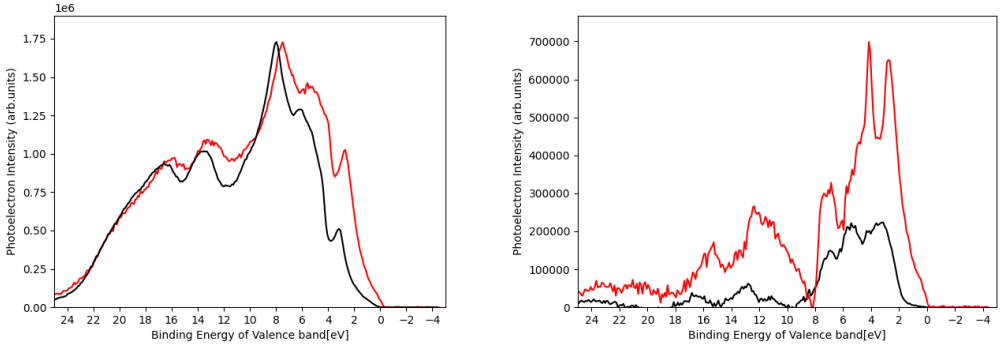

FIGURE 1. (a) The PES spectra of SWCNTs with and without Se at LT, (b)The PES spectra of Se@SWCNT at RT and LT.

The most interesting result from the EXAFS analysis is the temperature-dependent variation of the coordination number (N) of Se covalent bonds. At RT, the value of N is close to two, indicating that the two-fold covalent bonds remain intact even in Se@SWCNT. However, the value decreases to about 1.8 at LT. If we simply consider it, this suggests that the covalent bonds partially break as the temperature decreases.

We will discuss these interesting results in conjunction with the PES and EXAFS studies with other consideration.

REFERENCES

1. A. Shirley, Phys. Rev. B 5, 4709-4714 (1972).

23BG021 HiSOR, BL-1/UVSOR BL7U

Observation of electronic structure of chiral magnet $GdNi_3Ga_9$ by ARPES

Y. Tanimoto[a], Y. Nakashima[a] H. Sato[b], M. Arita[b], Y. Miyai[a], K. Shimada[c], K. Tanaka[c], S. Nakamura[d], S. Ohara[d]

[a]*Graduate School of Advanced Science and Engineering, Hiroshima University, Higashi-Hiroshima 739-8526, Japan*
[b]*Hiroshima Research Institute for Synchrotron Radiation Science, Higashi-Hiroshima 739-0046, Japan*
[c]*UVSOR synchrotron Facility, Institute for Molecular Science, Okazaki 444-8585, Japan*
[d]*Graduate School of Engineering, Nagoya Institute of Technology, Nagoya 466-8555, Japan*

Keywords: chiral magnetic crystal, helical magnetism, angle resolved photoemission spectroscopy

Trigonal $GdNi_3Ga_9$ has a chiral crystal structure belonging to space group of *R*32 (No. 155) [1] and is of interest as a 4*f* chiral metallomagnetic compound [2]. The localized Gd 4*f* spins are magnetically ordered below *T*=19.5 K, antiferromagnetic in the *c*-plane, and exhibit left-handed or right-handed helimagnetism with propagation vector $\boldsymbol{q}$=(0, 0, 1.485) [2]. Spin-polarized conduction electrons are thought to be responsible for this phenomenon. $GdNi_3Ga_9$ has the same crystal structure as $YbNi_3Al_9$, which is the first discovered 4*f* chiral metallomagnetic compound [3]. $YbNi_3Al_9$ exhibits a helimagnetism with propagation vector $\boldsymbol{q}$=(0, 0, 0.82), while ferromagnetic order in the *c*-plane in contrast to $GdNi_3Ga_9$ with antiferromagnetic order in the *c*-plane. Therefore a comparative study for $GdNi_3Ga_9$ is expected [3]. We have previously performed angle-resolved photoemission spectroscopy (ARPES) on $YbNi_3Al_9$ and observed five hole-like Fermi surfaces around $\bar{\Gamma}$ point and one electronic Fermi surface around $\bar{K}$ point [5]. In this study, we have performed ARPES on $GdNi_3Ga_9$ to observe the Fermi surface and the band structure of conduction electronic bands near the Fermi level (E_F). The experiments were carried out at BL-1 of Hiroshima Research Institute for Synchrotron Radiation Science (HiSOR) and at BL7U of UVSOR-III synchrotron. Single crystals used for the ARPES measurements were synthesized by the flux-method [2].

Figure 1 shows the ARPES intensity plots of $GdNi_3Ga_9$ measured at $h\nu$=70 eV with *p*-polarized geometry along the $\bar{\Gamma}$-$\bar{K}$ direction of the surface Brillouin zone. Some hole-like bands around the $\bar{\Gamma}$ point were observed. At k_x=1.0 ~ 2.5 Å^{-1}, several convex-downward bands crossing E_F, the M-shaped band and the V-shaped band shown by the yellow dashed lines are observed. The shape of some hole-like bands around the $\bar{\Gamma}$ point is similar to that observed in the ARPES spectrum of $YbNi_3Al_9$. On the other hand, the M-shaped band is not observed in $YbNi_3Al_9$.

Figure 2 shows the Fermi surface of $GdNi_3Ga_9$ measured at $h\nu$=70 eV with *p*-polarized geometry. The horizontal and vertical axes are the wavenumbers (k_x, k_y) along $\bar{\Gamma}$-$\bar{M}$ and $\bar{\Gamma}$-$\bar{K}$directions, respectively. At least two hole-like Fermi surfaces, (A, B), around the $\bar{\Gamma}$ point and one electronic-like Fermi surface were observed. Overall features of the Fermi surfaces are similar to $YbNi_3Al_9$. In addition to these Fermi surfaces, an arc-shaped Fermi surface connecting the electronic-like Fermi surface was observed as shown by dashed lines. This Fermi surface is not observed in $YbNi_3Al_9$.

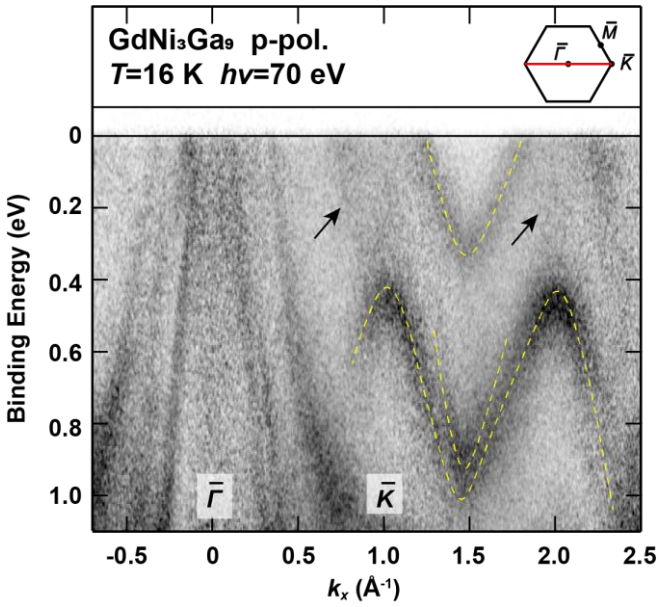

Fig. 1 ARPES intensity plots of $GdNi_3Ga_9$ measured along the $\bar{\Gamma}$-$\bar{K}$ direction and at $h\nu$=70 eV with *p*-polarized geometry.

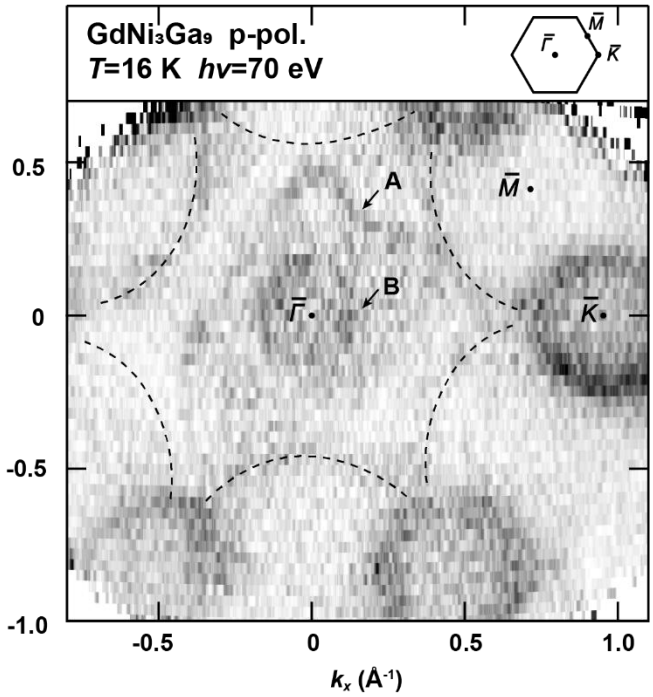

Fig. 2 Fermi surface of $GdNi_3Ga_9$ measured at $h\nu$=70 eV with *p*-polarized geometry.

REFERENCES

1. V. Topertser, R. Martyniak, N. Muts, Y. Tokaychuk and R. Gladyshevskii, Chem. Met. Alloys **12**, 21 (2019).
2. S. Nakamura, T. Matsumura, K. Ohashi, H. Suzuki, M. Tsukagoshi, K. Kurauchi, H. Nakao and S. Ohara, Phys. Rev. B **108**, 104422 (2023).
3. S. Ohara, S. Fukuta, K. Ohta, H. Kono, T. Yamashita, Y. Matsumoto and J. Yamaura, JPS Conf. Proc. **3**, 017016 (2014).
4. T. Matsumura, Y. Kita, K. Kubo, Y. Yoshikawa, S. Michimura, T. Inami, Y. Kousaka, K. Inoue and S. Ohara, J. Phys. Soc. Jpn. **86**, 124702 (2017).
5. Y. Tanimoto *et al.*, in preparation.

24AG038 BL-9A

Effects for the Electronic Structure by Oxygen Deficiency on the double-layer Cuprate High-T_c Superconductor, Bi2212

K. Kawamoto[a], H. Yamaguchi[b], Y. Miyai[b], Y. Onishi[b], M. Arita[c], K. Shimada[b,c,d,e], and S. Ideta[b,c]

[a] *Faculty of Science, Hiroshima Univ., Higashi-Hiroshima 739-8526, Japan*
[b] *Graduate School of Advanced Science and Engineering, Hiroshima Univ., Higashi-Hiroshima 739-8526, Japan*
[c] *Research Institute for Synchrotron Radiation Science (HiSOR), Hiroshima Univ., Higashi-Hiroshima 739-0046, Japan*
[d] *Research Institute for Semiconductor Engineering, (RISE), Hiroshima Univ., Higashi-Hiroshima 739-8527, Japan*
[e] *International Institute for Sustainability with Knotted Chiral Meta Matter (WPI-SKCM^2), Higashi-Hiroshima 739-8526, Japan*

Keywords: high-T_c cuprate superconductors, electronic structure, ARPES

Cuprate superconductors have been one of the materials which show the highest superconducting transition temperature (T_c) in superconductors under atmosphere. To elucidate the microscopic mechanism of the high T_c in cuprates; however, it has been unclear so far regardless of a lot of intensive studies [1]. Among Bi-based high-T_c cuprates, a double layer cuprate, $Bi_2Sr_2CaCu_2O_{8+\delta}$ (Bi2212) is a representative material which shows high-T_c superconductivity [2]. T_c and the electronic structure of cuprates dramatically changes with carrier doping, and therefore, one needs to understand the mechanism about these trends to achieve a higher T_c in superconductors.

According to the recent experimental study of Bi2212 using angle-resolved photoemission spectroscopy (ARPES), with increasing the hole carrier, the shape of the electronic structure shows a sudden discontinuous change around a hole doping level (p_c) of ~ 0.19 [3]. Therefore, the previous study suggests that the phase transition occurs at $p_c \sim 0.19$, but the origin of the phase transition has not been clear yet.

To investigate the electronic structure change with changing hole carrier, we have performed the temperature dependent ARPES study for two different Bi2212 samples with $p \sim 0.17$ and ~ 0.22. The ARPES spectra shows different shape compared with the previous results [3]. One of the unexpected features is that the peak-dip-hump structure at 20 K and 60 K, which was observed in the previous study, is not observed in the present experiment.

In this poster presentation, we will show the temperature dependent ARPES spectra in details and discuss the origin of the phase transition at $p_c \sim 0.19$.

REFERENCES

1. A. Damascelli *et al*., Rev. Mod. Phys. 75, 473 (2003).
2. H. Eisaki *et al*., Phys. Rev. B 69, 064512 (2004).
3. S. D. Chen *et al*., Science **366**, 1099-1102 (2019).

23BG012,23BU010 BL-9A, IPES

ARPES and IPES Studies for the Electronic Structure Derived by Quantum Charge Fluctuations on the Single-layer Cuprate Superconductor

Y. Onishi[a], Y. Miyai[a], Y. Tsubota[a], K. Tanaka[c], S. Ishida[d], H. Eisaki[d],

H. Sato[b], M. Arita[b], K. Shimada[a,b], and S. Ideta[a,b]

[a] *Graduate School of Advanced Science and Engineering, Hiroshima Univ., Higashi-Hiroshima 739-0046, Japan*
[b] *Hiroshima Synchrotron Radiation Center (HiSOR), Hiroshima Univ., Higashi-Hiroshima 739-0046, Japan*
[c] *UVSOR-III Synchrotron, Institute for Molecular Science, Okazaki, Aichi 444-8585, Japan*
[d] *National Institute of Advanced Industrial Science and Technology (AIST), Tsukuba, Ibaraki 305-8560, Japan*

Keywords: high- T_c superconductors, ARPES, IPES, charge fluctuations, electronic structure

To understand how the degrees of freedom in a solid (phonons, electron spins, orbitals, and charges) affect the electronic structure is essential for elucidating the microscopic mechanism behind the high superconducting transition temperature (T_c) in high-temperature superconductors. According to the previous studies by angle-resolved photoemission spectroscopy (ARPES), the electronic structure shows a kink in a band dispersion due to coupling with phonon and/or spin fluctuations [1, 2]. On the other hand, in recent resonant inelastic X-ray scattering (RIXS) studies, charge excitations have been observed in both hole-doped and electron-doped cuprates [4, 5]. However, direct experimental evidence how charge fluctuations affect the electronic structure for the high-T_c cuprates have been unclear so far.

In this study, we have performed an ARPES and an inverse photoemission spectroscopy (IPES) to directly observe the electronic structure in the occupied and unoccupied electronic states, respectively, of the single-layer copper oxide superconductor, $Bi_2Sr_{1.6}La_{0.4}CuO_{6+\delta}$ (Bi2201). If there is a contribution to the electronic structure from charge fluctuations, the experimental evidence could provide new key information into their role to the mechanism of superconductivity.

The ARPES and IPES results are shown in Figures 1 (left) and 1(right), respectively, and they reveal the electronic structure in both occupied and unoccupied energy regions. Notably, in the unoccupied states, we found that the structure exists around 1 eV and this result differs from the prediction of the density functional theory [6]. We believe that the present experimental results indicate that the structure above E_F around 1 eV is due to quantum charge fluctuations.

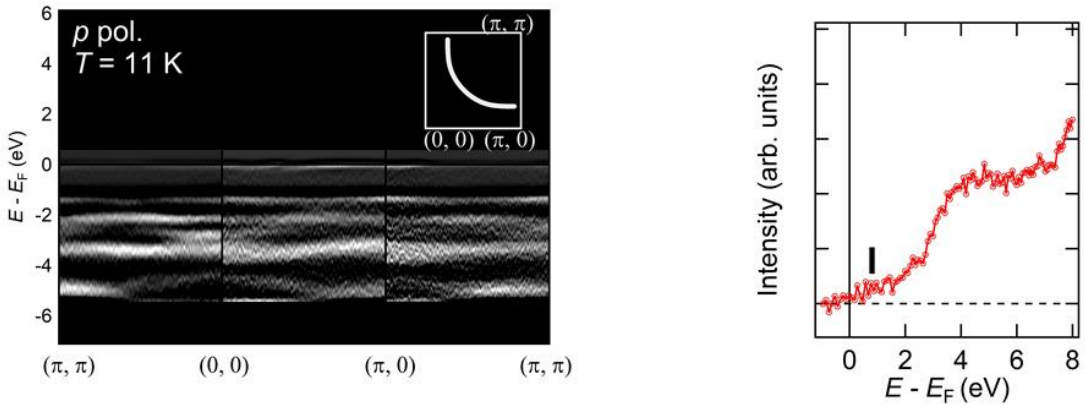

FIGURE 1. ARPES and IPES spectra for Bi2212. (Left) Intensity map of the first Brillouin zone of Bi2201 measured 21 eV. (Right**)** The IPES spectra observed in the unoccupied states of Bi2201at a certain momentum. Weak intensity is observed at the positions shown by a black bar.

REFERENCES

[1] A. Lanzara *et al.*, Nature **412**, 510 (2001).
[2] M. Zhu *et al*., Nat. Phys. **19**, 99-105 (2023).
[3] H. Yamase *et al*., Phys. Rev. B **104**, 045141 (2021).
[4] W. S. Lee *et al*., Nat. Phys. **10**, 883 (2014).
[5] A. Singh *et al*., Phys. Rev. B **105**, 235105 (2022).
[6] Jean-Baptiste Morée *et al*., Phys. Rev. B. **106**, 235150 (2022).

24AG040 BL-9B

Oxygen-termination effect of the spin-dependent electronic states in FeCo/Rh(001) thin film

Kaori Kunitomo[a], Kazuki Sumida[b], Koji Miyamoto[b], and Taichi Okuda[b,c,d]

[a] *Graduate School of Advanced Science and Engineering Hiroshima University, 1-3-1 Kagamiyama, Higashi-Hiroshima, 739-8526 Japan*
[b] *Research Institute for Synchrotron Radiation Science (HiSOR), Hiroshima University, 2-313 Kagamiyama, Higashi-Hiroshima, 739-0046 Japan*
[c] *International Institute for Sustainability with Knotted Chiral Meta Matter (WPI SKCM2) Hiroshima University, 2-313 Kagamiyama, Higashi Hiroshima, 739-0046 Japan*
[d] *Research Institute for Semiconductor Engineering (RISE) Hiroshima University, 1-4-2 Kagamiyama, Higashi-Hiroshima, 739-8527 Japan*

Keywords: FeCo thin films, perpendicular magnetic anisotropy, VLEED spin detection target, oxygen termination

The emergence of perpendicular magnetic anisotropy (PMA) in magnetic thin films is essential from a practical application standpoint, as it contributes to increasing the recording density of storage devices and reducing energy consumption. Many magnetic thin films exhibiting PMA, such as Co/Pt, Co/Pd, FePt, TbFeCo, and GdFeCo, have been extensively investigated. Among them, FeCo alloy films, which are free of rare-earth and noble-metal elements, are considered promising candidates exhibiting strong PMA. Burkert *et al*. predicted that the magnetic anisotropy energy may increase in FeCo alloys when the tetragonal distortion is applied [1]. Specifically, at a *c*/*a* ratio of approximately 1.20-1.25, the magnetic anisotropy energy exceeds 700-800 μeV/atom, which is one or two orders of magnitude greater than that of pure Fe or Co. The emergence of strong PMA was experimentally confirmed in tetragonally distorted FeCo ultra-thin films grown on Rh(001) (*c*/*a* = 1.24) with a thickness of 13-15 monolayers (ML) [2].

Furthermore, the FeCo thin films exhibiting PMA could be useful as a target for out-of-plane spin component in very low energy electron diffraction (VLEED) spin detectors [3,4]. In the present VLEED spin detector, Fe(001)*p*(1×1)-O films, which exhibit in-plane magnetic anisotropy and can detect only in-plane spin components (P_x, P_y), are widely used. However, to observe all components of spin polarization (P_x, P_y, P_z) with the VLEED detectors, a ferromagnetic thin film target with PMA is required in addition to the conventional Fe(001)*p*(1×1)-O films. Moreover, Fe(001)*p*(1×1)-O has an oxygen-adsorbed overlayer that serves as a protection layer from further oxidization and contamination, extending its lifetime from hours to weeks (or even several months or more with flash annealing). Thus, if the preparation method of oxygen-adsorbed protection layer on FeCo films is established, the FeCo-O films may be usable for long-term use as the VLEED targets for the out-of-plane spin component.

In this study, we fabricated the oxygen-terminated FeCo films on a Rh(001) single-crystal substrate and investigated the spin-polarized electronic structures and their lifetime utilizing spin- and angle-resolved photoemission spectroscopy (SARPES).

The samples were fabricated by using two different methods. In the first method, after cleaning the Rh(001) substrate by cycles of 2 keV Ar^+-ion sputtering and subsequent annealing at 1000 ˚C, FeCo was deposited at room temperature. Then, the FeCo film was exposed to approximately 30 L of oxygen and post-annealed at 300° C for 5 min. As a result, the low energy electron diffraction (LEED) pattern shows not only the 1×1 spots but also new superlattice spots [Fig. 1(b)]. Furthermore, while a clear out-of-plane spin polarization was observed at the pristine FeCo thin film [Fig. 2(a)], the spin polarization was almost diminished after oxygen exposure [Fig. 2(b)], indicating the loss of PMA.

Next, we explored a second method in which oxygen was introduced prior to the FeCo deposition, aiming to induce oxygen segregation. Specifically, after cleaning the Rh(001) substrate, oxygen exposure was exposed ~30 L to the substrate, followed by FeCo deposition and post-annealing at 300° C for 5 min. In this method, we obtained clear 1×1 LEED spots [Fig. 1(c)] similar to that of the pristine FeCo film [Fig. 1(a)].

More importantly, we observed a distinct out-of-plane spin polarization [Fig. 2(c)]. These results indicate that the FeCo thin film successfully retained perpendicular magnetic anisotropy even after oxygen termination.

Finally, to evaluate the protection effect of oxygen termination, we monitored the spin-polarization of both pristine FeCo and oxygen-terminated FeCo thin films over approximately one week. Figure 3 shows the time-dependent spin-polarization. Here, we estimated the time constant for an attenuation of out-of-plane spin-polarization, *i.e.* lifetime, by fitting the experimental results with an exponential function. As a result, the time constant of the oxygen-terminated FeCo thin film was approximately 5.5 times longer than that of the pristine FeCo thin film. This finding suggests that, similar to Fe(001)p(1×1)-O, the oxygen termination provides an effective surface protection effect for FeCo thin films.

Based on these results, oxygen-terminated FeCo thin films appear to be highly promising as targets for out-of-plane spin component in VLEED spin detector.

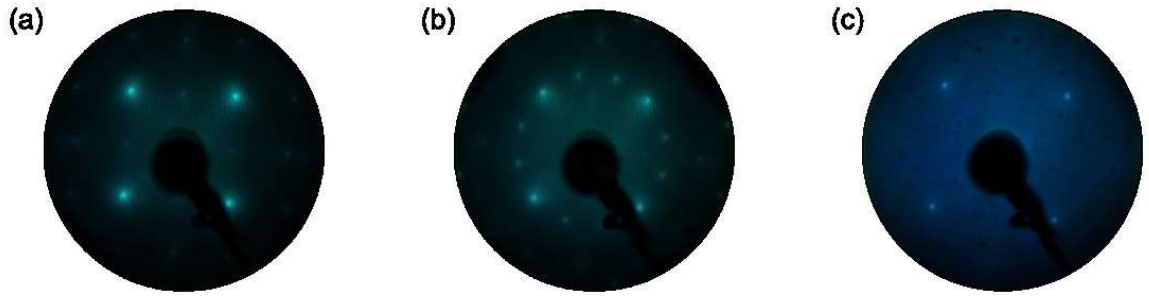

FIGURE 1. LEED patterns of the pristine FeCo thin film (a) and the oxygen-exposed FeCo film fabricated by the methods I (b) and II (c) taken at 90 eV.

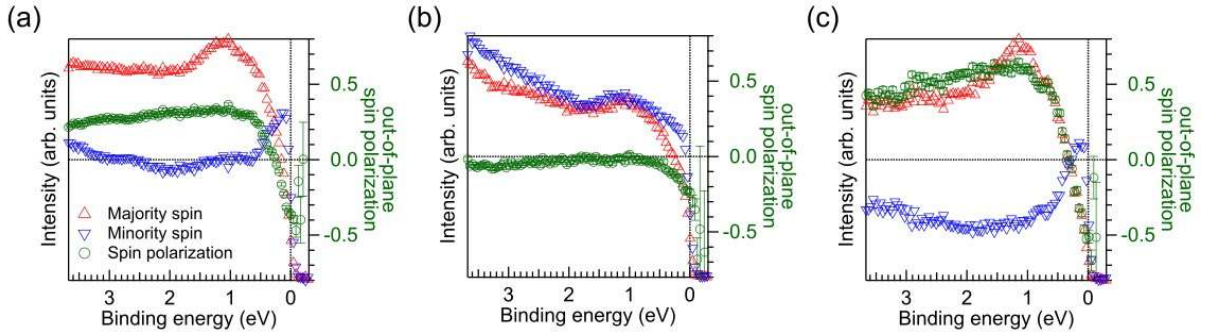

FIGURE 2. Out-of-plane spin-resolved photoemission spectra taken at 21.2 eV (He discharge lamp). The samples correspond to those in Fig. 1. A magnetic field was applied in the out-of-plane direction prior to the measurement. Red (blue) represents the majority (minority) spin, and green represents the out-of-plane spin polarization.

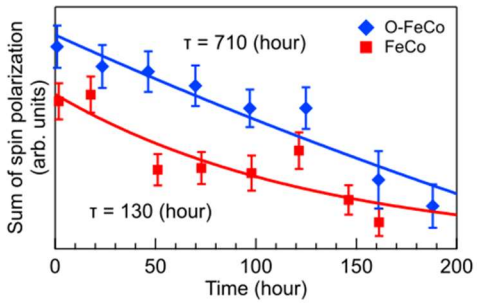

FIGURE 3. Comparison of the time constant for an attenuation of out-of-plane spin polarization. Red (blue) represents FeCo thin film (oxygen-terminated FeCo thin film).

REFERENCES

1. T. Burkert *et al.*, Phys. Rev. Lett. **93**, 027203 (2004).
2. F. Yildiz *et al.*, Phys. Rev. B **80**, 064415 (2009).
3. T. Okuda *et al.*, Rev. Sci. Instrum. **79**, 124117 (2008).
4. T. Okuda *et al.*, Rev. Sci. Instrum. **82**, 103302 (2011).

23AG036 BL-9B

Anisotropic Topological Surface States Induced by One-Dimensional Structure and Their Thickness Dependence

R. Yamamoto[a], Y. Fujisawa[b], K. Sumida[b], H. Sato[b], K. Miyamoto[b],

and T. Okuda[b,c,d].

[a]*Graduate School of Advanced Science and Engineering Hiroshima University, 1-3-1 Kagamiyama Higashi-Hiroshima 739-8526, Japan*
[b]*Research Institute for Synchrotron Radiation Science (HiSOR), Hiroshima University, 2-313 Kagamiyama, Higashi-Hiroshima 739-0046, Japan*
[c]*International Institute for Sustainability with Knotted Chiral Meta Matter (WPI-SCKM2), Hiroshima University, 2-313 Kagamiyama, Higashi-Hiroshima 739-0046, Japan*
[d]*Research Institute for Semiconductor Engineering (RISE), Hiroshima University, 1-4-2 Kagamiyama, Higashi-Hiroshima 739-8527, Japan*

Keywords: Topological Surface States, Silicon Vicinal Surface, Anisotropy of Band Structure, Bi_2Te_3 film

Topological insulators have spin-polarized metallic surface states called topological surface states (TSS). As in the Fig. 1(a), in the TSS, the spin direction of electrons is locked by their momentum resulting the helical spin-texture. The unique helical spin-texture is considered to prohibit complete backscattering by non-magnetic impurities. This property is expected to realize long spin coherent length and applied for spintronics devices. However, other backscattering passes except for the complete backscattering are not prohibited completely [Fig.1(a)]. One solution to overcome this problem is to form an anisotropic TSS, ideally a one-dimensional TSS [Figs. 1(b) and 1(c)] in which the direction of spin becomes closer to anti-parallel at the opposite k-point.

In the previous research, it has been reported that a quasi-one-dimensional band structure can be realized in the Ag films on Si(111)-(4 × 1)-In surface in which Ag film has regular step and terrace structure [1]. Thus, we expected that a similar effect might occur in the topological insulator film on vicinal surface with atomically regular step arrays. To investigate this hypothesis, we tried to fabricate Bi_2Te_3 film on silicon vicinal surface and measure its electronic structure.

Bi_2Te_3 ultrathin films were grown by molecular beam epitaxy on Si(111) and Si(557), which were used as a flat and a vicinal surface substrate, respectively. Si(557) is a surface tilted by 9.5° from Si(111), and has a Si(111) plane with a terrace width of 1.8 nm. The qualities of these films are evaluated by low energy electron diffraction (LEED) and auger electron spectroscopy (AES). Figure 2 shows LEED pattern and AES spectrum of the Bi_2Te_3 film on each substrate. As in Fig. 2(b) and (d), we can see clear spots in LEED and peak of Bi and Te in AES indicating that we succeeded in growing the Bi_2Te_3 film on both surfaces.

To observe the band structure of the fabricated films, angle-resolved photoemission spectroscopy (ARPES) measurements were performed at BL-9B in HiSOR using He Iα (21.2 eV) light. Figure 3(a), (b) shows the Fermi surface (top) and band structure (bottom) of 5 quintuple layer (QL) Bi_2Te_3 film on Si(557) surface. In these results, we can see the anisotropic TSS and Dirac point at around – 0.4 eV, which indicates that TSS is expanded to the direction perpendicular to the step by the effect of electron confinement. Figure 3(c), (d) and Figure 3(e), (f) show the results of 1~2 QL sample and less than 1 QL sample, respectively. In Figure 3(c), (d), we can see the anisotropic Fermi surface, but in Figure 3(e), (f), the anisotropy of Fermi surface and band structure is much weaker compared to 1~2 QL sample. Additionally, comparing the elongation of the Fermi surface, Fig. (c) (1~2 QL sample) shows the strongest anisotropy. This means the band anisotropy induced by evaporating on vicinal surface depends on the film thickness and quality of

substrate.

In conclusion, we succeeded in growing the Bi_2Te_3 film on vicinal silicon surface and observing the anisotropic topological surface states. In addition, we could also investigate the properties of the thin film on the vicinal surface. From these results, we found that it is possible to fabricate the one-dimensional topological insulator. Additionally, to effectively utilize the spin-texture of the anisotropic TSS, controlling the film thickness and ensuring the quality of substrate are important. These results will contribute to realizing the long spin coherent length and the future spintronics applications.

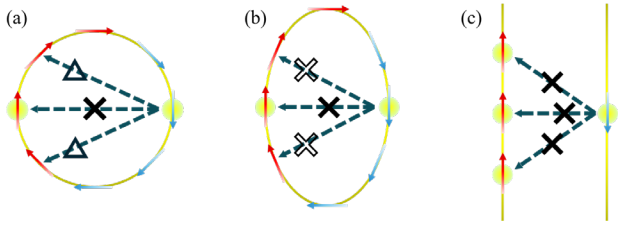

FIGURE 1. Schematic spin-texture of (a) isotropic, (b) anisotropic, and (c) one-dimensional Fermi surfaces (c) of topological insulators.

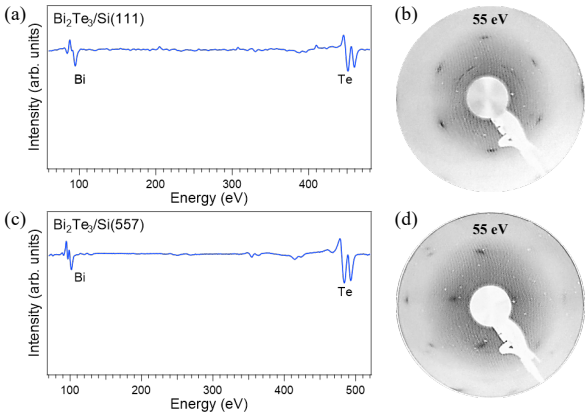

FIGURE 2. (a) AES spectrum of Bi_2Te_3/Si(111) (b)LEED pattern of Bi_2Te_3/Si(111) taken at 55 eV. (c),(d) the same as (a), (b) but of Bi_2Te_3/Si(557)

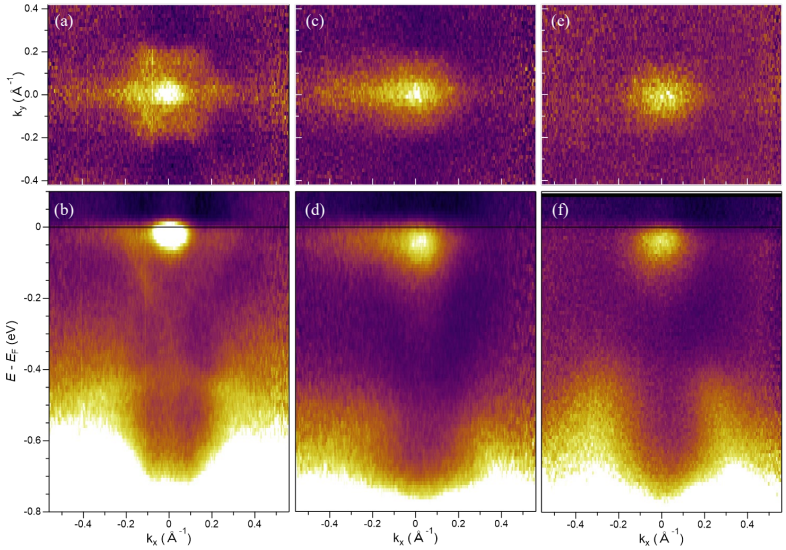

FIGURE 3. (a) Fermi surface and (b) band structure of 5 QL Bi_2Te_3/Si(557). (c), (d) the same as (a), (b) but of 1~2 QL Bi_2Te_3/Si(557). (e), (f) the same as (a), (b) but of less than 1 QL Bi_2Te_3/Si(557). All the data were measured by He Iα (21.2 eV) light.

REFERENCES

1. N. Nagamura *et al.*, Phys. Rev. Lett. **96**, 256801 (2006).
2. S. Hatta *et al.*, Sci. Rep. **11**, 5742 (2021).

24AU020 BL-9B

The observation of electronic structures on Pt/Fe/MgO and the design of operand sample holder

T. Asano[a], K. Sumida[b], T. Okuda[b,c,d], and K. Miyamoto[b]

[a]*Graduate School of Advanced Science and Engineering, Hiroshima University, 1-3-1 Kagamiyama, Higashi-Hiroshima 739-8526, Japan.*
[b]*Research Institute for Synchrotron Radiation Science (HiSOR), Hiroshima University 2-313 Kagamiyama, Higashi-Hiroshima 739-0046, Japan.*
[c]*International Institute for Sustainability with Knotted Chiral Meta Matter (SKCM^2), Hiroshima University, 1-3-1 Kagamiyama, Hiroshima 739-8526, Japan.*
[d]*Research Institute for Semiconductor Engineering (RISE), Hiroshima University, 1-4-2 Kagamiyama, Higashi-Hiroshima, 739-8527, Japan.*

Keywords: Spin Hall effect, Angle-resolved photoemission spectroscopy, *operando* measurements

Spin Hall effect is an important physical phenomenon that generates spin-polarized currents and is essential for the development of spintronics devices. The spin Hall effect in metals has attracted attention because conductance mismatches are markedly suppressed at an interface with ferromagnet and compared to the semiconductors and allows the use of spin-polarized current supplied by the ferromagnet [1]. Among many metals, elemental Pt is extensively investigated by experiment and theory [2,3]. T. Kimura *et al*. reported that the Pt wire exhibits largest spin hall conductivity as large as 2.4×10^4 S/m at room temperature, which is 4 orders of magnitude larger than that of typical semiconductors, such as GaAs [2]. In order to inject spin-polarized current into ferromagnets more efficiently, the orientation of spin current must be precisely controlled, i.e., it is necessary to observe its spin orientation. In previous studies, the rough spin orientation of spin currents induced by spin Hall effects has been obtained by using the magneto-optical Kerr effect [4]. However, the experimental method to precisely detect the spin orientation induced by the spin Hall effect has not been established yet. One solution is *operando* spin-resolved photoemission spectroscopy (PES) measurements under an external electric field.

In this presentation, we introduce two key developments for realizing this experimental technique. The first key development is the preparation of a platinum thin film. The second one is the design of a sample holder for the *operando* measurements.

For the Pt(001) thin film preparation, a thin Fe buffer layer was epitaxially grown on a MgO(001) substrate by molecular beam epitaxy (MBE) at room temperature (RT), in an ultrahigh vacuum (UHV) chamber with a base pressure of 8×10^{-7} Pa. The deposition of Fe was done at the substrate temperature of 600 °C. At a next growth stage, Pt was deposited on the Fe layer at RT. The quality of the Pt/Fe/MgO sample was evaluated using low-energy electron diffraction (LEED) and angle-resolved photoemission spectroscopy (ARPES). ARPES measurement was done using He discharge lamp with photon energy of 21.218 eV (He Iα).

Figure 1(a) shows the LEED pattern of the Pt/Fe/MgO sample. A distinct 1 × 1 LEED pattern with 4-fold symmetry indicates the successful growth of Pt(001) thin film. Moreover, the Fermi surface with 4-fold symmetry (**FIGURE 1(b)**), and the observed clear band structure forming a large electronic band (not shown here) are another indication of the high-quality Pt(001) film.

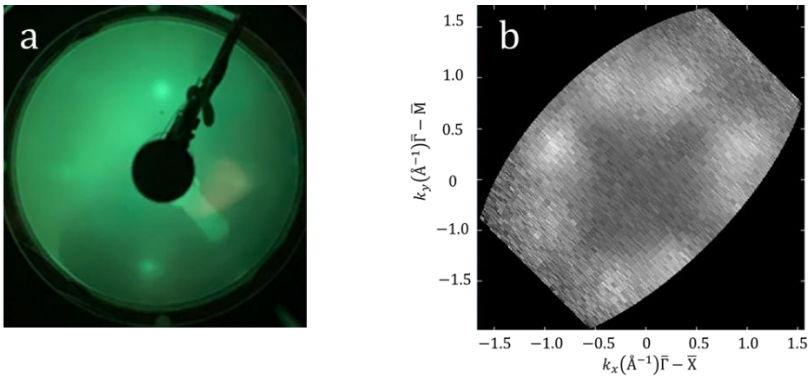

FIGURE 1. (a):(01)LEED-spot of Pt thin film sample at E_K = 73.4 eV**.** Pt film thickness is 22 nm. (b) Fermi surface of Pt(001)/Fe(001)/MgO(001) measured by ARPES at $h\upsilon$ = 20.218 eV. Pt film thickness is 36 nm.

For the *operando* measurement we have also developed the sample holder including the following two key functions:

1. Electrodes with a function to contact directly to the thin film sample in order to apply an electric field.
2. A function to heat the sample for preparation and cleaning.

We designed a sample holder that incorporates these two functions as shown in **FIGURE 2.** In our design, a filament for heating the sample is built into the sample holder.

In the future, we will develop the associated software, aiming to perform *operando* measurements of the spin Hall effect. More details will be presented in my poster.

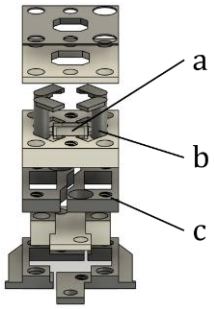

FIGURE 2. Sample holder design for *operando* measurements. a: Sample, b: Electrostatic field application terminal, c: Filament base.

REFERENCES

1. G. Schmidt, *et al*, Phys. Rev. B **62**, R4790(R) (2000).
2. T. Kimura, *et al.*, Phys. Rev. Lett. **98**, 249901 (2007).
3. G. Y. Guo, *et al.*, Phys. Rev. Lett. **100**, 096401(2008).
4. Y. K. Kato, *et al.*, Science **306**, 5703 (2004).

In house BL-9B

Improving the accuracy of spin detection using lock-in techniques

Yuma Ikeo[a], Koji Miyamoto[b] , and Taichi Okuda[b,c,d]

[a] *Faculty of Science, Hiroshima University, 1-3-1 Kagamiyama Higashi-Hiroshima 739-8526, Japan*
[b] *Research Institute for Synchrotron Radiation Science (HiSOR), Hiroshima University, 2-313 Kagamiyama, Higashi-Hiroshima 739-0046, Japan*
[c] *International Institute for Sustainability with Knotted Chiral Meta Matter (WPI-SCKM2), Hiroshima University, 2-313 Kagamiyama, Higashi-Hiroshima 739-0046, Japan*
[d] *Research Institute for Semiconductor Engineering (RISE), Hiroshima University, 1-4-2 Kagamiyama, Higashi-Hiroshima 739-8527, Japan*

Keywords: lock-in techniques, spin-resolved photoemission spectroscopy, VLEED spin detector

Spin-resolved photoemission spectroscopy is an experimental technique that can measure not only the binding energy and momentum of electrons in a material but also spin information (spin-polarization and spin-orientation). To obtain spin information Very Low Energy Electron Diffraction (VLEED) spin detector is utilized at HiSOR, in which spin-polarization is observed by measuring the intensity asymmetry between the reflected electrons by the positively and negatively magnetized target[1].
However, spin detection is generally inefficient and the spin-resolved photoemission measurement is time-consuming, which presents challenges such as (1) detecting small spin polarization and (2) sample degradation over time, affecting measurement reliability.

To overcome this problem, in this study, we tried to develop a lock-in detection system in spin detection to improve the measurement accuracy of spin-resolved photoemission. In order to utilize the lock-in technique into the VLEED spin detection the continuous modulation of some signals relating to the spin-polarization is needed. To this end, we tried to use the two different working points (i.e. two different electron injection energies to the target) where the intensity asymmetry by spin-dependent electron reflection in VLEED becomes positive and negative at the each working point instead of changing the magnetization of target positively and negatively as in the conventional VLEED spin detection[1]. We sought the condition where the intensity asymmetry of reflected electrons between the two working points matches that between the positively and negatively magnetized targets.

Figure 1(a) and (b) show the results of the spin-polarization measurement of Bi(110) Rashba state at some specific *k*-point taken with the conventional VLEED spin detection measurement by electron reflection intensities from the positively and negatively magnetized target as well as by electron reflection intensities at two different working points. As seen in the figures, it was clarified that almost the same results were obtained by both methods. Thus, we have confirmed that the periodic signal modulation necessary for the lock-in technique can be obtained by the periodic change of the working points in VLEED spin detection. We plan to perform actual lock-in measurements in near future.

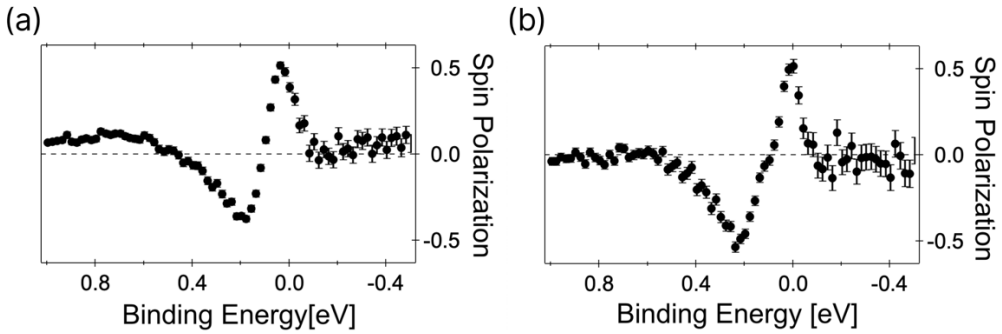

FIGURE 1. (a)Spin polarization of Bi(110) at the specific k-point measured by conventional method using magnetization reversal of target. (b) the same as (a) but by the new method using the two different working energy points (two different electron injection energies).

REFERENCES

1. T. Okuda and A. Kimura, *Spin- and Angle-Resolved Photoemission of Strongly Spin-Orbit Coupled Systems*, J. Phys. Soc. Japan **82**, 1 (2013).

24AG012 BL-12

Structural Dynamics of α_1-Acid Glycoprotein in the Membrane Interaction Revealed by Time-Resolved Vacuum-Ultraviolet Circular Dichroism

Satoshi Hashimoto[a] and Koichi Matsuo[a,b,c]

[a]*Graduate School of Advanced Science and Engineering, Hiroshima University, 1-3-1 Kagamiyama, Higashi-Hiroshima 739-8526, Japan*
[b]*Research Institute for Synchrotron Radiation Science, Hiroshima University, 2-313 Kagamiyama, Higashi-Hiroshima 739-0046, Japan*
[c]*International Institute for Sustainability with Knotted Chiral Meta Matter (WPI-SKCM2), Hiroshima University, 2-313 Kagamiyama, Higashi-Hiroshima 739-0046, Japan*

Keywords: Circular dichroism, α_1-Acid Glycoprotein, Membrane interaction, Secondary structures

α_1-acid glycoprotein (AGP) binds to drugs such as steroid hormones and releases them through membrane interactions, inducing its β-α structural transition[1]. Thus, AGP is used as a model protein for drug transport into the cell membrane. Studies have shown that two α-helices in the N- and C-terminal regions are key interaction sites[2,3] but the detailed membrane interaction mechanism, including electrostatic and hydrophobic forces, remains unclear. Recently, we developed a time-resolved (TR) vacuum-ultraviolet circular dichroism (VUVCD) spectrophotometer using synchrotron radiation to observe hierarchical protein structural transitions[4]. This study employed TR-VUVCD to analyze AGP's structural transitions and membrane interactions. TR-VUVCD spectra of AGP interacting with DMPG liposomes were measured within a 260–180 nm wavelength and 1–700 seconds (FIGURE 1). Analysis of TR data revealed that 90% of AGP's β-α transition occurred within 10 seconds of mixing with liposomes. Additionally, two distinct rate constants indicated that the transition from the native (N-) state to the membrane-bound (M-) state proceeded via an intermediate (I-) state. Secondary structure contents, segments, and sequences of AGP in the N-, I-, and MB-states were calculated from spectra. Physical parameters of each helical segment suggested that in the first step, two helices in the N-state interacted with the membrane, forming three new helices (I-state), and in the second step, an additional helix formed on the membrane (M-state). These insights provide valuable information for understanding AGP's drug delivery mechanism.

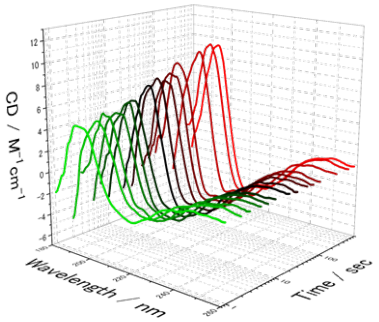

FIGURE. TR-VUVCD data sets in the interaction process between AGP and DMPG liposome.

REFERENCES

1. K. Nishi, T. Mayumura, HB. Halsall, T. Handa, M. Otagiri, *Biochemistry* **43**, 10513-10519 (2004)
2. K. Matsuo, H. Namatame, M. Tanighchi, K. Gekko, *Biochemistry* **48**, 9103-9111 (2009)
3. K. Matsuo, K. Kumashiro, K. Gekko, *Chirality* **32**, 594-604 (2020)
4. S. Hashimoto and K. Matsuo, *Anal. Chem.* **96**, 10524-10533 (2024)

24AG012 BL-12

Structural Dynamics of β-Lactoglobulin in the Interaction Processes with Sodium Dodecyl Sulfate Micelles Observed by Time-Resolved Vacuum-Ultraviolet Circular Dichroism

Satoshi Hashimoto[a] and Koichi Matsuo[a,b,c]

[a]Graduate School of Advanced Science and Engineering, Hiroshima University, 1-3-1 Kagamiyama, Higashi-Hiroshima 739-8526, Japan
[b]Research Institute for Synchrotron Radiation Science, Hiroshima University, 2-313 Kagamiyama, Higashi-Hiroshima 739-0046, Japan
[c]International Institute for Sustainability with Knotted Chiral Meta Matter (WPI-SKCM^2), Hiroshima University, 2-313 Kagamiyama, Higashi-Hiroshima 739-0046, Japan

Keywords: Circular dichroism, β-Lactoglobulin, Membrane interaction, Secondary structures, Time-resolved measurement

Structural transition of proteins induced by the membrane interaction alter their biological function. Hence, the structural dynamics in the membrane-interaction processes is key information to elucidating the mechanisms of expressed function. While vacuum-ultraviolet circular dichroism (VUVCD) spectroscopy has been widely applied to the studies of membrane-bound structures of proteins[1,2], the previous investigations were limited to the static conditions (before and after membrane interaction). To address this, we developed a time-resolved VUVCD (TR-VUVCD) method, enabling real-time observation of structural dynamics[3]. This study analyzed the interaction processes between β-lactoglobulin (bLG) and sodium dodecyl sulfate (SDS) micelles using TR-VUVCD and molecular dynamics (MD) simulations. First, we obtained a TRCD dataset in the 178–260 nm wavelength range within one second, which reflected the structural transitions of bLG due to the SDS interaction. Our analysis identified a single intermediate state, revealing a step-by-step transition of the native (N-) state → intermediate (I-) state → micelle-bound (M-) state. Secondary structure analysis showed that the I-state formed six helices, which were extended and stabilized in the M-state. Second, we conducted the MD simulations to confirm the binding potential of these helices to the micelle surface. Our analysis on the physicochemical properties (charge, hydrophobicity) of each helix and MD-derived parameters such as peptide-micelle distance, hydrogen bonding, and micelle penetration, characterized the key driving forces on the interactions, in which electrostatic interactions contributed at the initial stage (I-state) while hydrophobic interactions played a significant role in stabilizing the final structure (M-state). These results demonstrate that TR-VUVCD combined with MD simulations is a powerful method for characterizing protein dynamics in the processes of membrane interaction, contributing to a deeper understanding of the mechanism of function expression at molecular level.

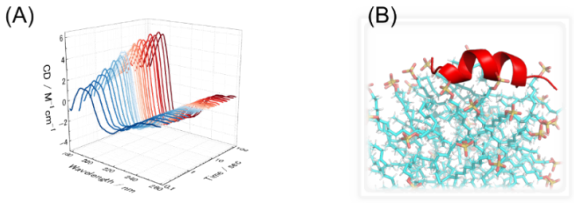

FIGURE. (A) TR-VUVCD data sets in the interaction process between bLG and SDS micelle. (B) The snapshot of MD simulation using Amber program.

REFERENCES

1. K. Matsuo, K. Kumashiro, K. Gekko, *Chirality* **32**, 594-604 (2020)
2. R. Imaura, Y. Kawata, K. Matsuo, *Langmuir* **40**, 20537–20549 (2024)
3. S. Hashimoto and K. Matsuo, *Anal. Chem.* **96**, 10524-10533 (2024)

24BG003 BL-12

Development of a Vertical Circular Dichroism Apparatus for Measuring Aggregated Biomolecules

Aoyama Kuya[1], Imaura Ryota[1], Hashimoto Satoshi[1], Haga Tastuki[1], Mohamed Ibrahim[2], Matsuo Koichi[1,2]

[1]*Graduate School of Advanced Science and Engineering, Hiroshima University*
[2]*Research Institute for Synchrotron Radiation Science, Hiroshima University*

Keywords: Circular Dichroism, Imaging

Circular dichroism (CD) measurements in the vacuum ultraviolet region (~140 nm) using synchrotron radiation are widely utilized for the precise structural and functional research of biomolecules in solutions. However, for solid and semi-solid biomolecules, such as amyloid fibrils which are causative materials of Alzheimer's disease, liquid-liquid phase separation involved in cellular and biological function regulation, and polymer hydrogels, accurate CD measurements are often difficult due to sample locality and anisotropy, which poses an obstacle to structural and functional research. Therefore, we developed a vertical circular dichroism apparatus and attempted to resolve these issues by using spatially resolved measurements with focused light from lenses and mirrors (which would address sample locality) and by introducing a new optical system [1] to resolve sample anisotropy.

As part of the performance evaluation of vertical apparatus, we measured the CD spectrum of camphor sulfonic acid solution, a standard CD sample, and confirmed an intensity ratio of 1:2 at 290 nm and 190 nm. Spatially resolved measurements were performed on the sample containing L- and D-alanine solutions, as well as on alginate gel sample. Although the resolution was low, the intensity and sign of circular dichroism depended on the position and types of samples. We will present the methods capable of removing sample anisotropy, comparing the conventional system.

REFERENCE

1. G. E. Jellison and F. A. Modine "Two-modulator generalized ellipsometry: theory" *Appl. Opt.* **36**(31) 8190-8198 (1997).

24AG015 BL-12

Monitoring the Self-Assembly of Alginate Induced by Calcium Ions Using Circular Dichroism

Tatsuki Haga[a], Masaya Yoshid[a], Takeharu Haino[a], Koichi Matsuo[b] and Mohamed I.A. Ibrahim[b]

[a]*Graduate School of Advanced Science and Engineering, Hiroshima University.*
[b]*Research Institute for Synchrotron Radiation Science (HiSOR), Hiroshima University, 2-313 Kagamiyama, Higashi-Hiroshima, Hiroshima 739-0046 Japan.*

Keywords: Self-assembly, Hydrogel, Circular Dichroism, Phase diagram

Circular dichroism (CD) spectroscopy is a valuable technique for analyzing the secondary structures of proteins and peptides [1]. However, its application to polysaccharide structural studies remains limited. Therefore, evaluating the feasibility of CD spectroscopy for polysaccharide analysis is essential. The alginate (Alg) polysaccharide is known to transition from liquid to gel when exposed to polyvalent ions [2]. This study used CD experiments to investigate the effect of calcium ions (Ca^{2+}) on the structural changes of Alg during self-assembly and hydrogel formation.

In the absence of Ca^{2+}, the CD spectrum of Alg exhibited a peak around 200 nm and a trough near 215 nm (Figure 1a). Both peak intensities and positions gradually changed with increasing Ca^{2+} concentration. Additionally, CD spectra of dried samples closely resembled those of liquid samples, indicating minimal structural changes due to drying. By analyzing the peak intensities and positions in the CD spectra, a phase diagram illustrating self-assembly and aggregation phases was constructed (Figure 1b).

To validate this diagram, ATR and AFM measurements were conducted. ATR spectra showed a peak shift around 1600 cm^{-1}, identifying the concentration range where structural transitions occur, as observed in the CD experiments. AFM measurements were performed at three key concentrations corresponding to the self-assembly, aggregation, and gel states. As Ca^{2+} concentration increased, a densely entangled fibrous structure emerged, correlating with the transition from the self-assembly to aggregation and then to gel state, supporting our findings from CD experiments.

These results highlight the potential of CD spectroscopy for analyzing structural changes in Alg-Ca^{2+} hydrogel system.

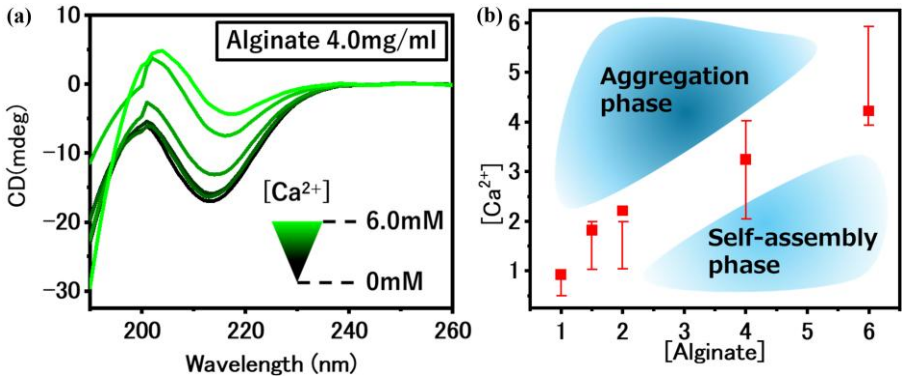

FIGURE 1. CD spectrum of Alg (4.0 mg/ml) as a function of calcium concentration (liquid sample), and (b) proposed phase diagram of Alg-Ca^{2+} system based on CD findings.

REFERENCES

1. K. Matsuo, G. Kunihiko, *Bull. Chem. Soc. Jpn.*, 2013, **86**, 675-689.
2. H. Wang, Y. Wan, W. Wang, W. Lia, and Jie Zhu, *Int. J. Food Prop.*, 2018, **21**, 1995-2006.

24AG028 BL-12

Optical Activity Emergence of Amino-acid Films under Circularly Polarized Lyman-α Light Irradiation

Gen Fujimori[a,b], Masahiro Kobayashi[c], Jun-ichi Takahashi[d], Hiroshi Ota[e,f], Koichi Matsuo[g], Yoshitaka Taira[e], Masahiro Katoh[e,g], Kensei Kobayashi[a,b], Yoko Kebukawa[b], Hiroaki Nakamura[c]

[a]*Yokohama National University, 79-5 Tokiwadai, Hodogaya-ku, Yokohama 240-8501, Japan*
[b]*Institute of Science Tokyo, 2-12-1 Ookayama, Meguro-ku, Tokyo 152-8551, Japan*
[c]*National Institute for Fusion Science, 322-6 Oroshi-cho, Toki 509-5292, Japan*
[d]*Kobe University, 5-1-1 Fukaeminami-cho, Higashinada-ku, Kobe 658-0022, Japan*
[e]*UVSOR Synchrotron Facility, 38 Nishigo-Naka, Myodaiji, Okazaki 444-8585, Japan*
[f]*Japan Synchrotron Radiation Research Institute, 1-1-1 Kouto, Sayo-cho, Sayo-gun 679-5198, Japan*
[g]*Research Institute for Synchrotron Radiation Science, 2-313 Kagamiyama, Higashi-Hiroshima 739-0046, Japan*

Keywords: Homochirality, Amino Acid, Optical Activity, Circularly Polarized Light, Lyman- α , Circular Dichroism.

The origin of homochirality in terrestrial biomolecules (L-amino acid and D-sugar dominant) remains one of the most mysterious problems in the research for the origins of life. One theory about the origin of homochirality is that racemic amino acids produced in outer space were exposed to polarized quantum radiation, such as circularly polarized photons or spin-polarized electrons, inducing asymmetric reactions, which then became asymmetric seeds and were transported to Earth [1, 2].

Among the polarized quantum radiation sources, circularly polarized light (CPL) has been proposed as a source of symmetrical breaking. Recent theoretical calculations have shown that background light scattering by aligned dust particles in interstellar space causes ultraviolet light to become circularly polarized [3], and it is possible that circularly polarized Lyman alpha emitted from star-forming regions in galaxies plays an important role in the origin of homochirality [4].

To verify the cosmogenesis scenario, several ground-based simulation experiments have been investigated using ultraviolet CPL from high-energy particle accelerators. In this study, we focused on the hydrogen Lyman α wavelength of 121.6 nm, where strong emission lines are observed in star-forming regions. We conducted experiments in which a racemic alanine film sample was irradiated with Lyman-α CPL to investigate the photoreaction of biomolecules. Thin solid film samples of a racemic mixture of alanine (DL-alanine) were prepared on CaF_2 substrates from crystalline powder of DL-alanine by vacuum deposition. The irradiated CPL wavelength corresponds to photon absorption bands with the chromophores from the electronic transitions of carboxyl and amino groups (π-σ*) of alanine molecules [5, 6]. The CD spectra of the specimen, before CPL irradiation, were measured using the synchrotron radiation CD beamline BL-12 at the Research Institute for Synchrotron Radiation Science (HiSOR), Hiroshima University, and with the J-1500 CD spectrometer (JASCO Corporation) at the Institute for Molecular Science. The samples were irradiated with L-CPL or R-CPL at hydrogen Lyman-α wavelength of 121.6 nm using undulator beamline BL1U of UVSOR-III. The samples were set in a vacuum sample chamber preventing attenuation by air absorption. The total photon beam intensity irradiated on the sample was monitored with photoelectron current of a silicon photodiode settled at the beam downstream side of the sample holder. The 121.6 nm wavelength radiation from the undulator is reflected by a gold coated mirror located in the mirror chamber directly beam upstream of the sample chamber and then enters the sample chamber. On the beam entrance side of the vacuum sample chamber, a gate valve with an MgF_2 vacuum sealing window (0.5 mm in thickness) was mounted. The use of gold-coated mirror reflections has made it possible to suppress high-energy higher-order light from the undulator source expecting to reduce the transmittance loss of the MgF_2 window due to high-energy radiation induced defects.

After CPL irradiation, the CD spectra was measured by rotating the sample in a plane perpendicular to

the CPL beam by 45° increments to eliminate the effect of the linear component [7]. The obtained CD spectra were averaged to minimize the effects of linear dichroism and birefringence. Circular dichroism (CD) spectrum measurements revealed that irradiation with right-handed (left-handed) CPL induced a positive (negative) anisotropy coefficient g in the wavelength range of 180–240 nm. However, the spectrum was different from that of enantiopure alanine, showing a broad wavelength range and no sign change.

Further studies on the photo-reactions of solid biomolecules under VUV CPL irradiation are required to elucidate the mechanism of optical activity emergence.

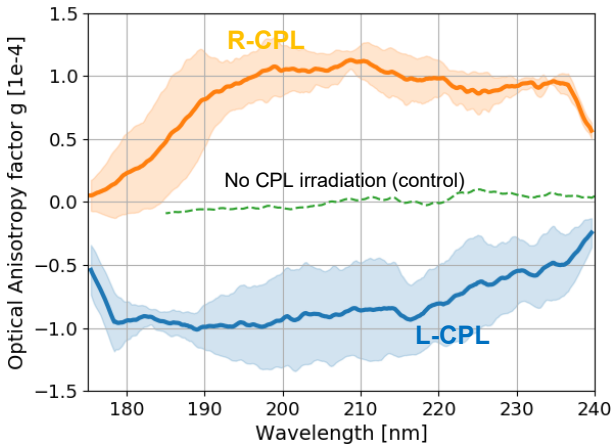

FIGURE 1. Optical anisotropy factor *g* of the DL-alanine samples after Lyman-α R- (orange) and L- (blue) CPL irradiation. Data from three samples were averaged for each case, with error bars representing the 95% confidence interval. The case without CPL irradiation is indicated by the dashed line.

REFERENCES

1. W. A. Bonner, *Orig. Life Evol. Biosph.*, **21**, 407 (1991).
2. J. Takahashi, K. Kobayashi, *Symmetry,* **11**, 919 (2019).
3. H. Fukushima, H. Yajima, M. Umemura, *Monthly Notices of the Royal Astronomical Society*, **524**, 2114 (2023).
4. A. Sato, M. Shoji, N. Watanabe, M. Boero, Y. Shigeta, M. Umemura, *Astrobiology*, **23**, 1 (2023).
5. M. Tanaka, Y. Kodama, K. Nakagawa, *Enantiomer*, **7**, 185 (2002).
6. F. Kaneko, K. Yagi-Watanabe, M. Tanaka, K. Nakagawa, *J. Phys. Soc. Jpn.*, **78**, 013001 (2009).
7. M. Kobayashi, J. Takahashi, H. Ota, K. Matsuo, M. I. A. Ibrahim, T. Minato, G. Fujimori, M. Katoh, K. Kobayashi, Y. Kebukawa, H. Nakamura. *Chirality*, **36**, e70004 (2024).

24BG010 BL-13

Determination of organic molecular film thickness on gold substrates using soft X-ray photoelectron spectroscopy

Shogo Tendo[a], Kakuto Yoshioka, Akinobu Niozu, Shohei Asakura, Yuri Ohura, and Shin-ichi Wada

[a]*Graduate School of Advanced Science and Engineering, Hiroshima University, Higashi-Hiroshima 739-8526, Japan*

[b]*Graduate School of Humanities and Social Sciences, Hiroshima University, Higashi-Hiroshima 739-8524, Japan*

[c]*Research Institute for Synchrotron Radiation Science, Hiroshima University, Higashi-Hiroshima 739-0046, Japan*

Keywords: Self-assembled monolayer (SAM), X-ray photoelectron spectroscopy (XPS), Thickogram analysis.

Self-assembled monolayers (SAMs) enable nanoscale surface functionalization by taking advantage of molecular design flexibility, and are expected to have a wide range of applications including electronic devices, catalysts, biosensors, and solar cells [1]. The electronic conductivity, surface energy, and reactivity of SAMs vary significantly depending on molecular film thickness and orientation. Therefore, precisely determining these structural properties is essential for the design and application of SAMs. In this study, we determined the molecular film thickness using X-ray photoelectron spectroscopy (XPS) and evaluated its validity based on molecular orientation angles determined by near-edge X-ray absorption fine structure (NEXAFS) spectroscopy and structural optimization through density functional theory (DFT) calculations.

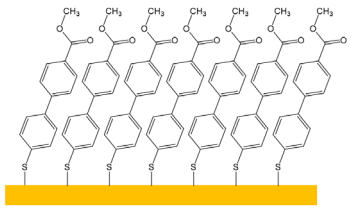

FIGURE 1. Graphical image of MBP SAM.

The experiments were conducted at HiSOR BL-13, a bending magnet beamline suitable for analyzing surfaces composed of light elements. The target samples were SAMs formed by chemisorption via thiol groups onto gold substrates, consisting of six different molecules with varying aromatic backbone structures, each terminating in a methyl ester group. In this study, the methodology for determining film thickness is presented using biphenyl (MBP) SAMs as an example, as shown in FIGURE 1. A wide-scan XPS spectrum of MBP SAMs, acquired with a hemispherical electron energy analyzer at a photon energy of 396 eV, is shown in FIGURE 2.

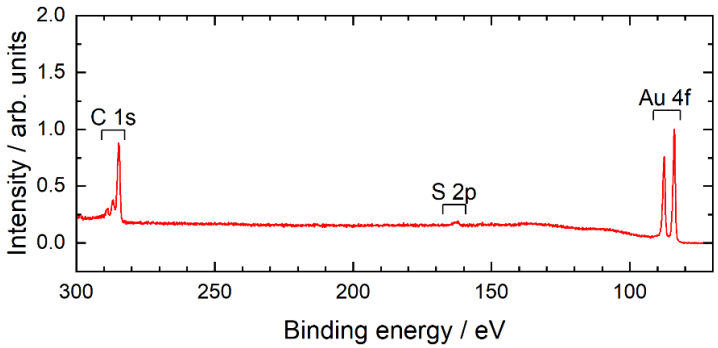

FIGURE 2. Wide-scan XPS spectrum of MBP SAM. The spectrum was acquired at a photon energy of 396 eV, with the intensity normalized to the Au $4f_{7/2}$ peak.

Since photoelectrons undergo inelastic scattering within the molecular film, the intensity of the Au 4f photoelectron peak, I_{Au}, is expressed by equation

$$I_{Au} = s_{Au}\exp(-t/\lambda_{Au}\cos\theta), \quad (1)$$

where t represents the molecular film thickness and θ is the emission angle (0° in this study). The intensity of the C 1s photoelectron peak, I_C, is given by equation

$$I_C = s_C\exp(-t/\lambda_C\cos\theta). \quad (2)$$

λ_{Au} and λ_C denote the inelastic mean free paths (IMFPs) of Au 4f and C 1s photoelectrons, respectively, while s_{Au} and s_C represents their corresponding detection sensitivities. The sensitivity ratio of s_{Au} / s_C was determined using hexadecanethiol SAMs of known molecular film thickness (17.3 Å) [2]. Based on these equations (1) and (2), Cumpson derived the Thickogram equation

$$\ln\left(\frac{I_C\, s_{Au}}{I_{Au}\, s_C}\right) = \ln\sinh\left(\frac{1}{2\lambda_C\cos\theta}\right) + \left[\left(\frac{E_C}{E_{Au}}\right)^{0.75} - \frac{1}{2}\right]\frac{t}{\lambda_C\cos\theta} + \ln 2 \quad (3)$$

for film thickness determination using XPS [3].The IMFP ratio was estimated using an empirical formula based on the ratio of kinetic energies: $\lambda_C/\lambda_{Au} = (E_C/E_{Au})^{0.75}$. Further data analysis was performed using the electron spectroscopy analysis software COMPRO12, developed by Yoshihara. [4], leading to the determination of an MBP SAM thickness of 14 Å. The film thickness was estimated based on the determination of the molecular orientation angle using NEXAFS spectra and the calculation of molecular length via DFT. Figure 3 shows the polarization-dependent NEXAFS spectra at the carbon K-edge. The absorption intensity of the π* peak increased and that of the σ* peak decreased when the angle of incidence of soft X-rays was varied from 20° to 90°. This dependence indicates that the molecules are oriented upright on the substrate. From the fitting analysis of the first peak with an excitation energy of about 285 eV to the π* orbital of the phenyl ring, the molecular orientation angle was determined to be 19°. The film thickness predicted from this orientation angle, the molecular length (12 Å) calculated using DFT (B3LYP/6-31G**), and the S–Au bond length (2.3 Å [5]) was 14 Å, which agreed with the result of Thickogram analysis. This agreement validates the method for determining the thickness of organic molecular films using XPS.

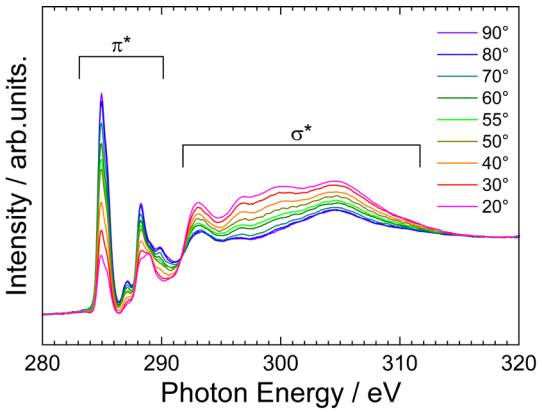

FIGURE 3. NEXAFS spectra of MBP SAM at the carbon K-edge. The polarization dependence was measured by varying the incident angle of soft X-rays from 20° (grazing incidence) to 90° (normal incidence) relative to the substrate.

Thickogram analysis was found to be applicable not only to SAMs on gold substrates but also to SAMs on nanoparticle surfaces [6]. This suggests that the method is a valuable tool for evaluating the thickness of organic thin films in fields requiring nanoscale molecular film control, such as electronic devices, catalysts, and biosensors.

REFERENCES

[1] J. C. Love, L. A. Estroff, J. K. Kriebel, R. G. Nuzzo, and G. M. Whitesides, Chem. Rev. **105**, 1103 (2005).
[2] H. A. Biebuyck, C. D. Bain, and G. M. Whitesides, Langmuir **10**, 1825 (1994).
[3] P. J. Cumpson, Surf. Interface Anal. **29**, 403 (2000).
[4] K. Yoshihara, JSA **23**, 138 (2017).
[5] C. Battocchio, F. Porcaro, S. Mukherjee, E. Magnano, S. Nappini, I. Fratoddi, M. Quintiliani, M. V. Russo, and G. Polzonetti, J. Phys. Chem. C **118**, 8159 (2014).
[6] S. Tendo, A. Niozu, K. Yoshioka, M. Tabuse, J. Adachi, H. Tanaka, and S. Wada, Phys. Chem. Chem. Phys. **27**, 388 (2025).

23BG034, 24BG009 BL-13

DFT calculations for NEXAFS analysis measured for organic molecules

Shohei Asakura[a], Hashimoto Genki[b], Ohura Yuri[a], Shogo Tendo[a], Kakuto Yoshioka[a], Akinobu Niozu[c], and Wada Shin-ichi[a,b,d]

[a] *Faculty of Science, Hiroshima University, Higashi-Hiroshima 739-8526, Japan*
[b] *Graduate School of Science and Engineering, Hiroshima University, Higashi-Hiroshima 739-8526, Japan*
[c] *Graduate School of Humanities and Social Sciences, Hiroshima University, Higashi-Hiroshima 739-8526, Japan*
[d] *Research Institute for Synchrotron Radiation Science, Hiroshima University 739-0046, Japan*

Keywords: NEXAFS (near edge X-ray absorption spectroscopy), DPPC, Phospholipids, DFT(density functional theory)

Density functional theory (DFT) is a powerful technique that allows theoretical predictions of electronic states and is also effective in interpreting X-ray absorption spectra (NEXAFS). However, proper implementation of DFT calculations requires setting parameters and mastering analysis techniques according to the characteristics of the target molecules. Gaining insights into the structure and order of molecular membranes, which are aggregates, is particularly challenging. Therefore, we focused on phospholipid molecules as the molecules forming the molecular membrane and performed DFT calculations on these.

Phospholipids play a vital role in living organisms, especially in forming the basic structure of cell membranes. These membranes are not just physical barriers but also function as sites for information transmission and protein function regulation, deeply involved in fundamental biological activities. Therefore, understanding the structure and properties of cell membranes is crucial for elucidating biological processes. Recent research has advanced by forming biomimetic membranes supported on metal substrates to study their structure and properties. In this context, understanding the electronic structure of lipid membranes is essential, and DFT calculations have gained attention as one method for this analysis.

Additionally, the hydrocarbon chains of lipid molecules are desirable systems for the introduction of DFT calculations. Hydrocarbon chains in lipid molecules are generally composed mostly of saturated chains without carbon-carbon double bonds. This characteristic provides ideal conditions for implementing DFT calculations and is suitable for verifying whether the analysis technique is appropriate through comparison with experimental results. Therefore, in this study, we focused on the hydrocarbon chains of lipid molecules and reproduced NEXAFS spectra using DFT calculations to examine their effectiveness by comparing with experimental results.

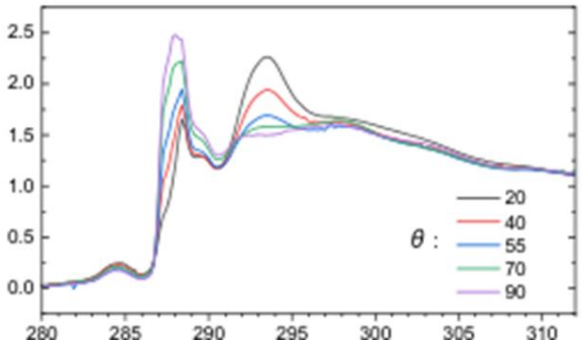

FIGURE 1. The carbon K-edge NEXAFS spectra of phospholipid membranes supported on metal substrates obtained from experiments. θ represents the angle between the soft X-ray and the substrate. The intensity of the spectra changes with θ, indicating orientation dependence.

The carbon K-edge NEXAFS spectra of phospholipid membranes supported on metal substrates obtained from previous studies are shown in Fig. 1. Strong polarization dependence at 288 eV and 293 eV can be observed in these spectra. Previous studies attributed this polarization dependence to the hydrocarbon chains that significantly contribute to the order of the molecular membrane and discussed the orientation and order of the phospholipid membranes on metal substrates. In this study, to verify the transitions attributed in previous studies, we focused on the hydrocarbon chains of DPPC as shown in Fig. 2(a) and assumed a model molecule as shown in Fig. 2(b). Calculations were performed on this molecule, with the superscript letters of each carbon atom representing the labeling used in the spectrum calculation. This model molecule includes carbons thought to be related to the orientation of the lipid membrane. The calculation results of this model molecule allow the decomposition of the soft X-ray absorption spectra of phospholipids into each carbon atom. This information is expected to provide detailed insights into the spectrum.

In the actual calculations, we performed structural optimization of the model molecule using DFT calculations, followed by reproducing the NEXAFS spectra using the TP method, which calculates the energy difference between the ground state and the excited state of the obtained structure. Gaussian16 was used for structural optimization with DFT calculations. The functional used was B3LYP, and the basis set was 6-31G. StoBe/Demon was used for TP method calculations.

The green dashed line in Fig. 3(b) indicates the calibrated position where the first peak of the experimental data matches the *π(C=O) peak from the calculation result of C1. At this point, it was found that the low-energy peak of the experimental data is composed of three peaks originating from C-H* and a peak originating from *π(C=O). The first peak originating from C-H* on the higher energy side of the green dashed line is composed of contributions from carbon atoms adjacent to electronegative oxygen or carbonyl carbons, such as C2, C3, and C4. The remaining peaks originating from C-H* are composed of contributions from C6, C7, and C8 in the hydrocarbon chain. This reveals which positions in the molecule contribute to the three peaks originating from C-H* and the peak originating from π*(C=O) that constitute the first peak of the experimental data.

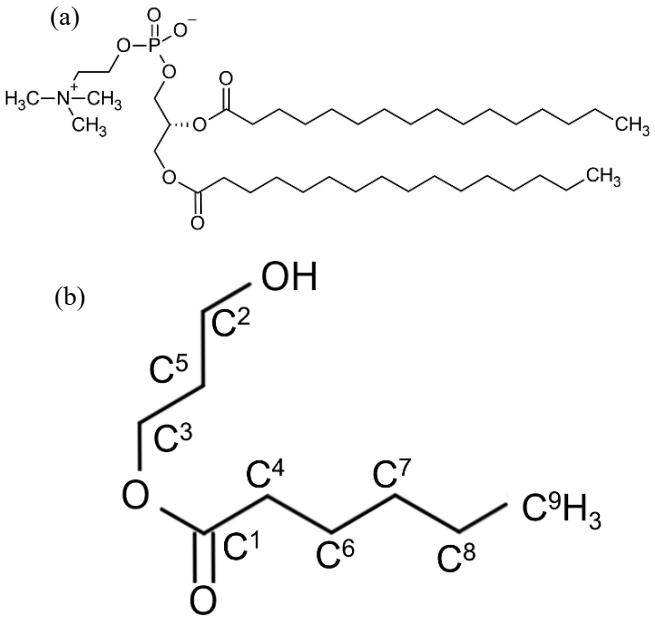

FIGURE 2. (a) Structural formula of DPPC. (b) Structural formula of the model molecule used for theoretical calculations. The superscript letters of each carbon atom represent the labeling used in the calculations.

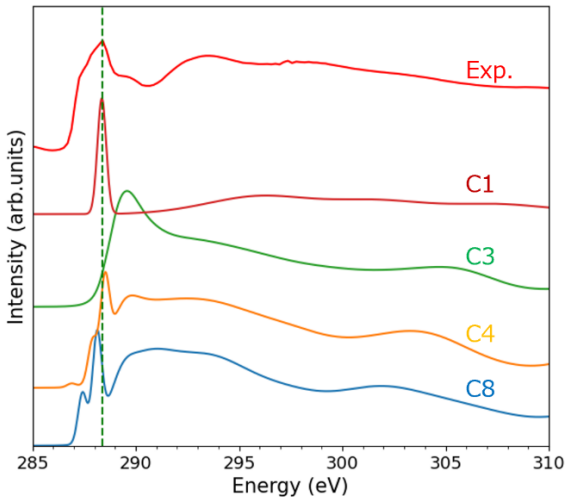

FIGURE 3. Comparison between the NEXAFS spectra obtained from calculations and experimental results.

23BG033, 24BG008 BL-13

Fluorine substitution dependence of ultrafast electron transport in biphenyl monolayers induced by resonant core-excitations

Hayate Inoue[a], Kakuto Yoshioka[b], Shohei Asakura[b], Yuri Ohura[b], Shogo Tendo[b], Akinobu Niozu[c], and Shin-ichi Wada[a,b,d]

[a]*School of Science, Hiroshima University, Higashi-Hiroshima 739-8526, Japan*
[a]*Graduate School of Advanced Science and Engineering, Hiroshima University, Higashi-Hiroshima 739-8526, Japan*
[b]*Graduate School of Humanities and Social Sciences, Hiroshima University, Higashi-Hiroshima 739-8524, Japan*
[c]*Research Institute for Synchrotron Radiation Science, Hiroshima University, Higashi-Hiroshima 739-0046, Japan*

Keywords: Self-assembled monolayer, Auger electron spectroscopy, Core-hole clock.

In recent years, the development of organic materials has attracted much attention in the field of electronic and optical devices. To realize industrial applications of organic materials, it is essential to optimize their electron transport properties and elucidate the correlation between molecular design and electron transport. For this reason, studies investigating the electron transport properties of various molecular systems have been actively conducted [1]. Among these studies, fluorine substitution has been suggested to control electron transport properties. As a method to evaluate electron transport properties, we focused on a technique to investigate the electron transport properties of molecules by observing the Auger decay process with electron transport after inner-shell resonance excitation using soft X-rays [2]. As a platform for this purpose, we focused on self-assembled monolayers (SAMs) where the end groups of molecules are located on the topmost surface of the substrate [3], which allows us to efficiently observe the electron transport from the end groups to the substrate. In this study, we investigated the effect of fluorine substitution positions on electron transport by measuring the kinetic energy of Auger electrons generated after soft X-ray irradiation for biphenyl SAMs with different fluorine substitution sites, as shown in Fig. 1.

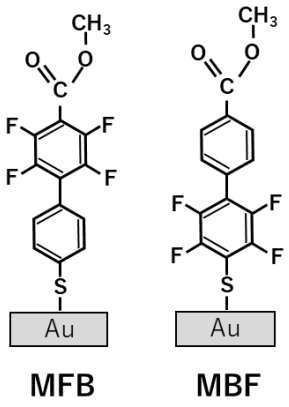

FIGURE 1. Fluorine-substituted SAMs.

Fluorine-substituted SAMs were prepared by immersing gold substrates in 1 mM ethanol solution of each sample for 24 hours and then rinsing with ethanol. Near-edge X-ray absorption fine structure (NEXAFS) and Auger electron spectroscopy (AES) measurements were performed on the prepared fluorine-substituted SAMs at HiSOR BL-13. NEXAFS measurements were performed in the carbon and oxygen K-edge regions, and the carbon K-edge region was measured in the range from 20° to 90° by changing the soft X-ray incidence angle by 10° (Fig. 2). The π* peak was mainly observed at photon energies lower than the ionization threshold (IP), while the σ* peak was observed at higher photon energies. The MFB and MBF molecules were found to be oriented perpendicularly to the gold substrate.

Next, AES measurements were performed on fluorine-substituted SAMs and insulating alkyl chain SAMs, where electron transport cannot occur. Fig. 2 shows the AES spectra of the carbonyl group when excited at 532 eV, which is the excitation energy from the oxygen 1s orbital to the π*(C=O) orbital, where the resonant

Auger decay and electron transport processes compete. The AES spectrum at 525 eV was used to subtract the photoelectron signal from the AES spectra at 532 eV and 540 eV. The 532 eV AES spectra of fluorine-substituted SAMs, shown as white circles in Fig. 2, are the pure resonance AES spectra of insulating alkyl chain SAMs, shown as yellow-green lines, and the equivalent Auger decay spectrum with electron transport, shown as gray lines. The AES spectrum at 532 eV of insulating alkyl chain SAMs was reproduced as shown in the red fitted line by fitting analysis using a linear combination of the pure resonance AES spectrum of insulating alkyl chain SAMs (yellow-green line) and the AES spectrum of normal Auger decay, which is equivalent to Auger decay with electron transport (gray line). To quantitatively compare the electron transport processes, the analysis was performed using the core-hole clock method, which determines the electron transport time with respect to the core-hole lifetime τ_{core}= 3.85 fs [4] for oxygen 1s from the fraction P of the normal Auger component.

$$\tau_{CT} = \tau_{CH} \frac{1-P_{CT}}{P_{CT}}. \quad (1)$$

The electron transport times were 15.7 ± 0.4 fs for MFB and 16.8 ± 0.4 fs for MBF, indicating that electron transport in MFB is about 1 fs faster. To discuss the results, we performed first-principles calculations of the lowest unoccupied molecular orbitals (LUMOs) involved in electron transport and found no clear difference in the LUMO shapes of the two molecules that could explain the difference in electron transport time. Since the molecular orbitals of the chemisorbed species are expected to change due to orbital hybridization with the Au substrate, a detailed understanding of each molecule would be obtained by performing first-principles calculations that consider the effect of the Au substrate.

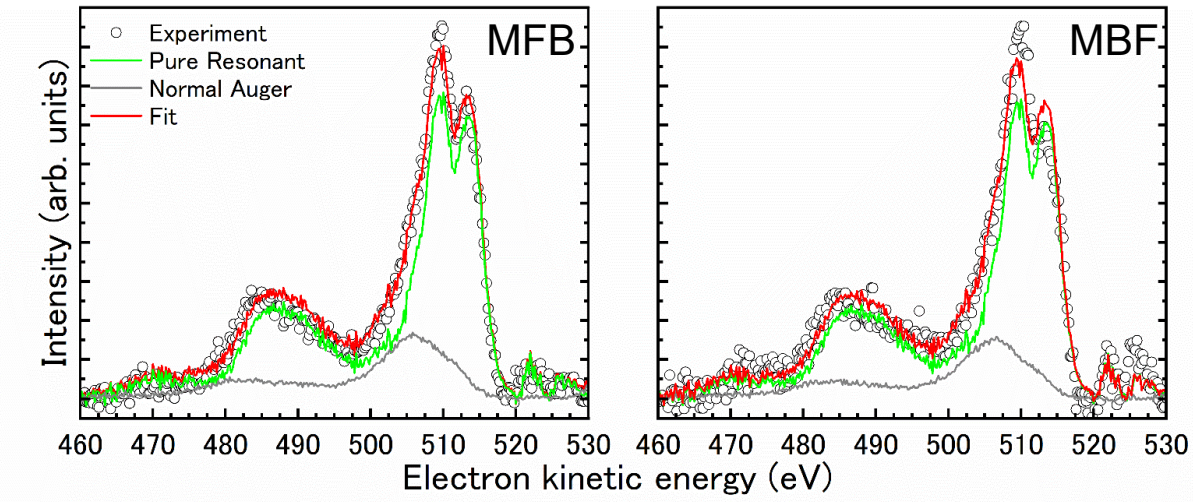

FIGURE 2. AES spectra (white circles) of MFB (left) and MBF (right). The fitted lines (red) are obtained by linear combination of the resonant Auger component (green) and the electron transport component (gray).

REFERENCES

[1] R. L. Carroll and C. B. Gorman, Angewandte Chemie International Edition **41**, 4378 (2002).
[2] M. Zharnikov, Acc. Chem. Res. **53**, 2975 (2020).
[3] J. C. Love, L. A. Estroff, J. K. Kriebel, R. G. Nuzzo, and G. M. Whitesides, Chem. Rev. **105**, 1103 (2005).
[4] C. Nicolas and C. Miron, Journal of Electron Spectroscopy and Related Phenomena **185**, 267 (2012).

BL-14

Structural analysis of Co/h-BN/Ni(111) using low-energy electron diffraction

Shen Zili [a] and Masahiro Sawada [b]

[a] *Graduate School of Advanced Science and Engineering, Hiroshima University*
[b] *Research Institute for Synchrotron Radiation Science, Hiroshima University*

Keywords: Hexagonal boron nitride (h-BN), Magnetic tunnel junction (MTJ), Low energy electron diffraction (LEED)

TMR devices used in magnetic read heads, magnetic memory (MRAM), magnetic field sensors, etc. have a ferromagnetic tunnel junction (MTJ) structure (ferromagnet/insulator/ferromagnet layers) whose interfacial structure and magnetic state are crucial for performance of the TMR effect. In this study, we focus on a junction structure using a single layer of hexagonal boron nitride (h-BN) as an insulator layer in the MTJ structures. Hexagonal boron nitride is chemically inert and can be used as a monoatomic barrier layer because of its insulating band gap of about 6eV, and its elastic chemical bond network of honeycomb structure has an advantage to uniform formation of monatomic films with few defects and pinholes. Furthermore, magnetic transition metals such as Ni, Co, and Fe are expected to form ideal epitaxial interfaces because of their good lattice matching with the h-BN honeycomb [1]. In order to utilize MTJ structures consisting of a single h-BN burrier layer as high-performance TMR devices, it is necessary to establish monatomic control of film fabrication and investigate their interfacial magnetism and interface structure. In a previous study [2], it has been shown that ultrathin Co layers two-dimensionally grown on h-BN/Ni(111) exhibit antiferromagnetic interlayer magnetic interactions between Co layer and Ni substrate, but their interface structures have not sufficiently been investigated.

In this study, we fabricated ultrathin films of Co grown on h-BN/Ni(111) and analyzed the interface structure in atomic-scale. Quantitative analysis of low energy electron diffraction (LEED) allows the atomic arrangement in the near-surface region to be determined with sub-angstrom accuracy, where the diffraction spot intensities are carefully measured as a function of the electron beam energy (LEED I-V). A numerical package [3] is used to determine the bast structural model reproduces the experimental LEED I-V, whose numerical calculation can simulate realistic LEED diffraction intensities by means of a multiple scattering model. The calculations for 1ML and 2ML-Co/h-BN/Ni(111) have provided best-fit structural models as shown in Figure 1. Parameters of interlayer distance are optimized for Co-BN and Co-Co layers. In both cases of overlayer thickness of 1ML and 2ML, the Co-BN distance (1.85Å and 1.88Å) are similar, indicating the stable atomic distances in the interface of Co/BN and no modification in the interfacial magnetic interaction between Co and Ni thorough a h-BN layer.

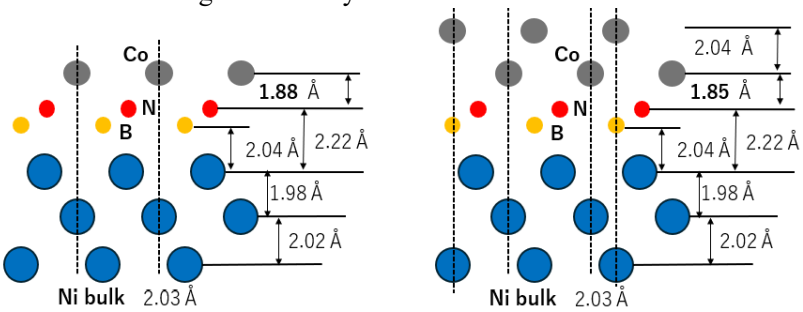

FIGURE1 Structure models for (a) 1ML and (b) 2ML-Co/h-BN/Ni(111) optimized by LEED I-V calculation.

REFERENCES

1. A. Nagashima *et al.*, Phys. Rev. Lett. 75, 3918 (1995).
2. Wataru Tadano, Masahiro Sawada, Hirofumi Namatame, Masaki Taniguchi Journal of Electron Spectroscopy and Related Phenomena 220 (2017) 105-10; Master's Thesis by Ichikawa (2018) Hiroshima Univ.
3. Barbieri/Van Hove STALEED and Phase Shift package

BL-14 (HiSOR beamline number)

Magnetic and Transport Properties of Thin Films of MnTe Altermagnet Candidate

H.Sato[a] and Y.Fujisawa[b]

[a] *Faculty of Science, hiroshima University*
[b] *HiSOR*

Keywords: Enter keywords.

In recent years, magnetic materials called alternating magnetic materials have been attracting attention. Alternating magnets are antiferromagnets that break time-reversal symmetry by multiple sublattices consisting of magnetic atoms and surrounding nonmagnetic atoms[1].

This magnetic material has spin splitting of the bands originating from time-reversal symmetry breaking, and various physical phenomena related to it are expected to occur [2]. In particular, the anomalous Hall effect in this magnetic material occurs despite the fact that the overall magnetization is zero, and the characteristic electronic state is considered to be the origin [3].

MnTe, the subject of this study, consists of two types of Mn sublattices, one consisting of magnetic Mn atoms and the other of nonmagnetic Te atoms, and its two spins are alternately aligned along the c-axis, thus satisfying the conditions for alternating magnetism (Fig.1).

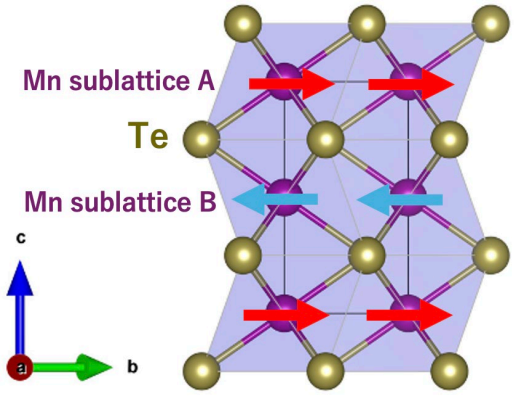

Fig.1 Crystal and magnetic structure of MnTe

The electronic state can be observed by SARPES, and it has been reported that when alternating magnets are grown as thin films on single-crystal substrates by molecular beam epitaxy (MBE), their physical properties differ depending on the substrate used, including magnetization, Hall resistance behavior, and strain [4].

MnTe thin film on SrF_2 substrate has an antiferromagnetic magnetization curve and hysteresis of Hall resistance due to anomalous Hall effect, while MnTe thin film on GaAs substrate has a weak ferromagnetic magnetization curve with small hysteresis and no hysteresis Hall resistance observed (Fig. 2).

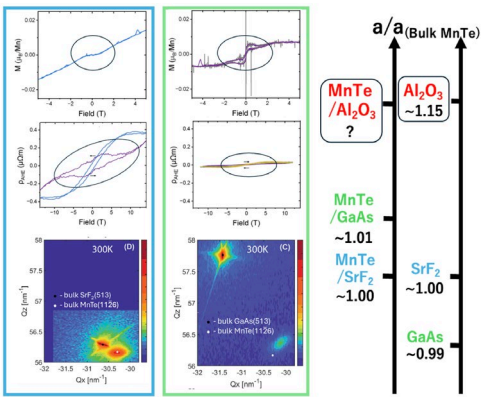

Fig2. Magnetic field dependence of magnetization and Hall resistance of MnTe thin films grown on different substrates using MBE: SrF_2 substrate (blue box), GaAs substrate (green box)[6], Ratio of the in-plane lattice constant (a) of the MnTe film and substrate on each substrate to the lattice constant (a_0) of bulk MnTe

This difference is expected to be due to the strain that the MnTe films are subjected to from the substrate, and the magnitude of the difference in lattice constant of these MnTe films from bulk MnTe, MnTe/GaAs>MnTe/SrF_2. However, the magnitude of the difference in lattice constant between the epitaxial surface of the substrate and bulk MnTe is GaAs<SrF_2, and the magnitude of strain is not simply determined by the difference in lattice constant between the substrate and MnTe (Fig.2).

Therefore, in this study, we newly set up an MBE apparatus to measure the strain applied to the thin film and its physical properties using an Al_2O_3 substrate, which has a larger difference in lattice constant from bulk MnTe than SrF_2 and GaAs, and to verify the relationship between the strain applied to the thin film and the physical properties.

As a result, the following physical property behaviors were observed in the MnTe/Al_2O_3 prepared in this study.

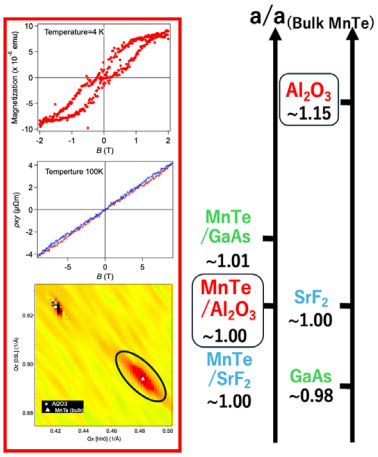

Fig.3Results of this study

There is hysteresis in the magnetization and no hysteresis in the Hall resistance (Fig. 3). This behavior is similar to that of MnTe/GaAs, but the distortion is closer to that of MnTe/SrF_2 (Fig. 3).

This suggests that the difference in physical properties is not due solely to substrate distortion.

REFERENCES

[1]. Libor Šmejkal, Jairo Sinova *et al*. PHYSICAL REVIEW X 12, 040501 (2022)
[2]. T. Osumi *et al*. PHYSICAL REVIEW B 109, 115102 (2024)
[3]. Libor Šmejikal *et al*. SCIENCE ADVANCES Vol 6, Issue 23 (2020)
[4]. Sara Bey *et al*. ArXiv,2409.04567(2024)

24AU015-17 Quantum leap

Activity and Characteristics of Ni-Based Hybrid Catalysts with Promoters for Ammonia Methanation

Reiji Sunamoto[a], Hiroki Miyaoka[a], Takayuki Ichikawa[a] and Hitoshi Saima[a]

[a]*Hiroshima University, Higashi-Hiroshima, Japan*

Keywords: carbon dioxide, ammonia, methane

Background:

As one of the carbon recycle techniques, we propose ammonia methanation, which directly synthesizes methane from carbon dioxide and ammonia. Ammonia methanation (1) is a combination of the Sabatier reaction (methane synthesis) (2) and ammonia decomposition (3).

$$CO_2 + 8/3\,NH_3 \rightarrow CH_4 + 4/3\,N_2 + 2H_2O \quad \Delta H = -42.5\ \text{kJ} \tag{1}$$

$$CO_2 + 4H_2 \rightarrow CH_4 + 2H_2O \quad \Delta H = -165.0\ \text{kJ} \tag{2}$$

$$8/3\,NH_3 \rightarrow 4/3\,N_2 + 4H_2 \quad \Delta H = -122.5\ \text{kJ} \tag{3}$$

Since the heat generation from ammonia methanation is about 1/4 compared with that of the Sabatier reaction (2), conventional adiabatic reactors can be used. On the other hand, the issue of ammonia methanation is that suitable catalysts to accelerate both reactions should be designed effectively. In a previous study, ammonia methanation was conducted using a hybrid catalyst consisting of Ni/Al_2O_3 for ammonia decomposition and Ni/CeO_2 for methane synthesis, achieving about 60% of methane yield at 500°C and 0.4 MPa. The ammonia decomposition rate in this condition was about 57%.[1] In this study, effective ammonia decomposition catalysts with promoters are prepared to enhance the catalysis at low-temperature regions, and their catalytic activity is investigated.

Experimental Methods:

Ni/Al_2O_3 (Ni: 10 wt%) was used as a catalyst for ammonia decomposition. Alkaline metals, which are K, Li, Na, K, Rb, and Cs, were added to the catalyst as promoters, where the number of promoters was 2 wt% to the Ni catalyst. The hybrid catalyst was prepared by mixing Ni-Ba/ Al_2O_3 and Ni/CeO_2(Ni: 20wt%) as a catalyst for ammonia methanation. The catalysts are characterized by X-ray absorption spectroscopy. (Quantum leap)

Results and discussion:

The results of ammonia decomposition at 500 °C by using the prepared catalysts with alkaline metals are shown as follows,

$$Ni/Al_2O_3\ (75\%) > K\ (71\%) > Na\ (67\%) > Cs\ (64\%) \approx Rb\ (63\%) > Li\ (51\%)$$

Ni/Al_2O_3 without a promoter showed the highest ammonia decomposition rate. Among the alkaline metal species, K showed the highest ammonia decomposition rate. A plot of the relationship between ammonia decomposition rate and electronegativity for catalysts with alkaline metal species showed a volcanic-type trend (Fig. 1). From the results, it was expected that the peak is in the region of 0.82~0.93, and the corresponding element is only Ba. Therefore, the catalyst with Ba was prepared, and its catalysis for the ammonia decomposition reaction was evaluated. As shown in Figure 1, the Ba-added catalysts showed the highest catalytic activity with a 77% decomposition rate. Fig.2 shows the XANES spectra. The spectrum

of Ni-Ba was slightly shifted to the oxidation side and different from the spectra of other catalysts. This chemical state might contribute to the highest catalytic activity of Ni-Ba.

The results of ammonia methanation experiments are shown in Fig. 3. The highest methane yield, 73%, was obtained by using the Ni catalyst at 550 °C and 0.5 MPa.

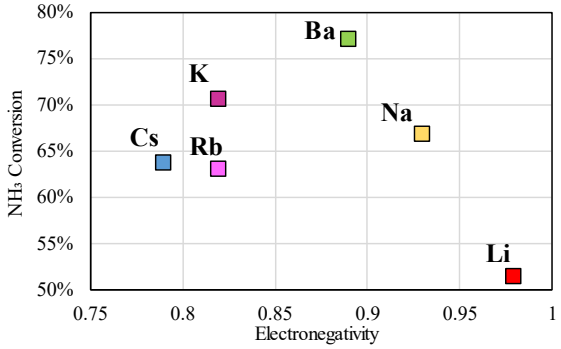

FIGURE 1. Relationship between ammonia decomposition rate and electronegativity

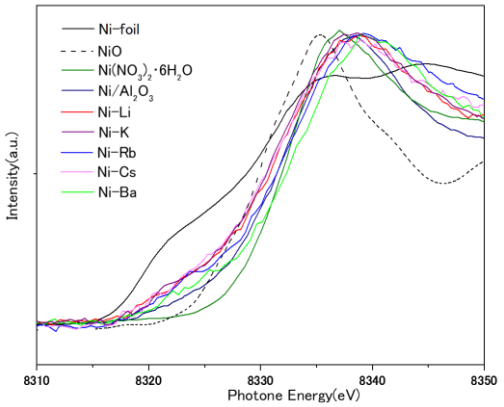

FIGURE 2. XANES spectra of the Ni-K edge.

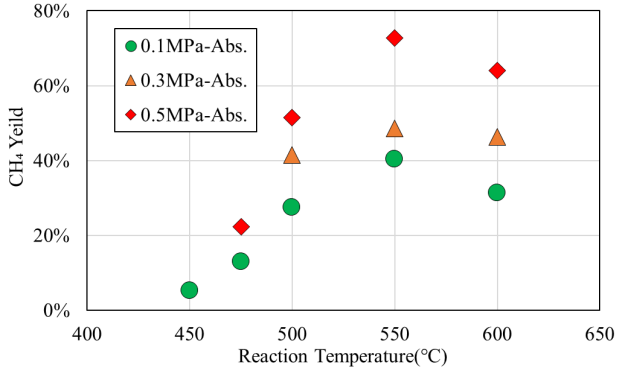

FIGURE 3. Methane yield of ammonia methanation with hybrid catalysts of Ni-Ba/Al_2O_3 and Ni/CeO_2

REFERENCES

1. Hitoshi Saima, Reiji Sunamoto, Hiroki Miyaoka, and Takayuki Ichikawa, *Ammonia Methanation of Carbon Dioxide with a Hybrid Catalyst*, JOURNAL OF CHEMICAL ENGINEERING OF JAPAN, 2023, Volume 56.

Experimental Study on Single Electron Storage in 2024

Y. Asai[a], M. Shimada[b,c], H. Miyauchi[b,c] and M. Katoh[c,d]

[a]*Graduate School of Advanced Science and Engineering Hiroshima University, 1-3-1 Kagamiyama Higashi-Hiroshima 739-8526, Japan*
[b]*High Energy Accelerator Research Organization (KEK), 1-1 Oho Tsukuba 305-0801, Japan*
[c]*Research Institute for Synchrotron Radiation Science, Hiroshima University, 2-313 Kagamiyama Higashi-Hiroshima 739-0046*
[d]*UVSOR Synchrotron Facility, 38 Nishigo-Naka Myodaiji Okazaki 444-8585, Japan*

Keywords: electron, photon, insertion device, undulator, synchrotron radiation, quantum mechanics

We have started single-electron storage [1] experiments at UVSOR-III since 2021 with the aim of conducting fundamental research on electromagnetic radiation. At BL1U, we extracted undulator light in the UV region at a wavelength of 355 nm into the atmosphere and observed its intensity using a photomultiplier tube. By using appropriate band-pass filters to reduce background light and a beam scraper to decrease the electron beam intensity, we succeeded in observing a step-function-like intensity change [1] under a small number of electron storage conditions with a good SN ratio, confirming single-electron storage.

In the fiscal year 2022, we advanced the sophistication and labor-saving of single electron storage technology and began experiments to observe synchrotron radiation from single electrons. As a result, we successfully confirmed that the undulator radiation from a single electron follows a Poisson distribution, with the number of emitted photons per pass being much less than one, which is consistent with the theoretical calculations based on classical electrodynamics [2]. In addition, we also observed the photon statistics from numerous electrons of the order of 10^8 and the results are also consistent with Poisson statistics. Additionally, as part of the beam dynamics research related to single electron storage, we investigated the relationship between the insertion depth of the beam scraper, and the beam lifetime. The results suggest that the lifetime weakly depends on the insertion depth when it is a few hundred microns from the beam center but strongly depends on it when it is closer. We speculate that the gas-scattering lifetime is dominant in the former region but the quantum one in the latter.

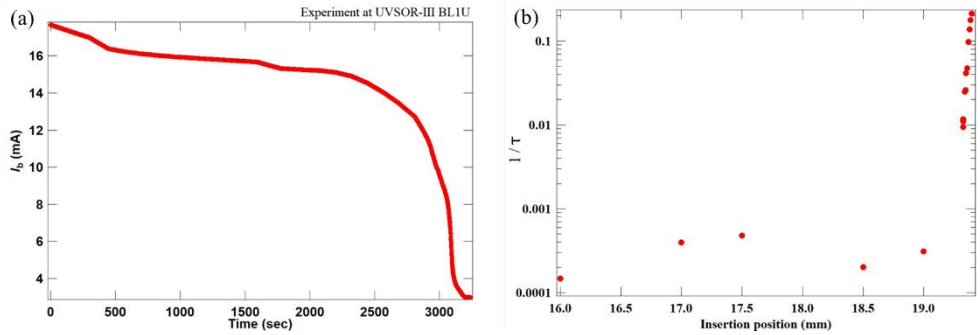

FIGURE 1. Relationship between beam scraper insertion position and beam lifetime

REFERENCES

1. R. Klein, R. Thornagel, and G. Ulm, *Metrologia* **47**, R33 (2010).
2. K. J. Kim, "CHARACTERISTICS OF SYNCHROTRON RADIATION" in *Physics of Particle Accelerators: Fermilab Summer School, 1987; Cornell Summer School, 1988*, edited by M. Month et al., AIP Conference Proceedings 184, American Institute of Physics, New York, 1989, pp. 589-601.

Application of Machine Learning to Accelerator Beam Transport Systems

R. Sakurai[a] , M. Shimada[a,b] , H. Miyauchi[a,b] , T. Obina[b] and M. Katoh[a,b,c,d]

[a] *Faculty of Science, Hiroshima University, 1-3-1Kagamiyama Higashi-Hiroshima 739-8526, Japan*
[b] *High Energy Accelerator Research Organization (KEK), 1-1 Oho Tsukuba 305-0801, Japan*
[c] *Research Institute for Synchrotron Radiation Science, Hiroshima University, 2-313 Kagamiyama Higashi-Hiroshima 739-0046*
[d] *UVSOR Synchrotron Facility, 38 Nishigo-Naka Myodaiji Okazaki 444-8585, Japan*

Keywords: Light Source, Accelerator, Electron Beam, Machine Learning

In recent years, the need for sustainability has driven efforts to improve energy efficiency and reduce operational workload in synchrotron light sources. For small-scale facilities like HiSOR at Hiroshima Synchrotron Radiation Center, which is being operated with a few staff members, automation of accelerator tuning is particularly crucial. The next-generation HiSOR-2 plans to introduce top-up operation [1], requiring stable injection efficiency over long periods, making automation indispensable.

This study focuses on the automatic tuning of beam transport systems using machine learning. Experiments were conducted at the Photon Factory (PF) at KEK to automate the beam injection process from the injector to the storage ring. We aimed to suppress stored beam oscillations and maximize injection efficiency using Bayesian optimization. Simulations compared two approaches: (1) minimizing the Courant-Snyder invariant and (2) minimizing orbit deviation at a specific point in the ring, with the latter chosen for experiments. The experimental results showed that automatic adjustment of the kicker magnet effectively suppressed stored beam oscillations. Additionally, tuning the kicker and septum magnets improved injection efficiency.

Furthermore, we explored the simultaneous optimization of oscillation suppression and injection efficiency. The results demonstrated that automatically adjusting multiple injection system parameters could enhance efficiency while minimizing oscillations. These findings contribute to the advancement of automation technology in small-scale synchrotron light sources, providing a foundation for future implementations, including in HiSOR-2. As synchrotron facilities increasingly require stable, efficient, and low-maintenance operations, these automation techniques are expected to play a crucial role in next-generation accelerator systems.

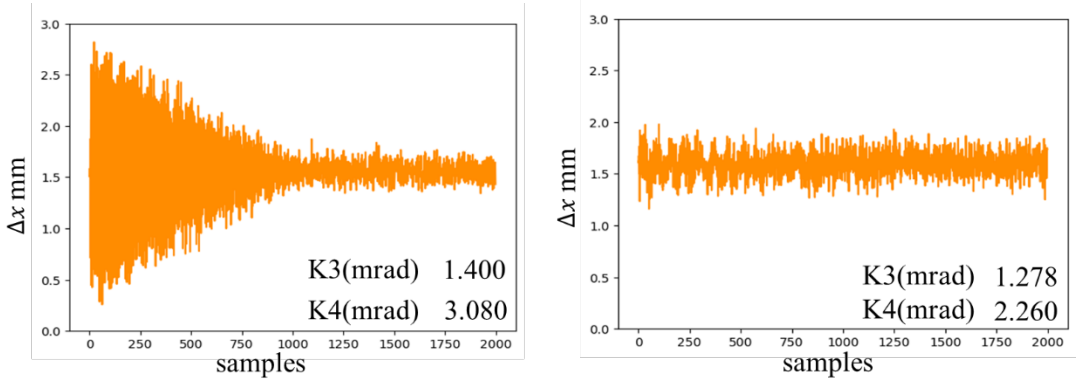

Figure 1: Changes in Electron Oscillations Before and After Optimization

REFERENCES

1. M. Katoh et al., AIP Conf. Proc. 1234, 531 (2010)

Observing Electronic Dynamics within 100 fs in 2H-$MoTe_2$ by Double-excitation Ultrafast Electron Diffraction

Yui Iwasaki[a], Gaël Privault[a], Haruki Taira[a], Ryota Nishimori[a], Takumi Fukuda[b], Muneaki Hase[a], Yusuke Arashida[a], and Masaki Hada[a]

[a]*University of Tsukuba, Tsukuba, Ibaraki 305-8573, Japan*
[b]*Okinawa Institute of Science and Technology, Kunigami-gun, Okinawa 904-0495, Japan*

Keywords: Pump-probe experiments, Ultrafast electron diffraction, Nonlinear optical effect, Saturable absorption, Femtosecond carrier dynamics, Transition metal dichalcogenides

Transition metal dichalcogenides (TMDs) are two-dimensional layered materials, especially $MoTe_2$ which exhibits a semiconductor, semimetal and Weyl semimetal phases [1,2]. Understanding the carrier dynamics in semiconducting materials is important because the properties of these compounds are affected by the behavior of hot carriers in the conduction and valence bands. Electronic relaxations have been directly observed by two-photon photoelectron spectroscopy and time-resolved angle-resolved photoemission spectroscopy [3,4]. We proposed a unique method to understand the electronic relaxation dynamics in semiconducting materials. The use of a double-optical-pulse excitation ultrafast time-resolved electron diffraction measurements under saturable absorption conditions [5] enabled to observe electronic relaxation of hot carriers in the conduction band of 2H-$MoTe_2$ [6]. We found that the momentum relaxation of excited electrons occurred within 100 fs in the conduction band of 2H-$MoTe_2$. Because the time constant of the momentum relaxation was comparable to the duration of the excitation pulse, it was required to measure the time constant of the electronic scattering more precisely. To measure extremely fast electron scattering (within 100 fs), we need to use an ultrafast time-resolved electron diffraction setup with shorter excitation optical pulses. Our laboratory constructed a setup that generates an ultrashort optical beam (wavelength: 800 nm, duration: 35 fs) and an electron pulse (duration: ~100 fs) with a compression cavity [7]. We introduced the double-pulse excitation system with a Mach-Zehnder interferometer in the pump line for the double-optical-pulse ultrafast time-resolved electron diffraction measurement. We measured the pulse duration of the excitation beam (wavelength: 400 nm) by auto- and cross-correlation to be approximately 62 fs (FWHM). This result shows that we can observe the momentum relaxation of electrons with a time resolution of approximately 30 fs. Then, we measured the fluence range to induce a saturable absorption in the 2H-$MoTe_2$ sample at approximately 3–8 mJ/cm^2. After setting up the systems, the electron relaxation in the momentum direction will be investigated by using the ultrafast time-resolved electron diffraction setup, with the electron compression system.

REFERENCES

1. D. H. Keum, et al., *Nature Physics* **11**, 482-486 (2015).
2. K. Deng, et al., *Nature Physics* **12**, 1105-1110 (2016).
3. U. De Giovannini, et al., *Nano Letters* **16**, 7993-7998 (2016).
4. L. Wang, et al., *Nano Letters* **18**, 5172-5178 (2018).
5. T. Fukuda, et al., *Journal of Physical Chemistry C* **127**, 13149-13156 (2023).
6. Y. Iwasaki, et al., *Applied Physics Letters* **123**, 181901 (2023).
7. K. Takubo, et al., *Review of Scientific Instruments* **93**, 053005 (2022).

Direct Measurement of Compressed Electron Pulse Duration through the Interaction with Terahertz Waves

Haruki Taira[a], Ryota Nishimori[a], Kaito En-ya[a], Godai Noyama[a], Gael Privault[a], Yusuke Arasida[a], Kou Takubo[b], Sin-ya Koshihara[b], Shoji Yoshida[a] and Masaki Hada[a]

[a] *University of Tsukuba, 305-8573, Tsukuba, Japan*
[b] *Institute of Science Tokyo, 152-8550, Ookayama, Japan*

Keywords: Ultrafast time-resolved electron diffraction, Terahertz wave, Electron beam, Terahertz streaking, Pulse duration measurement.

Ultrafast time-resolved electron diffraction is one type of pump-probe measurement that uses an electron pulse as a probe. This methodology directly observes the structural dynamics of atomic and molecular rearrangements induced by photoexcitation on the femtosecond to the picosecond timescales [1]. Since the electrons are charged particles, they can be controlled with an external electrical field. Recently, the probe electron pulses for ultrafast time-resolved electron diffraction and electron microscopy have been controlled with the terahertz (THz) wave [2,3], where the THz wave can be used to accelerate or deflect the electron pulses and to measure the duration of the electron pulses. The THz wave has also been employed as a pump pulse [4]. Here, we are developing a time-resolved electron diffraction measurement setup with a radio-frequency cavity to compress the electron pulses [5]. To measure the compressed electron pulse, we conducted a THz streaking experiment. This experiment generates an instantaneous electric field by irradiating a metal resonator with a THz pulse. The electric field deflects the electron pulse as it passes through the metal resonator. According to the time evolution of the beam width or center position of the electron pulses, we can directly measure the pulse duration of the electron pulse.

The THz generation system is based on an organic BNA crystal. The THz wave is focused on the metal resonator using a lens with a focal length of 30 mm in the vacuum chamber. The polarization axis of the generated THz electric field is horizontal to the resonator; therefore, the electron pulse is horizontally deflected. Without compression by the RF cavity, the pulse duration was estimated to be 9.8 ps based on the spread of the electron beam width [Fig. 1(a)]. With the RF cavity activated, both the spread of the electron beam width and the oscillations in its center position were observed. Several Gaussian functions, synchronized with the oscillation of the center position of the electron beam and sharing the same full width at half maximum (FWHM), were fitted to the temporal profile of the electron beam width to determine the pulse duration [Fig. 1(b)]. Since the FWHM of the electron beam width was measured to be 2.3 ps, the compressed electron pulse duration was determined to be less than this value. Further improvements in the setup and additional analysis will enable more precise pulse duration measurement.

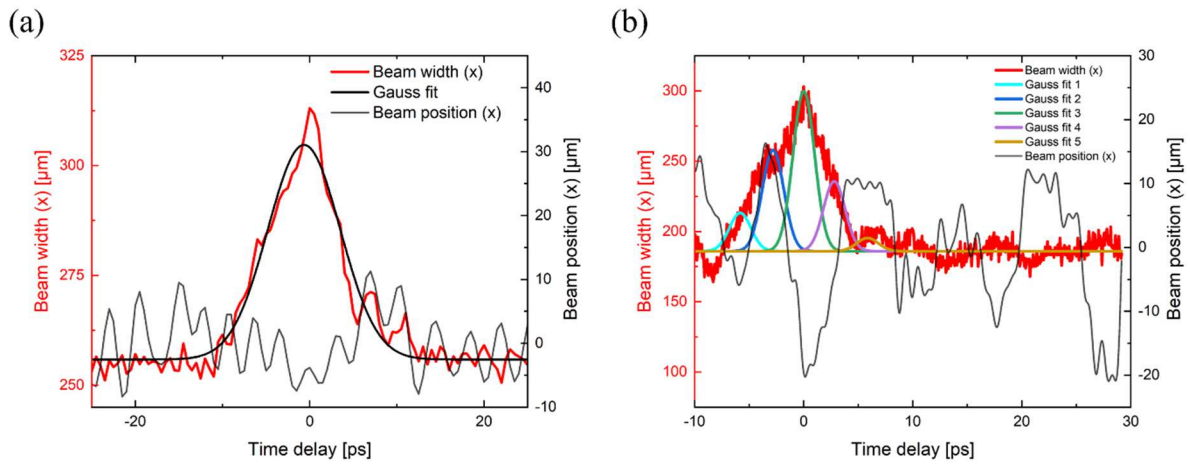

FIGURE 1. Time evolution of the beam width (red line) and center position (gray line) of the electron pulse. (a) Without electron pulse compression. The black line indicates the fitted Gaussian function, with the FWHM of the electron beam width being 9.8 ps. (b) With electron pulse compression. The colored lines (except for the red one) indicate the fitted Gaussian functions, synchronized with the oscillation of the center position of the electron beam and sharing the same FWHM (2.3 ps).

REFERENCES

1. R. J. D. Miller, *Science* **343**, 1108-1116 (2014).
2. C. Kealhofer, W. Schneider, D. Ehberger, A. Ryabov, F. Krausz and P. Baum, *Science* **352**, 429-433 (2016).
3. D. Zhang, A. Fallahi, M. Hemmer, X. Wu, M. Fakhari, Y. Hua, H. Cankaya, A.-L. Calendron, L. E. Zapata, N. H. Matlis, F. X. Kärtner, *Nature Photonics* **12**, 336-342 (2018).
4. B.K. Ofori-Okai, M.C. Hoffmann, A.H. Reid, S. Edstrom, R.K. Jobe, R. Li, E.M. Mannebach, S.J. Park, W. Polzin, X. Shen, S.P. Weathersby, J. Yang, Q. Zheng, M. Zajac, A.M. Lindenberg, S.H. Glenzer, and X.J. Wang, *Journal of Instrumentation* **13**, P06014 (2018).
5. K. Takubo, S. Banu, S. Jin, M. Kaneko, W. Yajima, M. Kuwahara, Y. Hayashi, T. Ishikawa, Y. Okimoto, M. Hada, S. Koshihara, *Rev. Sci. Instrum.* **93**, 053005 (2022).

Hydration structure of inorganic salt solutions at various concentrations: A molecular dynamics approach

Ayana Sato [a], Nanami Shima [b], Osamu Takahashi [c]

[a] *Department of Chemistry, Faculty of Science, Hiroshima Univ.*
[b] *Chemistry Program, Graduate School of Advanced Science and Engineering, Hiroshima Univ.*
[c] *Research Institute for Synchrotron Radiation Science, Hiroshima Univ.*

Keywords: Molecular dynamics (MD) simulation, soft X-ray emission spectroscopy (XES), computational chemistry

Traditionally, water treatment membranes have been considered to function based on the molecular sieving principle. However, ion permeability measurements using a liquid crystal polymer membrane developed by Watanabe et al. [1] showed that $MgSO_4$ exhibited than NaCl. This suggests that the selective ion permeability is influenced not only by the ions themselves but also by the hydrogen bonding structure and stability of water molecules surrounding the ions.

To understand ion permeability, it is first necessary to examine the hydration structures of salt ions in detail. Therefore, we investigated the behavior of ions in salt solutions and the structure of water molecules.

Molecular dynamics (MD) simulations were performed for NaCl and $MgSO_4$ aqueous solutions at various concentrations up to saturation. The radial distribution function was calculated, several properties of the hydrogen bonding in solutions were analyzed. Furthermore, using structures obtained from the simulations, an X-ray emission spectroscopy (XES) spectrum calculation was performed on a 20-molecules cluster, which consisted of one water molecule selected randomly and the 19 surrounding water molecules.

First, the results of the radial distribution function confirmed that Mg^{2+} is closer to water than Na^+. Next, an analysis of the number of hydrogen bonds, their types, and their distribution revealed that, in the first hydration shell, all ions caused significant deviations from that of pure water. Comparing Mg^{2+} with Na^+, Mg^{2+} was found to be closer to water, with an overwhelming number of water molecules acting as hydrogen donors around it. In contrast, around Na^+, the water molecules were positioned farther away compared to Mg^{2+}, resulting in a dominance of water molecules acting as hydrogen acceptors.

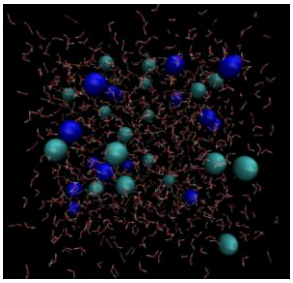

FIGURE 1. MD simulation of 1M NaCl solution

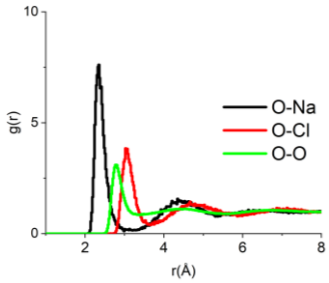

FIGURE 2. Radial distribution function of 1M NaCl solution

REFERENCES

1. R. Watanabe, "Ion Selectivity of Water Molecules in Subnanoporous Liquid-Crystalline Water-Treatment Membranes: A Structural Study of Hydrogen Bonding" *Angew. Chem.*, **59**, 23461 (2020).

Concentration dependence of mixtures of water and 3-methylpyridine using MD simulations

Kouki Ozeki[a] and Osamu Takahashi[b]

[a] *Department of Chemistry, Faculty of Science, Hiroshima Univ.*
[b] *Research Institute for Synchrotron Radiation Science, Hiroshima Univ*

Keywords: Molecular dynamics (MD) simulation, Fourier Transform Infrared Spectroscopy (FT-IR), X-ray absorption spectroscopy (XAS), computational chemistry

Hydrogen bonding is extremely important as a factor governing the physicochemical properties of aqueous solutions. It is expected that a better understanding of its nature will lead to its application in various research fields. In this study, we investigated the behavior of hydrogen bonding in mixtures of water and organic compounds using Fourier Transform Infrared Spectroscopy (FTIR) and theoretical calculations. As an organic compound, 3-methylpyridine (3MP) was chosen. In this compound, it is known that OH...N hydrogen bonds are formed between a lone pair of nitrogen atoms in the pyridine ring and water molecules in aqueous solution.

First, Attenuated Total Reflection (ATR) FT-IR measurements were performed using mixed solutions of various concentrations, and it was found that the peak of the in-plane angular vibration of the pyridine ring corresponding to the vibration at 1029 cm^{-1} (Figure 1) shifted to the higher wavenumber side as the ratio of water increased. This peak shift was also observed for other organic compounds with pyridine rings. The smaller the dipole moment, the weaker the hydrogen bond formed, so the experiment was conducted using chloroform as the solvent. Since the peak shift was smaller than that of water, we considered that this peak change was due to hydrogen bonding.

Next, several aqueous solution models were created with different concentrations of water molecules and 3MP molecules, totaling 50000 molecules, and Molecular Dynamics (MD) simulations were performed with ambient conditions under NPT ensemble. After equilibration, phase separation was observed in each model (Figure 2). This suggests that phase separation may occur even at room temperature in this mixed solution from a microscopic viewpoint.

X-ray absorption spectroscopy (XAS) calculations were performed. The calculations were performed using a cluster model consisting of 19 molecules around a single molecule of water. In the obtained spectra, no pre-edge peaks were observed, which were observed experiments.

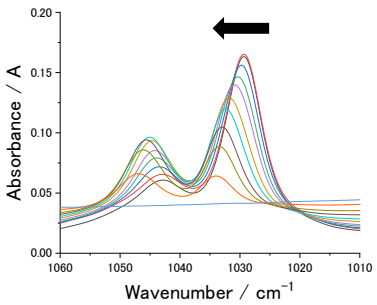

Figure1 ATR FT-IR spectra of water/3MP mixture

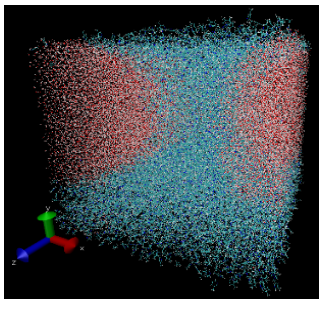

Figure2 Results of MD simulation of water/3MP mixture

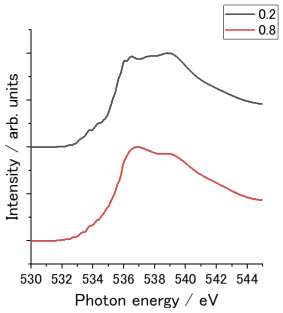

Figure3 Results of XAS calculations for water/3MP mixtures

Structure of maleic and succinic acid in aqueous solution by soft X-ray absorption spectroscopy

Risa Okada[a] and Ryosuke Yamamura[a] and Osamu Takahashi[b]

[a]*Graduate School of Advanced Science and Engineering, Hiroshima University, 1-3-1 Kagamiyama, Higashihiroshima City, Hiroshima 739-8526, Japan*
[b]*Research Institute for Synchrotron Radiation Science, Hiroshima University, 2-313 Kagamiyama, Higashihiroshima City, Hiroshima 739-0046, Japan*

Keywords: X-ray absorption spectroscopy(XAS), soft X-ray, Molecular dynamics(MD)

In our laboratory, we have performed X-ray absorption spectroscopy (XAS) spectral calculations of a series of monocarboxylic and dicarboxylic acids aqueous solutions, and discussed the structures of the acids. In the XAS spectra of oxalic acid, the first peak at 532 eV was blue-shifts due to the break of the orbital π resonance caused by the twisting of the carboxylic group with increasing pH [1]. In this study, we performed theoretical XAS calculations for maleic and succinic acids, which include four carbon atoms in the molecule, and investigated their structures in aqueous solution.

Succinic and maleic acids have multiple stable conformations depending on the orientation of the substituent, so the most stable conformations were determined for neutral, anionic, and dianionic acids, respectively. From the molecular dynamics (MD) simulations at 300 K and 1 bar under the NPT ensemble, a cluster structure consisting of a dicarboxylic acid molecule and 30 water molecules around it was extracted, and XAS spectra were calculated for the cluster structure and compared with experimental spectra. Experimental XAS spectra at the O K-edge were measured at room temperature and atmospheric pressure at the soft X-ray beamline BL17SU at SPring-8. 0.3 M aqueous succinic acid at pH 0.01, 4.98, and 12.37 and 0.2 M aqueous maleic acid at pH 1.38, 4.16, and 11.70 were prepared.

Fig. 1 shows the experimental and theoretical XAS spectra of aqueous succinic and maleic acid. In the XAS spectra of aqueous succinic acid, the first peak around 533 eV shifts to higher energy with increasing pH, similar to acetic acid and malonic acid. In contrast, in aqueous maleic acid, the peak of neutral maleic acid is seen at a higher energy than the peak of anionic maleic acid. The XAS spectra of both succinic and maleic acid were theoretically reproduced. XAS spectra were calculated for a single molecule of neutral maleic acid by rotating the carboxy group, and it was confirmed that the peak shifts to higher energy as the carboxy group becomes more perpendicular to the molecular plane and the orbital resonance between the two carboxy groups is broken. This suggests that the orbital resonance between the carboxy groups is broken, so that the first peak of neutral maleic acid appears on the high energy side.

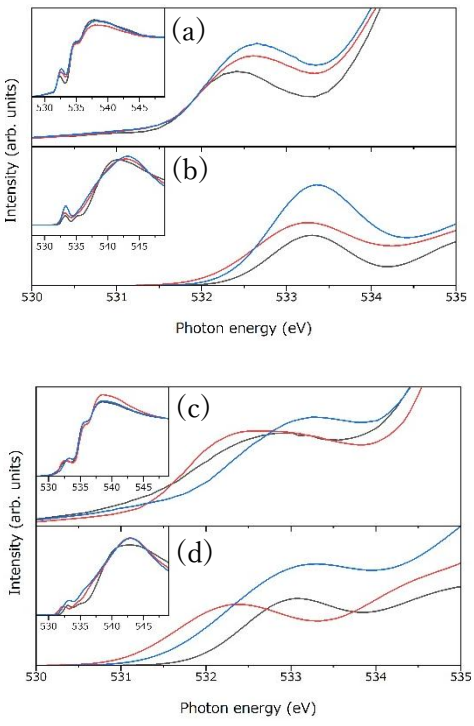

FIGURE 1. (a) experimental and (b) theoretical XAS spectra of aqueous succinic and (c) experimental and (d) theoretical XAS spectra of aqueous maleic acid.

REFERENCES

1. Yamamura, R et al, *Chem. Phys. Lett*, **738**, 136895 (2020).

Theoretical calculations of resonant inelastic soft X-ray scattering based on semi-classical approximation -Application to methanol-

Hikari Sato[a] and Osamu Takahashi[b]

[a] *Department of Chemistry, Faculty of Science, Hiroshima Univ.*
[b] *Research Institute for Synchrotron Radiation Science, Hiroshima Univ.*

Keywords: resonant inelastic soft X-ray scattering (RIXS), soft X-ray emission spectroscopy (XES), Computational chemistry

In our laboratory, various types of X-ray spectroscopy calculations are performing for several liquids. In this study, we performed soft X-ray emission spectroscopy (XES) calculations and resonant inelastic soft X-ray scattering (RIXS) calculations for liquid methanol, which is a typical example as a liquid with simple hydrogen bonds.

In these spectroscopic calculations, especially the system including the second-row elements, it is important to consider the dynamic effects of the intermediate state, i.e., the core hole state. The Kramers-Heisenberg equation unifies the formation of the core excited state due to the absorption of incident photons and the emission of X-rays accompanying the transition of valence electrons to the core hole. In this study, we performed the calculations using the semi-classical Kramers-Heisenberg approximation.[1] By applying the semi-classical approximation, it is possible to perform the XES calculations that take vibrational effects into account while keeping the calculation cost down.

$$\sigma(\omega,\omega') = \frac{\omega'^{\Gamma_f}}{\omega\pi}\sum_f \left\langle F_{if}^{+}(\omega,\omega'-\omega)F_{fi}(\omega,\omega'-\omega)\right\rangle \quad (1)$$

$$F_{fi}(\omega,\omega'-\omega) = -i\alpha\sum_n \frac{\tilde{D}_{ni}(R)}{\omega - E_{ni}(R) + i\Gamma}\left(\int_0^\infty dt'\tilde{D}_{fn}^{+'}(t')e^{i\int_0^{t'}d\tau E_{nf}(\tau)}e^{-i[\omega-E_{ni}(R)]t'}e^{-\Gamma_f t'}e^{i\omega' t'}\right) \quad (2)$$

Molecular dynamics (MD) simulations of a liquid methanol with condition were performed, and several dimer model structures were extracted. Based on this dimer model, theoretical calculations of XES and RIXS spectra were performed, and the obtained spectra were compared with the results of previous studies.

The RIXS spectrum showed a blunt peak change near the first resonance excitation compared to the previous study [2], which is considered to be due in part to the difference in the dimer model.

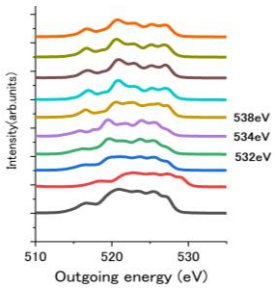

Figure 1. Calculated RIXS spectra of methanol dimers

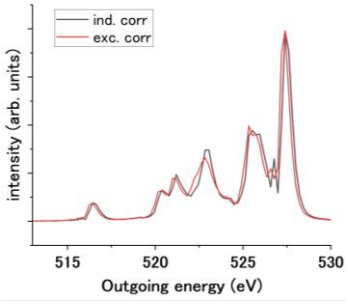

Figure 2. Calculated XES spectra of methanol dimers

REFERENCES

1. M. P. Ljungberg, Phys. Rev. B 96, 2017.
2. M. P. Ljungberg, I. Zhovtobriukh, O. Takahashi and L. G. M. Pettersson, JCP, 2017.

Improvement of the calculation method for X-ray Emission Spectroscopy based on Slater's transition state theory

Yuika Watari[a] and Osamu Takahashi[b]

[a]*Graduate School of Advanced Science and Engineering, Hiroshima Univ.*
[b]*Research Institute for Synchrotron Radiation Science, Hiroshima Univ.*

Keywords: X-ray emission spectroscopy (XES), Density functional theory, Koopmans' theorem, Ionization potential.

Our group is actively working on theoretical calculations of core-excited states using the density functional theory. For X-ray emission spectroscopy (XES) calculations our code estimates the state based on Koopmans' theorem. This theorem has the advantage that the relative energy difference can be evaluated to some extent by the orbital energy, but it has the disadvantage that the orbital relaxation due to the electron number change is not taken into account, which leads to large errors.

Recently, Hirao et al. calculated ionization potentials (IP) using three different methods that extend Slater's transition state theory [1]. The three methods are called the AVG, STS, and RPT3 methods. In these methods, to calculate the IP of one orbital, orbital energies are required for the ground state, the monovalent ionic state with one electron missing from the orbital for which the IP is to be calculated, and the divalent ionic state with one half electron missing. Therefore, while this method is highly accurate, it has the disadvantage of requiring a large amount of computational effort when obtaining IPs for multiple energy levels. In this study, we aim to improve the theoretical calculations of XES so as to eliminate such effort and to establish a practical theoretical calculation method.

Our procedure how to calculate the XES is described. In order to easily calculate IPs for all valence orbitals, we propose a method to remove electrons from the entire valence orbital. For example, consider the case of H_2O. H_2O has four valence electron orbitals, so if we remove 0.25 electrons from all valence electron orbitals, one electron is removed from the entire orbital. In the same way, 0.125 electrons are removed from all valence electron orbitals, resulting in a total of 0.5 electrons removed. By this improvement, the IPs of all levels can be calculated by calculating these three electronic states, which saves a lot of time and effort.

The improved method of XES calculation was validated on 28 molecules, and the errors compared to the experimental values were compared with Koopmans' theorem and the three methods. The results showed that the three methods were more accurate than Koopmans' theorem. Especially for the IP of HOMO, the average error from the experimental data was -0.14 eV for oxygen and -0.10 eV for carbon by the AVG method. In addition, XES spectra were calculated, and spectra with good reproducibility were produced for the peak positions.

TABLE 1. Average of error between calculated and experimental IP from HOMO in eV.

core level	Koopmans	AVG	STS	RPT3
C	-3.73	-0.14	-0.18	-0.17
N	-3.52	-0.10	-0.15	-0.13
O	-4.30	-0.34	-0.41	-0.39

REFERENCES

1. K. Hirao et al., *J. Chem. Phys*. **155**, 034101(2021).